Use of Small UAVs for Field Measurement of Hydraulic Parameters in Small Drainage Basins

February 2026
Final Report

Project number TR202510
MoDOT Research Report number cmr 26-004

PREPARED BY:

Jitae Do, Ph.D.

Binbin Wang, Ph.D.

Baolin Deng, Ph.D.

Yaw Adu-Gyamfi, Ph.D.

Kaitlin Belk

John Holmes, P.E.

University of Missouri-Columbia and Allstate Consultants

PREPARED FOR:

Missouri Department of Transportation

Construction and Materials Division, Research Section

TECHNICAL REPORT DOCUMENTATION PAGE

1. Report No. cmr 26-004	**2. Government Accession No.**	**3. Recipient's Catalog No.**
4. Title and Subtitle Use of Small UAVs for Field Measurement of Hydraulic Parameters in Small Drainage Basins		**5. Report Date** February 2026 Published: February 2026 **6. Performing Organization Code**
7. Author(s) Jitae Do, Ph.D. https://orcid.org/0000-0002-8018-3358 Binbin Wang, Ph.D. https://orcid.org/0000-0003-3799-2042 Baolin Deng, Ph.D. https://orcid.org/0000-0001-6569-1808 Yaw Adu-Gyamfi, Ph.D. https://orcid.org/0000-0002-1924-9792 University of Missouri Katilin Belk and John Holmes, P.E. Allstate Consultants		**8. Performing Organization Report No.**
9. Performing Organization Name and Address Department of Civil and Environmental Engineering University of Missouri-Columbia E2509 Lafferre Hall, Columbia, MO 65201 Allstate Consultants 3312 LeMone Industrial Blvd, Columbia, Missouri, 65201		**10. Work Unit No.** **11. Contract or Grant No.** MoDOT project # TR202510
12. Sponsoring Agency Name and Address Missouri Department of Transportation (SPR-B) Construction and Materials Division P.O. Box 270 Jefferson City, MO 65102		**13. Type of Report and Period Covered** Final Report (December 2024-February 2026) **14. Sponsoring Agency Code**

15. Supplementary Notes

Conducted in cooperation with the U.S. Department of Transportation, Federal Highway Administration. MoDOT research reports are available in the Innovation Library at https://www.modot.org/research-publications.

16. Abstract

This project evaluated the feasibility, accuracy, and practical use of small unmanned aerial vehicles (UAVs) for measuring hydraulic parameters, water-surface elevation (WSE), surface velocity, bathymetry, and discharge, in small to medium Missouri drainage basins. UAV-based measurements offer non-contact alternative to traditional field methods in hazardous environments or high-flow conditions. A comprehensive literature review of 522 publications (2010–2024) was conducted and found that reported errors showed radar-based WSE and hyperspectral/multispectral bathymetry as the most accurate, while PTV showed the highest accuracy with a mean absolute percentage error (MAPE) of 10.7%, while the surface velocity method (SV) yielded the lowest discharge error (MAPE = 12.4%). For the field studies in the next phase, six field sites were selected from 21 candidate locations, to represent diverse channel and hydrologic conditions. Five sites were surveyed using UAV photogrammetry, LiDAR, PIV/PTV, and sonar-based bathymetry. Discharge was estimated using GM and surface-velocity approaches (SV). GM used LiDAR geometry, bathymetry, roughness, and slope, while SV used PIV/PTV at all sites. UAV-based discharge estimates showed 22.2–25.3% difference relative to USGS rating curves. SV produced more consistent accuracy across sites, while GM was highly sensitive to roughness and geometry. SV is recommended when field time is limited, and GM when detailed channel data are available.

17. Key Words Unmanned aerial vehicles; Image velocimetry; Surface velocity; River flow monitoring; River discharge; Stream discharge	**18. Distribution Statement** No restrictions. This document is available through the National Technical Information Service, Springfield, VA 22161.

19. Security Classif. (of this report) Unclassified.	**20. Security Classif. (of this page)** Unclassified.	**21. No. of Pages** 98	**22. Price**

Use of Small UAVs for Field Measurement of Hydraulic Parameters in Small Drainage Basins

Jitae Do[1], Binbin Wang[1], Baolin Deng[1], Yaw Adu-Gyamfi[1], Katilin Belk[2], and John Holmes[2]

[1]University of Missouri, [2]Allstate Consultants

Prepared for

Missouri Department of Transportation

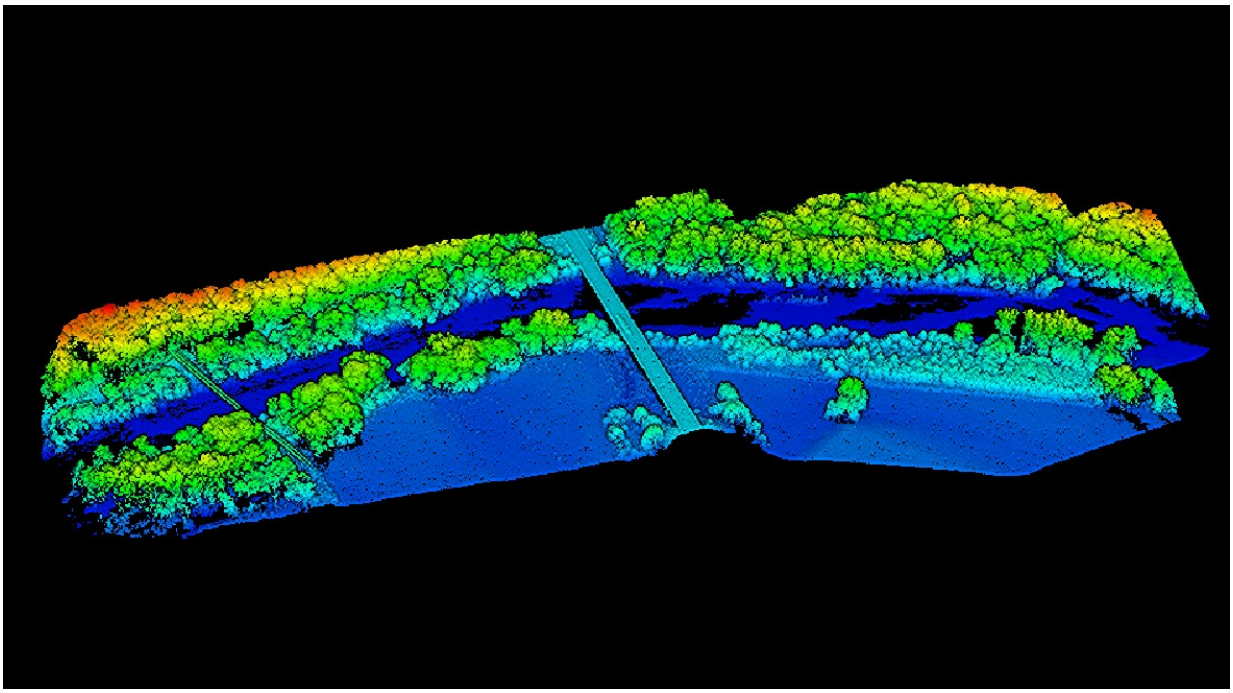

February 2026

Final Report

cmr 26-004

Copyright

Disclaimer

The contents of this report reflect the views of the author(s) who is (are) responsible for the facts and accuracy of the data presented herein. The contents do not necessarily reflect the official views or policies of the Missouri Department of Transportation or the Federal Highway Administration. This report does not constitute a standard, specification, or regulation.

Declaration of Generative Artificial Intelligence (AI), and AI Assisted Technologies

The use of unapproved, **open AI systems** (such as ChatGPT, Bing Chat, and other publicly available AI systems) for research report writing **is prohibited.** Open AI systems such as these, capture data that is entered into it and then uses that data for training their systems to respond to all users of the system. **This is the equivalent of publishing information onto a public website – a violation of MoDOT policy.** Researchers inputting data and information into an AI tool are prohibited from disclosing confidential data or information belonging to MoDOT or MoDOT's partners. Researchers must comply with MoDOT's policies concerning data and record retention, and the proper storage, handling and sharing of sensitive information.

Acknowledgments

The authors would like to acknowledge the Missouri Department of Transportation for funding this study. We are also grateful to the MoDOT personnel who provided valuable support with traffic control during field operations. Finally, we would like to thank the following MU graduate students and postdoctoral researchers for their contributions to field data collection: Dr. Ruichen Xu, Andrew Weber, and Muhammad Waqar Saleem.

Executive Summary

This project evaluated the feasibility, accuracy, and operational practicality of using small unmanned aerial vehicles (UAVs) to measure hydraulic parameters, including water surface elevation, surface velocity, bathymetry, and stream discharge, in streams of small to medium Missouri drainage basins. Traditional field methods such as wading, current metering, or acoustic doppler current profiler (ADCP) surveys can be hazardous, slow, or impractical during high-flow conditions. UAV-based remote sensing offers a non-contact alternative capable of rapidly acquiring spatially continuous data while reducing personnel risk.

The objectives of this study included the following:

- Conduct an in-depth literature review of past and current research on the use of UAVs for measuring key hydraulic parameters, including water surface elevation, flow velocity, bathymetry, and discharge.
- Determine best practices through field surveys and data processing for UAV-based field surveys in small drainage basins across different hydrological regions in Missouri.
- Support MoDOT's UAV-based hydraulic measurements by demonstrating best practices in the field, developing a step-by-step procedure manual, and presenting methods and results.

In-depth literature review was conducted. Five hundred twenty-two publications were found from 2010-2024 - they were categorized into three categories: river applications, non-hydraulic parameter related studies, and not related to the studies. For the river application studies, they were divided into four subcategories: water surface elevation (WSE), bathymetry, surface velocity, and discharge measurements.

From the literature review, UAV-based WSE measurement errors (ME) range from 0.16 to 0.61 ft, with radar-based WSE measurements showing the lowest error (ME = 0.16 ft). For bathymetry, measurement errors range from 0.3 to 1.0 ft, with hyperspectral/multispectral sensors (ME = 0.31 ft.) and bathymetric Light Detection and Ranging (LiDAR, ME = 0.30 ft.) providing the highest accuracy among the reviewed methods. Surface-velocity measurements show mean absolute percentage errors (MAPE) ranging from 10.7% to 37.7%, with Particle Tracking Velocimetry (PTV) yielding the lowest error (MAPE = 10.7%). For discharge estimation, MAPE ranges from 12.4% to 19.1%, with the surface velocity method (SV) providing the lowest error (MAPE = 12.4%). However, PTV and geometric method (GM) give mean percentage errors (MPE) of approximately +4.0% and –2.3%, respectively, which are larger in magnitude than the average MPE reported for surface-velocity measurements (–2.0%) and for overall discharge estimates (–1.0%). This indicates the presence of small systematic biases in both methods.

Initial site selection was conducted, resulting in twenty-one candidate sites. Among these candidates, a final set of field locations was selected for UAV-based hydraulic data collection. These sites were chosen to represent a broad range of channel sizes, geomorphic settings, and hydrologic conditions while ensuring safe and consistent UAV operation. A total of five field experiment locations were decided and evaluated based on photogrammetry, LiDAR, Particle

Image Velocimetry (PIV)/PTV, bathymetry, and discharge measurements. For discharge estimation, two different approaches were used: the GM and SV methods. Bathymetric data, LiDAR-derived hydraulic parameters, including hydraulic radius, flow area, and roughness coefficients, were used in the GM approach to compute discharge. For the SV method, PIV was applied at all sites except Tavern Creek, where clear-water conditions required the use of seeded tracers. Surface velocities obtained from PIV (or PIV and PTV at Tavern Creek) were then converted to discharge using the velocity–area method.

Overall, UAV-based discharge estimation resulted in measurement errors of 22.2–25.3% compared with the USGS rating curve. Based on these results, GM is generally applicable except in very small streams. GM produced an average difference of 22.2%, while the SV method produced an average difference of 25.3%. However, GM difference ranged widely from 0.3% to 40.7%, with an extreme value of 798% treated as an outlier when computing the mean, whereas SV differences were consistently within 14.2–43.2%. This indicates that SV provides more stable accuracy across different sites, while GM can exhibit large deviations when channel geometry or roughness estimates are uncertain. Therefore, when testing time is limited, SV may be the preferred approach; when sufficient time and site information are available, GM is recommended.

Based on field experience and data-processing outcomes, several recommendations are proposed to improve the reliability and efficiency of UAV-based hydraulic measurements:

- Adopt PTV with seeding particles for clear-water conditions. While PIV provides faster computation, PTV offers higher accuracy in resolving surface flow trajectories, especially when natural or artificial tracers are sparse. Despite its longer processing time, PTV is preferred for low-turbidity or smooth-surface flows where PIV correlation may be unreliable.
- Adopt PIV under flooded conditions. Although PTV yields better accuracy in clear water, it becomes less effective in flooded or highly reflective environments due to weak tracer contrast. PIV is recommended in such cases, as its correlation-based approach performs more robustly under variable lighting or surface disturbance.
- Establish standardized seeding protocols. Biodegradable tracers such as wood mulch improved surface texture and PTV detection. Seeding density and release location should be adjusted based on flow velocity and channel width to ensure uniform tracer distribution.
- Automate velocity extraction and discharge estimation. Developing semi-automated workflows in MATLAB or Python that integrate PIV/PTV outputs with DEM-based cross-sections can streamline data processing, reduce operator workload, and improve reproducibility.

Table of Contents

List of Figures

List of Tables

List of Equations

1. Introduction

Accurate characterization of streamflow and hydraulic parameters is essential for designing, evaluating, and maintaining transportation infrastructure such as bridges and culverts. Conventional discharge measurement techniques, such as current metering, Acoustic Doppler Current Profilers (ADCPs), or wading surveys, often require direct contact with the flow, which can be hazardous or impractical especially under high-flow or flood conditions.

Recent advances in unmanned aerial vehicle (UAV) technologies now enable non-contact measurements of river hydraulics using optical and Light Detection And Ranging (LiDAR) sensors. UAVs provide rapid, flexible, and cost-effective mapping capabilities while minimizing personnel exposure to unsafe flow environments. This manual presents a standardized workflow for collecting, processing, and integrating UAV-based LiDAR, photogrammetry, and optical velocimetry data to estimate surface velocity and discharge in Missouri streams.

The goal is to establish repeatable field and data-processing procedures that enable Missouri Department of Transportation (MoDOT) to acquire reliable hydraulic data in small to medium drainage basins.

The primary objectives of this project were to:

- Evaluate UAV-based Method Accuracy and Techniques: Measure water surface elevation, flow velocity, bathymetry, and discharge in small drainage basins, comparing UAV-based methods with traditional techniques.
- Develop Best Practices and Documentation: Provide MoDOT with detailed guidelines and recommendations to achieve accurate hydraulic measurements.
- Support MoDOT with Practical Applications: Provide a step-by-step procedure manual, ensuring safe and effective data collection, even in challenging conditions such as high-water flows

To meet the project objectives, the following tasks were completed:

- a comprehensive literature review of UAV-based hydraulic measurement methods and related studies;
- selection of five representative stream sites in Missouri that encompass a broad range of hydraulic and geomorphic conditions;
- data collection for the five sites: photogrammetry, LiDAR mapping, surface-velocity videos, and bathymetry;
- processing of UAV-based datasets including LiDAR point clouds, photogrammetric reconstructions, PIV/PTV surface-velocity fields, and bathymetry measurements;
- estimation of discharge using geometry-based and surface-velocity-based methods
- comparison of hydraulic measurement methods, including accuracy assessment and evaluation of applicability across different stream types.

This report details the tasks completed to address the above objectives and is organized to present the following information: background and literature review (Chapter 2), selection of study locations (Chapter 3), data-processing methods, hydraulic analysis results including surface velocity, water-surface elevation, bathymetry, and discharge estimation for each site (Chapter 4), and summary and recommendations for future implementation (Chapter 5). The bulk of the detailed results are provided in figures and tables throughout the report, with high-resolution graphics included in the appendices and representative examples presented in the main body of the report.

2. Background & Literature Review

Conventional field-based methods for measuring hydraulic parameters, such as water surface elevation, flow depth, surface velocity, and discharge, have been successfully used for decades. However, conventional methods typically rely on ground-based instruments such as total stations, current meters, ADCPs, and wading surveys. While effective, these approaches often require direct access to the channel, making data collection time-consuming, labor-intensive, and potentially hazardous during high flows. In addition, field accessibility, vegetation cover, and unstable channel conditions can limit the spatial resolution and repeatability of traditional measurements.

Recent advances in UAVs have enabled new approaches for measuring hydraulic parameters in rivers and small drainage basins, providing safe, rapid, and spatially continuous data collection even under challenging field conditions. UAVs can carry optical, LiDAR, hyperspectral, and acoustic sensors, allowing multiple hydraulic variables to be captured simultaneously, and enabling repeatable surveys that would otherwise be difficult or impractical using ground-based methods.

In this section, we provide an overview of the UAV-based methods relevant to hydraulic data collection, including LiDAR and photogrammetric approaches for mapping surface elevation and channel geometry, optical velocimetry techniques for estimating surface flow velocity, and supporting bathymetric methods used to complete channel characterization.

2.1 Literature Survey

An extensive literature search was conducted in the Web of Science database to identify studies that apply UAVs and related platforms for hydrological and hydraulic observations. The search combined key terms related to UAVs with water-related variables such as “water surface elevation,” “flow velocity,” “water velocity,” “surface flow,” “river discharge,” “stream discharge,” and “bathymetry.” The search string used was:

```
((UAV) OR (UAS) OR (Drone)) AND (“water surface elevation” OR “flow velocity” OR “water velocity” OR “surface flow” OR “river discharge” OR “stream discharge” OR “bathymetry”)).
```

This query yielded 522 publications in the Web of Science Core Collection as of October 2024. Figure 2.1 presents the annual distribution of publications during 2010–2024, showing a sharp rise after 2015 that reflects advances in UAV sensing technologies and image-processing methods. The number of publications exceeded 60 per year after 2020, indicating accelerated adoption of UAV-based approaches for hydrological and hydraulic observations.

To ensure comprehensive coverage of relevant hydraulic applications, we manually reviewed the retrieved papers, focusing on studies involving quantitative field measurements of hydraulic parameters such as water surface elevation, bathymetry, surface velocity, and discharge obtained using UAV-based techniques. Review papers and remote-sensing mapping studies unrelated to water dynamics were excluded from further consideration.

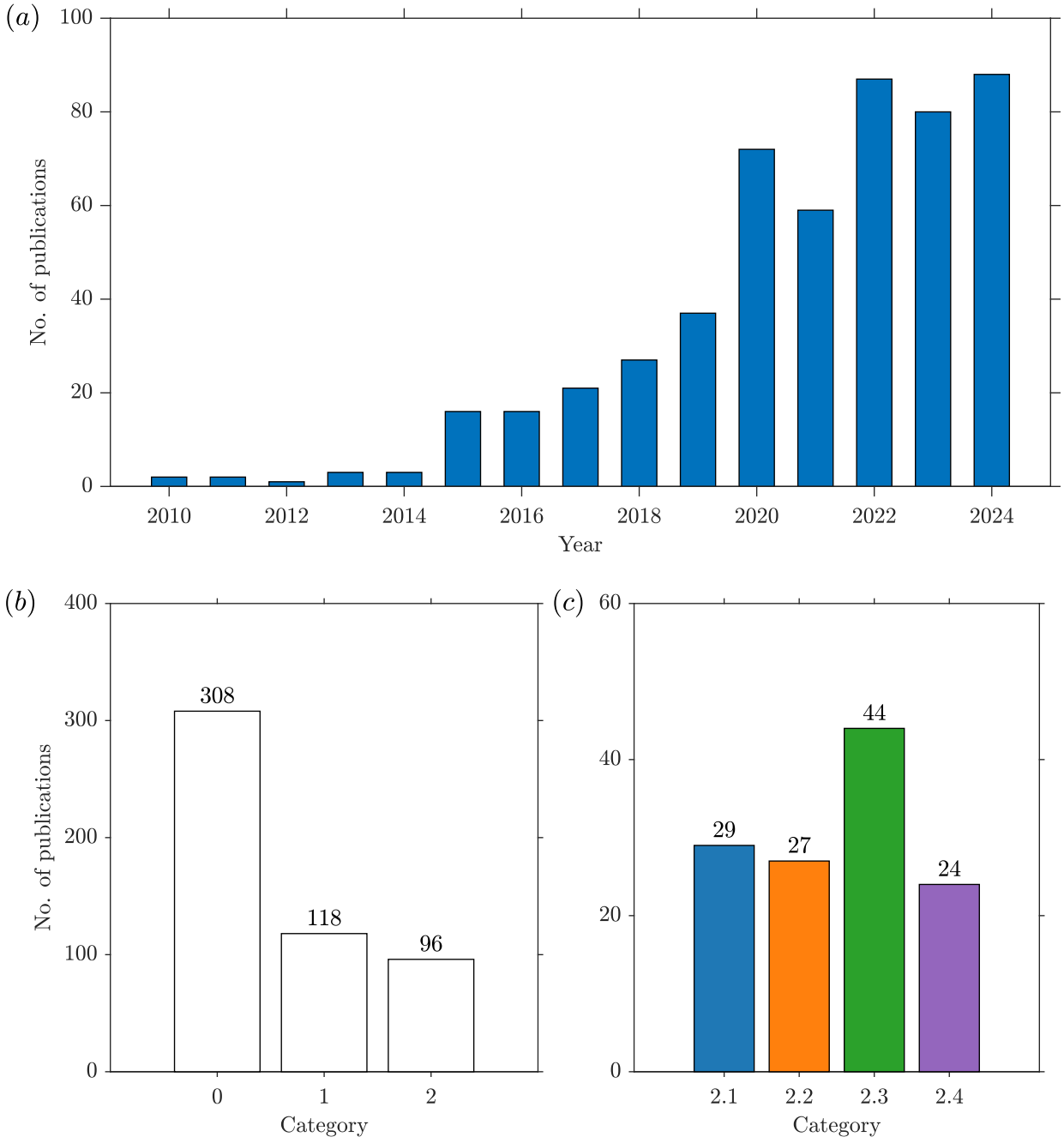

Figure 2.1 (*a*) Number of publications retrieved from the Web of Science during 2010–2024. (*b*) Classification of studies based on their relevance to river hydraulic measurements. (*c*) Subdivision of Category 2, where 2.1, 2.2, 2.3, and 2.4 correspond to water surface elevation, bathymetry, surface velocity, and discharge, respectively.

Table 2-1 Classification criteria used for categorizing UAV-based hydrological studies according to their relevance to river applications.

Category	Description	Examples / Focus Areas
0	Not related to river applications	Coastal and oceanic applications (seabed or seafloor, shallow water, nearshore, sea state, shoreline, seagrass, offshore), ponds, reservoirs, lakes, glaciers, aerodynamic and navigation systems, geodynamic processes, and other non-UAV, or non-hydraulic studies.
1	Related to river applications but not with hydraulic parameters	Groundwater, habitat, flood modeling, flash floods, river meandering, sediment transport, soil loss, riverbeds, rock glaciers, dams, temperature, headwaters, acid mine drainage, and others.
2	Related to river hydraulic parameters	Quantitative measurements of: 2.1 Water surface elevation 2.2 Bathymetry 2.3 Surface velocity 2.4 Discharge

Table 2-1 summarizes the classification criteria used to categorize UAV-based hydrological studies according to their relevance to river applications. Studies were grouped into three categories: Category 0 includes studies not related to river environments, such as coastal, oceanic, and other non-hydraulic applications; Category 1 includes studies related to river environments but not involving direct hydraulic measurements; and Category 2 comprises studies focused on quantitative measurements of hydraulic parameters such as water surface elevation, bathymetry, surface velocity, and discharge. Figures 2.1b–c present the distribution and characteristics of these categories. Figure 2.1b shows the proportion of papers across the three categories defined in Table 1, with Category 0 (non-river applications) representing the largest portion, followed by Category 1 (river-related but non-hydraulic) and Category 2 (hydraulic measurements).

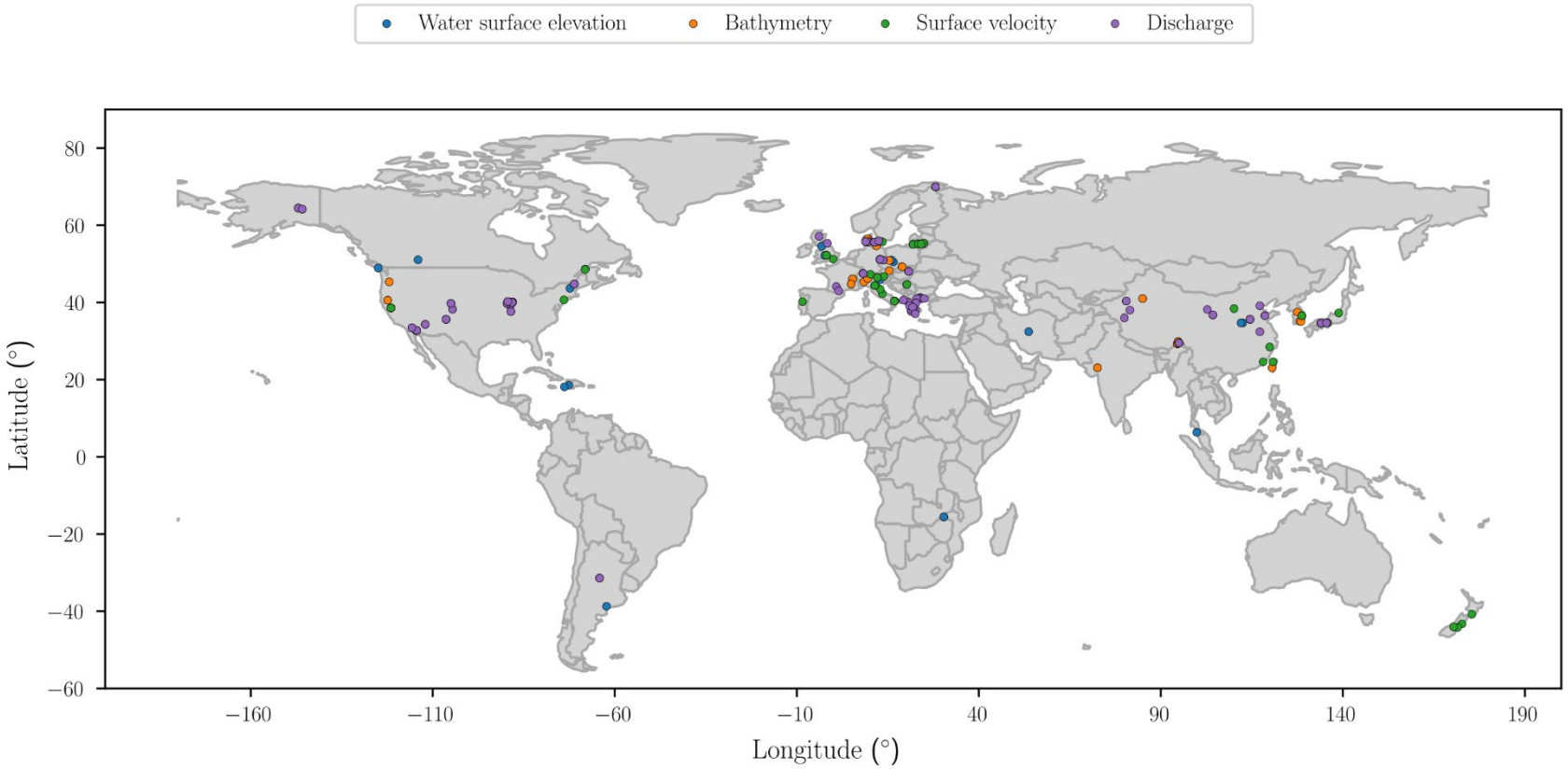

Figure 2.2 Global distribution of studies belonging to Category 2. Each point represents a published UAV-based field study involving quantitative hydraulic measurements, categorized into surface elevation, bathymetry, surface velocity, or discharge.

Figure 2.2 presents the spatial distribution of studies classified under Category 2, which includes UAV-based measurements of water surface elevation, bathymetry, surface velocity, and discharge. The spatial pattern indicates that most documented field applications are concentrated in Europe, East Asia, and North America, particularly in regions with well-established hydrological monitoring networks. In contrast, relatively few UAV-based hydraulic field studies have been reported in Africa, South America, and parts of Southeast Asia, highlighting clear regional disparities in the availability and use of UAV technologies for quantitative river measurements.

Collectively, these results illustrate the rapid expansion of UAV-based hydraulic research worldwide while showing significant regional gaps in field data availability. Building on these findings, the following sections provide an overview of UAV-based techniques relevant to hydraulic data collection and their application to stream environments.

In the following subsections, we review the methods used to measure each hydraulic parameter. Section 2.2 describes approaches for estimating water surface elevation. Section 2.3 summarizes bathymetric techniques. Section 2.4 reviews surface velocity estimation methods. Finally, Section 2.5 examines discharge estimation, establishing the foundation for the data processing presented in subsequent chapters.

2.2 Water Surface Elevation

UAV-based methods for estimating WSE have advanced rapidly in recent years. Based on the literature review, the primary approaches fall into three categories: photogrammetry, LiDAR, and radar. Each method relies on different sensing principles and offers distinct advantages depending on water clarity, illumination, and surface conditions. This section provides an overview of these techniques, outlining their operational characteristics, limitations, and applicability to riverine environments.

2.2.1 Photogrammetry

Photogrammetry can be used to estimate WSE by reconstructing the three-dimensional geometry of visible points near or beneath the water surface. However, when imaging through water, light rays refract at the air–water interface, causing underwater features to appear displaced from their true positions. This distortion must be corrected to obtain accurate elevation estimates.

Refraction is governed by Snell's Law using following (Equation 2.1):

$$n_1 \sin i = n_2 \sin r$$

where n_1 and n_2 are the refractive indices of air and water; i and r are the angles of incidence and refraction.

Equation 2.1. Snell's law for refraction at the air–water interface

By applying this refraction correction (Figure 2.3), the true depth of the underwater point can be recovered and combined with surrounding terrain information to estimate the local WSE.

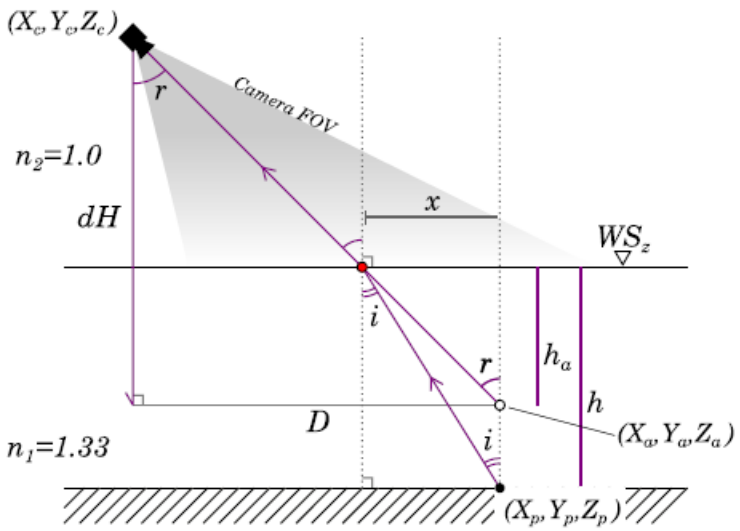

Figure 2.3 Trigonometry of the refraction angles for a single camera point combination (adapted from Dietrich 2017, with permission from Wiley).

This method is most effective in moderately clear water, where underwater features or bed textures provide enough contrast for photogrammetric reconstruction. In very clear water, however, the reconstructed point may correspond to the midpoint of the refracted light path rather than the true bed elevation, introducing additional uncertainty. Consequently, data quality and WSE accuracy depend strongly on water clarity, lighting conditions, and the availability of detectable underwater features.

2.2.2 LiDAR

UAV-mounted Light Detection and Ranging (LiDAR) systems provide high-resolution elevation data by emitting laser pulses and measuring their return time after reflection from the ground or other surfaces. The LiDAR workflow typically consists of (1) emission and reflection of laser pulses, (2) integration of multiple returns into a georeferenced point cloud, and (3) post-processing to generate a Digital Elevation Model (DEM). When operated from a UAV platform, LiDAR offers dense and spatially continuous elevation mapping of channel banks, floodplains, and surrounding terrain, as illustrated in Figure 2.4.

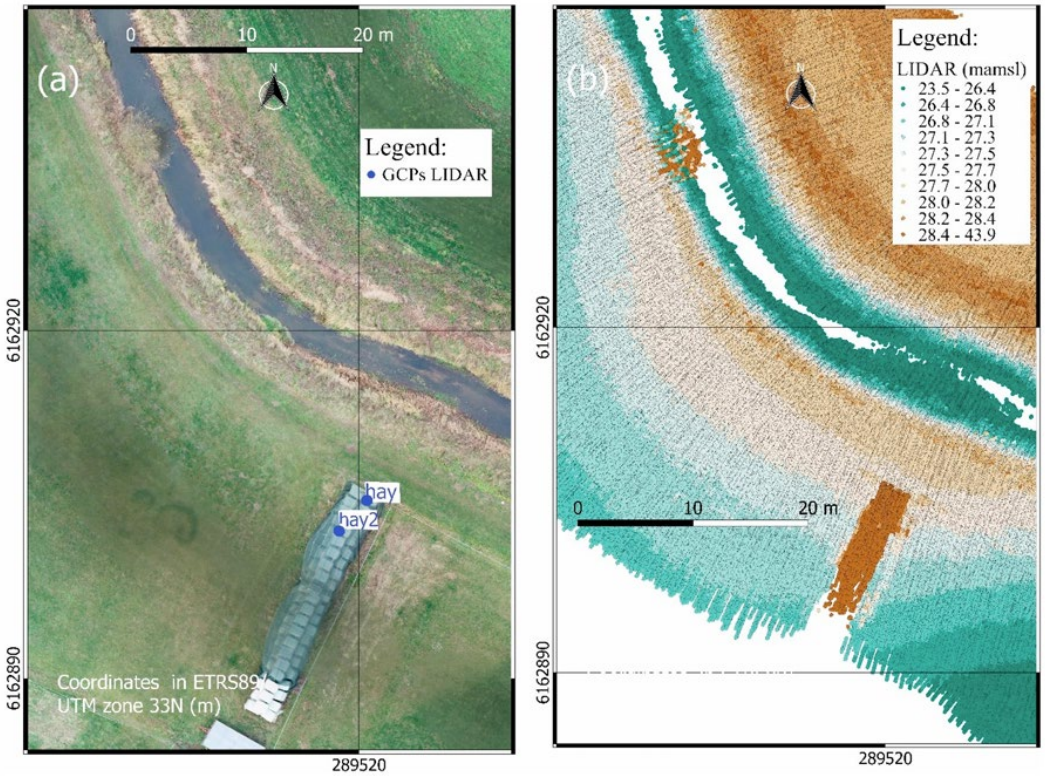

Figure 2.4 Example of UAV LiDAR data: comparison of photogrammetry and LiDAR point cloud. (a) Orthophoto of the study area. (b) LiDAR-derived point cloud for the same location, showing detailed elevation variation across the stream corridor (adapted from Bandini et al. 2020, with permission from Elsevier).

However, a key limitation of airborne LiDAR is its inability to reliably measure WSE over open water. Most rivers and streams do not provide sufficiently strong or consistent laser returns due to low reflectivity, surface smoothness, and absorption of the emitted LiDAR energy. As a result, direct LiDAR returns over the water surface are often absent or too sparse to characterize a continuous water surface.

Despite the inability to directly capture water returns, LiDAR remains essential for constructing accurate DEMs of the channel banks and adjacent floodplain, which provide critical inputs for hydraulic slope estimation, river bank topography, and geometry-based discharge calculations.

2.2.3 Radar

Radar sensors can be used to estimate WSE by measuring the range to the water surface and converting the returned signal into an elevation value using GNSS-derived aircraft or UAV altitude. Compared with optical methods, radar is less sensitive to water clarity and illumination conditions, making it suitable for turbid rivers or environments with limited visual contrast. Airborne radar returns provide a continuous profile of the reflecting surface along the flight path. As shown in Figure 2.5, radar power maps can identify key features such as bridges, vegetation, and differences in flight altitude between passes.

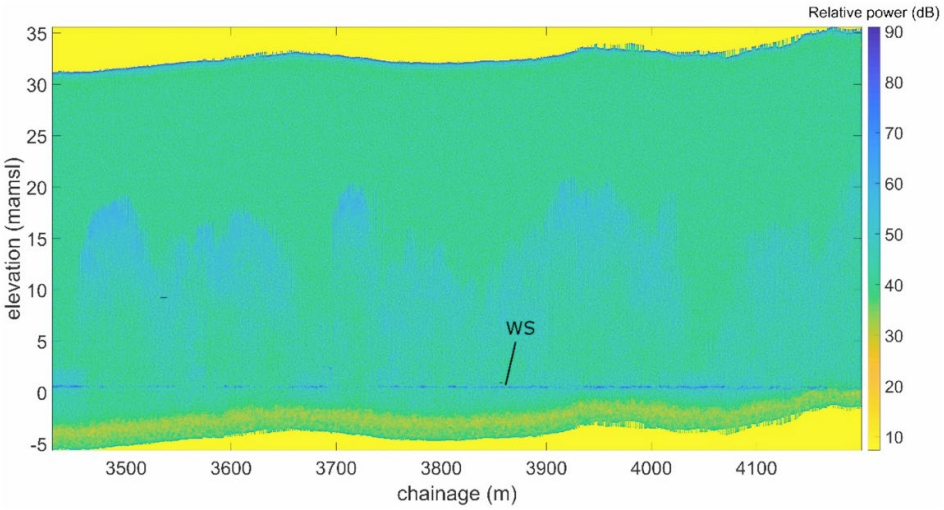

Figure 2.5 Example of a radar full waveform profile. The blue shadow-like patterns are the hyperbolic signatures produced by trees (adapted from Bandini et al. 2020, with permission from Elsevier).

Radar typically produces smoother and less noisy WSE estimates than optical point clouds, particularly under variable lighting or surface roughness. However, accuracy can be influenced by factors such as aircraft motion, antenna orientation, and surface conditions that affect backscatter intensity. Despite these limitations, radar offers a valuable alternative for estimating WSE, especially in highly turbid or dynamic river environments where optical methods are often challenged.

2.2.4 Comparative Assessment

A comparative assessment of UAV-based WSE methods, photogrammetry, Light Detection and Ranging (LiDAR), and radar, was conducted using published datasets reporting WSE accuracy under a range of environmental conditions. Across studies, all three methods show reasonable agreement with reference measurements, with most WSE estimates falling within typical error bounds reported for remote-sensing applications.

Table 2-2 Error statistics for UAV-derived water surface elevation estimates using photogrammetry, LiDAR, and radar.

Method	**No. of publications**	**Mean measurement error [ft]**
Photogrammetry	18	0.56
LiDAR	6	0.61
Radar	4	0.16
Total	28*	0.51

*The total number of publications does not equal the sum of individual categories because some studies used multiple methods, while others did not report method-specific error values.

Based on the compiled error statistics (Table 2-2), photogrammetry shows moderate accuracy across studies but exhibits higher variability in reported errors. LiDAR demonstrates consistent performance for elevations derived from bank-adjacent returns but displays reduced accuracy across the available datasets. Radar shows the lowest mean errors among the three methods, with reported values indicating smoother and less variable WSE estimates.

Each method, however, has notable limitations. Photogrammetry is constrained by water clarity, surface reflectance, and the visibility of underwater or edge features. LiDAR is limited by weak or absent returns over open water, requiring indirect estimation of WSE. Radar performance can be affected by platform motion, antenna geometry, and surface backscatter characteristics. Collectively, these results indicate that each method offers complementary strengths, and their suitability depends strongly on water clarity, surface conditions, and the required spatial resolution.

2.3. Bathymetry

For UAV-based hydraulic surveying, several complementary methods are available to estimate underwater topography depending on water clarity, depth, and site conditions. The primary UAV-enabled bathymetric approaches include photogrammetry, Green LiDAR, hyperspectral imagery, UAV-tethered sonar, and ground-penetrating radar (GPR). Each method relies on different sensing principles and exhibits varying levels of effectiveness based on factors such as water clarity, depth, substrate visibility, and overall environmental conditions. This section provides an overview of these techniques, outlining their operational characteristics, limitations, and applicability.

2.3.1 Photogrammetry

Photogrammetry can be used to estimate shallow-water depth by reconstructing the geometry of visible points beneath or near the water surface. However, light rays refract at the air–water interface, causing underwater features to appear displaced from their true position. This refraction must be corrected using Snell's Law to recover the true location and elevation of the submerged point. Without applying this correction, the reconstructed point lies along an incorrect line of sight, leading to systematic underestimation of depth, as illustrated in Figure 2.6.

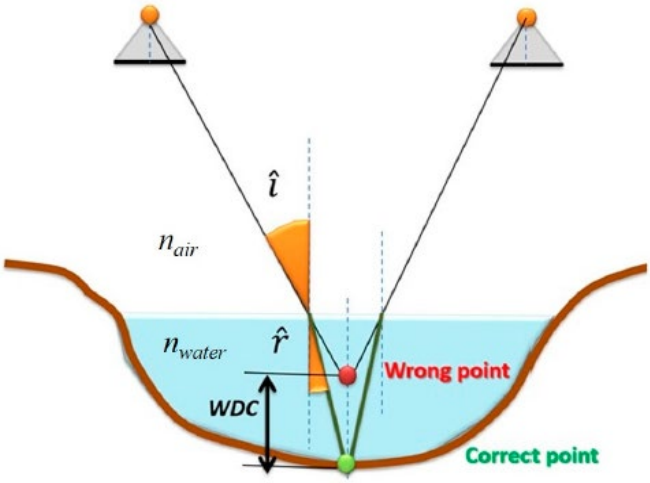

Figure 2.6 Illustration of refraction effects on underwater point reconstruction for a single-camera configuration (adapted from Emanuele et al., 2020, under CC BY 4.0).

This method is most effective in moderately clear water, where the channel bed or other submerged features provide sufficient texture for photogrammetric reconstruction. In very clear water, however, the apparent location of underwater points may lie partway along the refracted light path rather than at the true bed elevation, increasing depth uncertainty. As a result, accurate bathymetric estimation requires applying a refraction-correction procedure, and the overall data quality depends strongly on water clarity, lighting conditions, viewing geometry, and the visibility of underwater features.

2.3.2 Hyperspectral/Multispectral Sensor

Hyperspectral and multispectral sensors estimate water depth by analyzing how light at different wavelengths is absorbed and reflected by the water column and channel bed. By capturing dozens to hundreds of spectral bands, far beyond the limits of standard RGB imagery, these sensors allow depth-related spectral variations to be mapped across the channel. When paired with appropriate calibration data, empirical models can convert spectral information into continuous bathymetric surfaces, producing detailed maps of water depth (Figure 2.7).

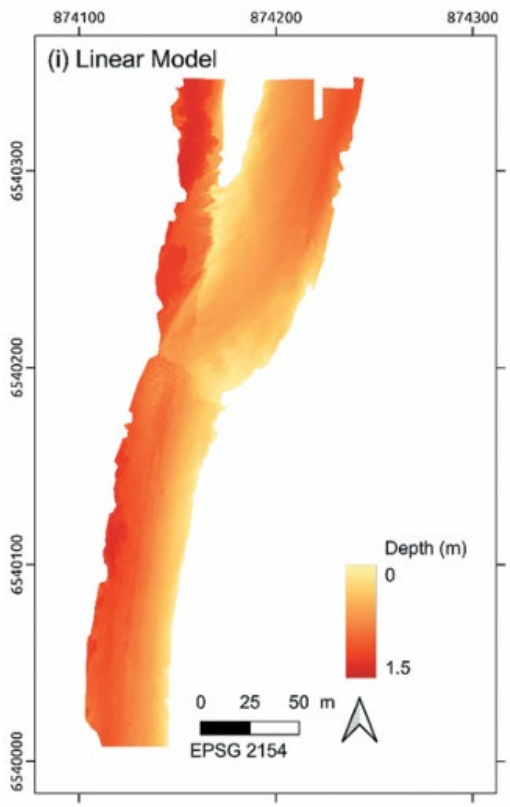

Figure 2.7 Example of hyperspectral sensor derived bathymetry: base flow depth map generated from UAV hyperspectral imagery (adapted from Godfroy., 2024, with permission from Taylor & Francis).

Hyperspectral bathymetry is most effective under conditions where water clarity allows sufficient light penetration, and where water-column properties remain relatively uniform. However, its performance reduces in deeper water depth due to limited light penetration, in areas affected by shadows or surface turbulence changes the spectral response. Environmental variability across long reaches can reduce the transferability of site-calibrated models, requiring additional calibration data. Despite these challenges, hyperspectral imaging remains a reliable option for UAV-based bathymetry, providing high-resolution, continuous depth mapping when conditions are suitable.

2.3.3 Bathymetric LiDAR

Bathymetric LiDAR systems use short-wavelength green laser light (≈532 nm) capable of penetrating the water column, enabling measurement of both the water surface and the channel bed when water clarity is sufficient. Unlike traditional near-infrared (NIR) LiDAR, which is almost completely absorbed by water, green LiDAR produces a multi-return waveform that typically includes a surface return, volumetric backscatter from suspended particles, and a bottom return. By analyzing the timing and intensity of these returns, water depth can be estimated (Figure 2.8).

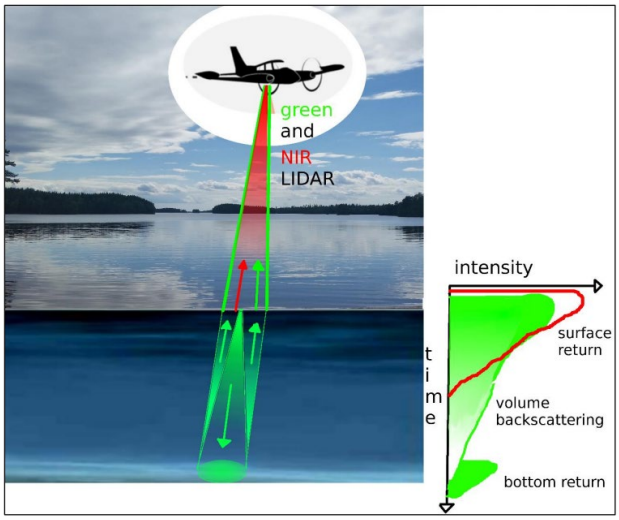

Figure 2.8 Conceptual illustration of UAV-based green LiDAR bathymetry: green and near-infrared (NIR) LiDAR waveform components used for detecting the water surface and channel bed (adapted from Bandini, 2017).

When mounted on UAV platforms, green LiDAR enables high-resolution bathymetric mapping of shallow streams, especially in clear to moderately turbid water. This capability is valuable for characterizing channel morphology, monitoring sediment transport, and providing input for hydraulic modeling. However, the performance of green LiDAR strongly depends on water clarity, depth, and bottom reflectivity. Highly turbid water, dense vegetation, or low-reflectance substrates can limit penetration and reduce the reliability of bottom returns.

2.3.4 UAV Tethered Sonar

UAV-tethered sonar systems enable bathymetric measurements by suspending a compact echo sounder beneath a multirotor platform. The sonar transducer, positioned at or just below the water surface, emits acoustic pulses that reflect off the channel bed, allowing depth to be measured independently of water clarity or lighting conditions. Dual-frequency configurations provide both wide-beam coverage for general depth profiling and narrow-beam returns for higher-resolution bottom detection. An example of a UAV-mounted tethered sonar system and its beam geometry is shown in Figure 2.9.

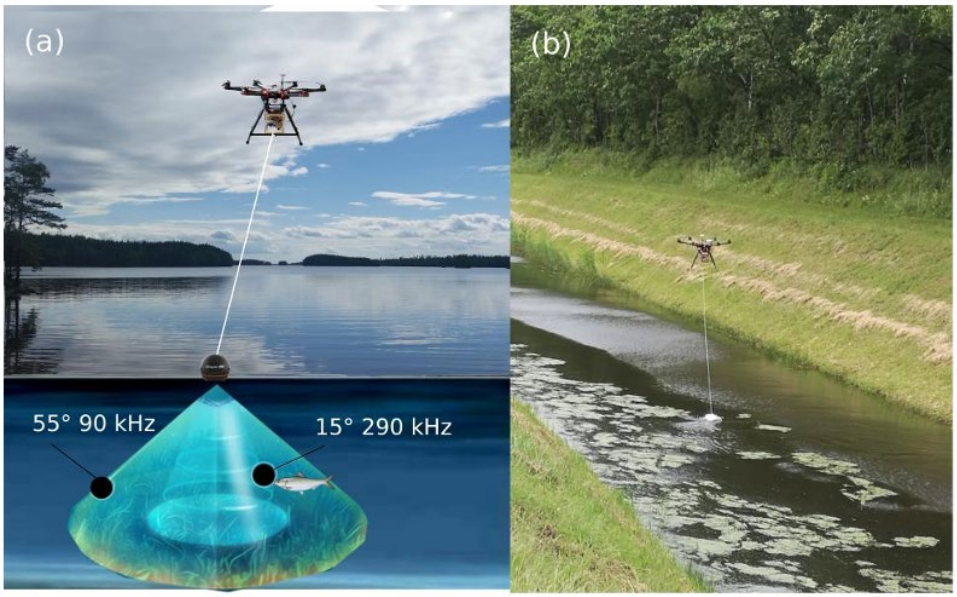

Figure 2.9 UAV-tethered sonar for bathymetric measurement. (*a*) Sonar measurement beams at two different frequencies, showing their respective beam divergences. (*b*) UAV in flight deploying the tethered sonar system (adapted from Bandini, 2017).

This approach enables bathymetric surveys in locations that are difficult or unsafe to access with boats or wading, such as narrow channels, steep banks, or high-flow conditions. UAV positioning offers rapid mobility along the channel and allows depth transects to be collected without direct human contact with the water, improving both efficiency and operator safety.

Limitations include sensitivity to UAV motion, cable sway, and flow-induced drag on the tethered transducer, all of which can influence positional accuracy and measurement stability. The measurable depth range is also constrained by the sonar transducer's specifications and the required clearance between the UAV and the water surface. Despite these challenges, UAV-tethered sonar provides a flexible and effective method for collecting bathymetric data in small to medium river systems.

2.3.5 Ground Penetrating Radar (GPR)

Ground Penetrating Radar (GPR) estimates bathymetry by transmitting electromagnetic waves that pass through the air–water interface, propagate through the water column, and reflect from the channel bed. When mounted on a UAV, the antenna can be flown along the channel to collect continuous depth information without needing to place instruments in the water. The resulting radar signal contains identifiable components related to transmission loss, propagation through water, and bed reflection, which can be used to infer depth (Figure 2.10).

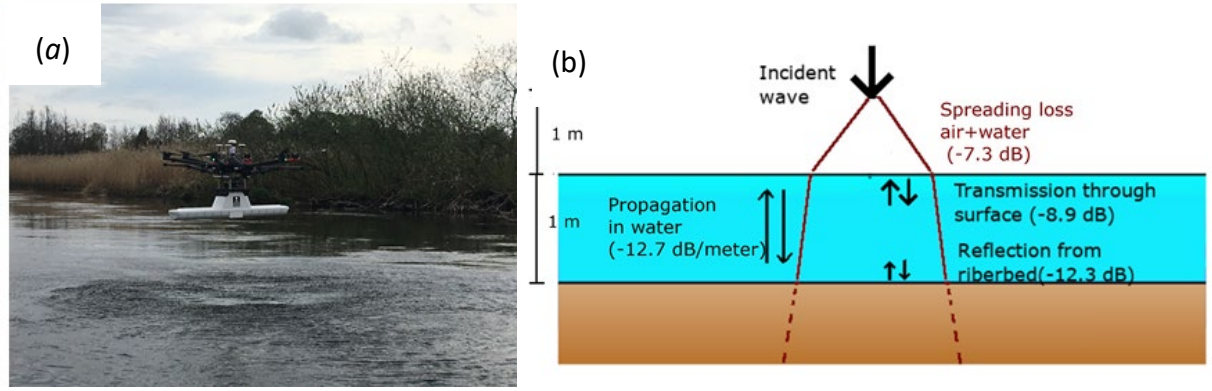

Figure 2.10 (*a*) UAV equipped with a Ground Penetrating Radar (GPR) system. (*b*) Illustration of major signal-loss components for GPR propagation, including spreading loss in air–water transmission, attenuation within the water column, and reflection losses at the riverbed (adapted from Bandini et al, 2023, licensed under CC BY 4.0).

GPR is most effective when the water column allows electromagnetic energy to travel to the river bed and back, and when the channel substrate provides a clear reflective boundary. A major advantage is its ability to detect the bed even in areas with submerged vegetation, where optical or acoustic methods may be insufficient. However, performance can be reduced by surface roughness, high electrical conductivity, or unstable flight conditions that introduce noise into the radar signal. Despite these limitations, UAV-based GPR provides a useful alternative for shallow-water bathymetry, particularly in environments where visibility, turbidity, or vegetation limit the use of optical and sonar methods.

2.3.6 Comparative Assessment

A comparative assessment of UAV-based bathymetric methods, photogrammetry, hyperspectral/multispectral sensors, bathymetric LiDAR, UAV-tethered sonar, and GPR, was conducted using published datasets that report depth-measurement accuracy under a range of environmental conditions.

Based on the error statistics in Table 2-3, UAV-based bathymetric methods show a wide range of performance across published studies. Hyperspectral/multispectral sensors and bathymetric LiDAR show the lowest mean errors among the available datasets, indicating relatively consistent depth retrieval when environmental conditions allow spectral or laser penetration.

Photogrammetry shows moderate accuracy but with higher variability, reflecting its dependence on visible bed features. UAV-tethered sonar produces reasonable depth estimates across studies but with greater spread in reported error, likely linked to platform stability and channel conditions. Ground Penetrating Radar, represented by a smaller number of studies, shows the highest mean error, reflecting both methodological sensitivity and limited dataset availability.

Table 2-3 Error statistics for UAV-derived bathymetry estimates using photogrammetry, LiDAR, and radar.

Method	**No. of publications**	**Mean measurement error [ft]**
Photogrammetry	10	0.78
Hyperspectral/Multispectral sensor	6	0.31
Bathymetric LiDAR	3	0.30
UAV tethered sonar	3	0.68
Ground Penetrating Radar	1	1.05
Total	25*	0.59

*The total number of publications does not equal the sum of individual categories because some studies used multiple methods, while others did not report method-specific error values.

Across studies, all methods demonstrate the ability to retrieve channel bed elevations with errors generally within the range expected for remote-sensing–based bathymetry. However, performance varies among techniques due to factors such as water clarity, substrate visibility, and sensor–environment interactions, resulting in differences in mean error and overall variability.

2.4. Surface Velocity

Surface velocity measurements are a key component of UAV-based hydraulic monitoring, providing direct information about flow patterns, channel conveyance, and discharge. A range of image- and signal-based approaches exist, including Particle Image Velocimetry (PIV), Particle Tracking Velocimetry (PTV), Spatial–Temporal Image Velocimetry (STIV), Optical Flow (OF), and Doppler radar. Each technique differs in its data requirements, sensitivity to surface texture, and suitability for specific flow conditions. The following subsections summarize these methods and their relative advantages and limitations for UAV-based applications.

2.4.1 Particle Image Velocimetry (PIV)

Particle Image Velocimetry (PIV), along with its field-scale adaptation known as Large-Scale PIV (LSPIV), is one of the most widely used optical methods for measuring river surface velocity. The technique computes two-dimensional velocity fields by cross-correlating small interrogation areas between sequential images, allowing motion patterns on the water surface to be quantified. LSPIV is particularly effective when natural tracers such as foam, bubbles, or floating debris are present. The use of UAVs enhances the method substantially: drones can hover to obtain nadir-oriented imagery, access remote or hazardous locations, and capture large spatial extents with high resolution. UAV-based LSPIV has been shown to provide consistent velocity distributions across a variety of stream sizes, and even low-cost unmanned aircraft can deliver reliable measurements when surface texture is adequate. Overall, PIV and LSPIV offer a flexible, non-contact approach for rapid surface velocity estimation using UAV video data.

PIV estimates surface velocity by tracking the collective motion of tracers, such as foam, debris, or natural texture, across sequential images. The image domain is divided into small interrogation windows, and cross-correlation is applied to determine the most probable displacement of tracer patterns within each window. As illustrated in the left panel of Figure 2.11, PIV computes velocity vectors on a fixed surface grid by comparing tracer motion within each interrogation area. This grid-based approach is well suited for flows with abundant surface texture and provides dense, spatially continuous velocity information across the channel.

2.4.2 Particle Tracking Velocimetry (PTV)

Particle Tracking Velocimetry (PTV) estimates surface velocity by following the movement of individual tracers across consecutive video frames. Unlike PIV, which evaluates the motion of tracer patterns within interrogation windows, PTV identifies and tracks discrete particles, allowing it to perform effectively even when seeding is sparse or uneven. This characteristic is particularly advantageous for UAV-based surveys, where natural tracers may be limited or distributed non-uniformly across the water surface. As illustrated in the right panel of Figure 2.11, PTV resolves trajectories of individual particles, enabling detailed characterization of flow paths and localized velocity variations. PTV performs especially well in small streams where only a few visible tracers are present.

The accuracy of PTV depends on adequate particle visibility, sufficient frame rate, and appropriate particle displacement between frames. Extremely dense or extremely sparse seeding can degrade tracking performance. When conditions are suitable, UAV-derived PTV offers high-fidelity surface velocity measurements and serves as a valuable complement to PIV-based velocity mapping.

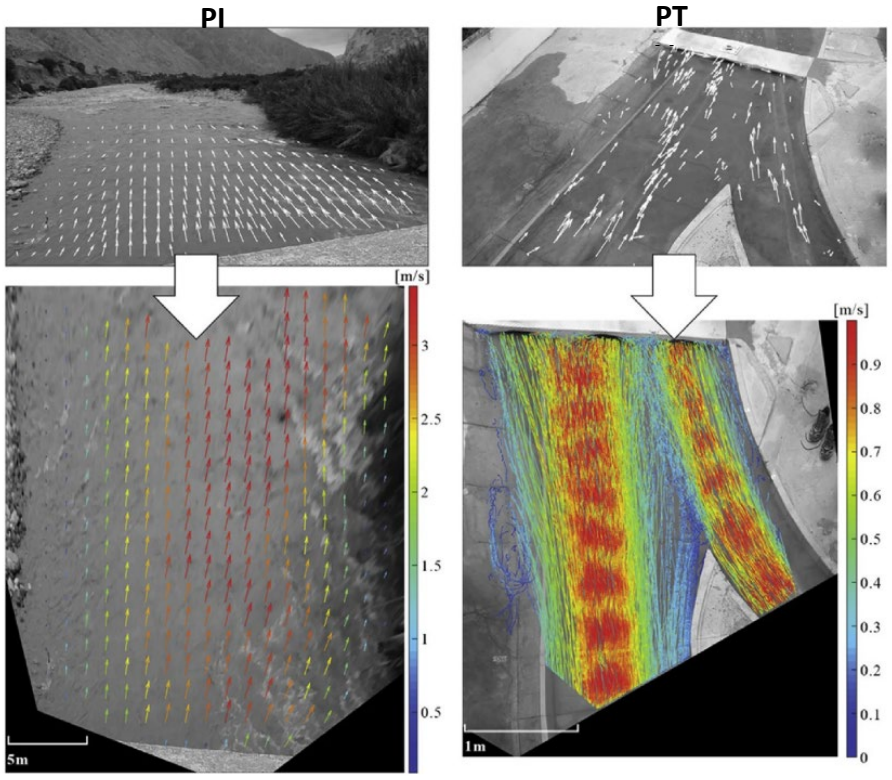

Figure 2.11 Comparison of UAV-based surface velocity estimation using PIV and PTV. (Left) PIV workflow showing tracer patterns and the resulting Eulerian velocity field derived through cross-correlation. (Right) PTV workflow illustrating individual tracer-tracking and the corresponding Lagrangian velocity map (adapted from Patalano et al., 2017, with permission from Elsevier).

2.4.3 Spatial Temporal Image Velocimetry (STIV)

Spatial–Temporal Image Velocimetry (STIV) is an image-based technique for estimating the one-dimensional surface velocity component along a predefined search line that is aligned with the primary flow direction. The method constructs a space–time diagram from sequential video frames, where the streak patterns produced by moving surface features form characteristic linear traces. As illustrated in Figure 2.12, the slope of these streaks corresponds directly to the advection speed of surface tracers, allowing velocity to be extracted without requiring full two-dimensional feature tracking.

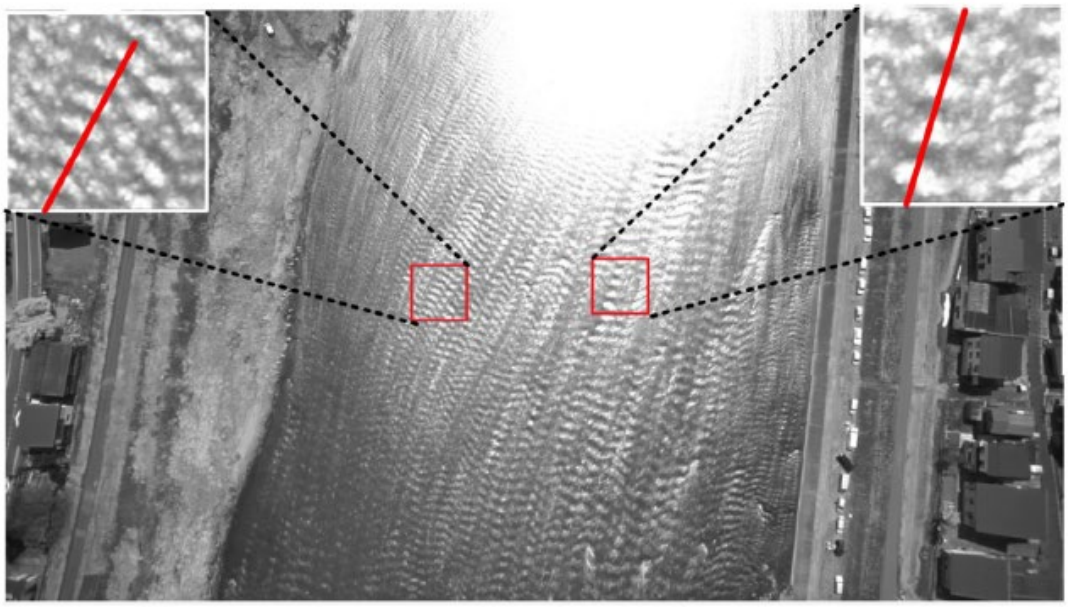

Figure 2.12 Example of Space–Time Image Velocimetry (STIV) analysis. A stabilized composite image generated from 300 frames collected over 10 seconds is shown. The red boxes denote local interrogation regions, and the inset panels display instantaneous texture patterns with the corresponding search line used for STIV processing (adapted from Fujita et al., 2015, licensed under CC BY 4.0).

Because STIV only depends on detectable texture along a narrow transect, it is well suited for UAV observations in rivers where surface contrast is limited or where PIV/PTV struggle to obtain dense velocity fields. The method is computationally efficient and reasonably robust under moderate lighting and texture conditions. However, its accuracy depends on reliable image stabilization and the presence of consistent tracers along the search line. Despite these limitations, STIV offers a practical and efficient approach for extracting velocity information from UAV video data, particularly in channels with relatively uniform flow direction.

2.4.4 Optical Flow (OF)

Optical flow (OF) methods estimate pixel-wise motion between consecutive image frames to derive dense surface velocity fields, making them effective even when visible tracers are sparse or absent. Unlike PIV and PTV, which rely on identifiable particles or texture patches, OF detects motion by analyzing changes in image intensity patterns. One of the earliest UAV-based OF implementations, the Kanade–Lucas–Tomasi Image Velocimetry (KLT-IV) algorithm, tracks local texture gradients and feature displacements across video sequences to compute velocity vectors (Figure 2.13).

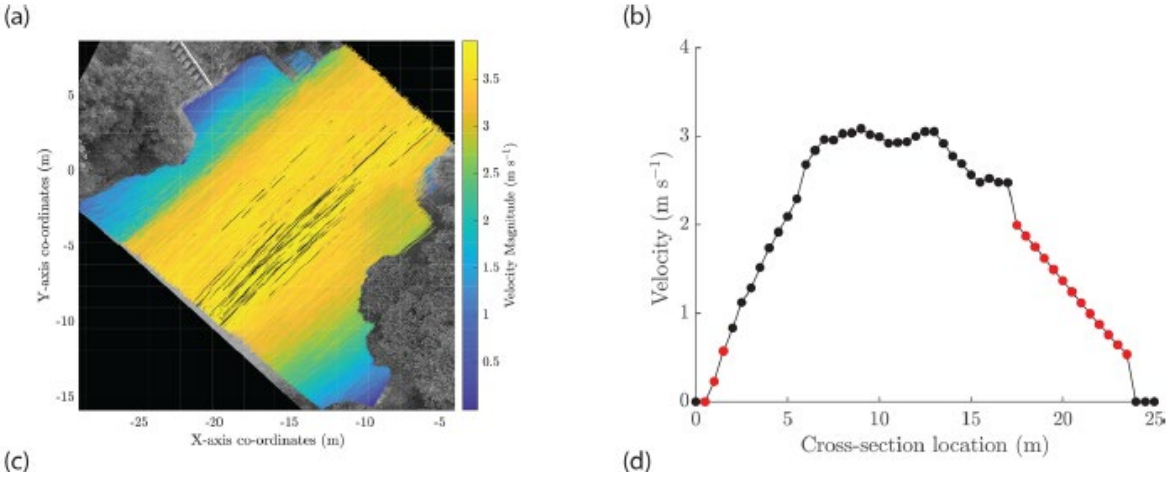

Figure 2.13 Example of optical flow-based surface velocity estimation. (a) Velocity magnitude map overlaid on the UAV image, with color shading indicating computed surface velocity. (b) Extracted cross-sectional velocity profile showing spatial variations in surface velocity along the channel (adapted from Perks, 2020, licensed under CC BY 4.0).

This approach provides high spatial resolution and is particularly well suited for identifying complex flow structures in environments where distinct tracers are limited. When combined with adaptive filtering or stabilization techniques, optical flow offers an efficient, tracer-independent method for UAV-based surface velocity mapping, though it generally requires longer computation times compared with PIV or PTV.

2.4.5 Doppler Radar (DR)

Doppler radar measures surface velocity by transmitting microwave signals toward the water surface and analyzing the frequency shift of the returned backscatter. When deployed on a UAV platform, the radar is typically angled upstream at a fixed incidence angle to maintain a stable illuminated footprint and consistent measurement geometry. This configuration allows the instrument to capture velocity information independent of visible tracers or illumination conditions. Figure 2.14 illustrates a UAV-mounted Doppler radar system, showing the upstream-oriented radar beam and the elliptical surface footprint used for velocity estimation.

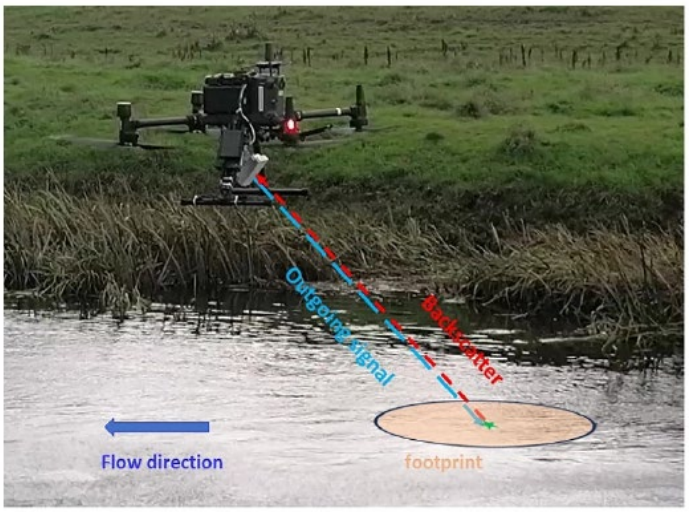

Figure 2.14 Overview of a UAS-borne Doppler radar measurement configuration. The radar is oriented upstream at a fixed incidence angle of 45°, allowing it to receive backscattered energy from the illuminated elliptical footprint on the water surface (adapted from Zhou et al., 2024, license under CC BY 4.0).

Doppler radar offers strong advantages for UAV-based surface velocity measurement, including the ability to operate effectively in turbid water, low-light environments, and conditions with limited surface texture, situations where optical methods often perform poorly. Additionally, radar measurements are less sensitive to tracer availability and can capture velocity even during high-flow or debris-laden conditions. However, accuracy can be affected by UAV motion, beam misalignment, and water-surface roughness, all of which influence backscatter strength and the reliability of the Doppler shift. As a result, while Doppler radar provides a robust complement to optical techniques, its performance depends heavily on stable sensor orientation and surface scattering conditions.

2.4.6 Comparative Assessment

A comparative assessment of UAV-based surface-velocity estimation methods, PIV, PTV, STIV, optical flow, and Doppler radar, was conducted using 1,020 velocity measurements compiled from 26 published datasets. Figure 2.15 compares UAV-derived velocities with reference data and shows that all methods generally follow the 1:1 agreement line, with most points falling within ±20% deviation. The inset panel highlights the low-velocity range (0–2 ft s^{-1}), where performance differences among methods are more pronounced due to reduced surface texture and increased sensitivity to noise.

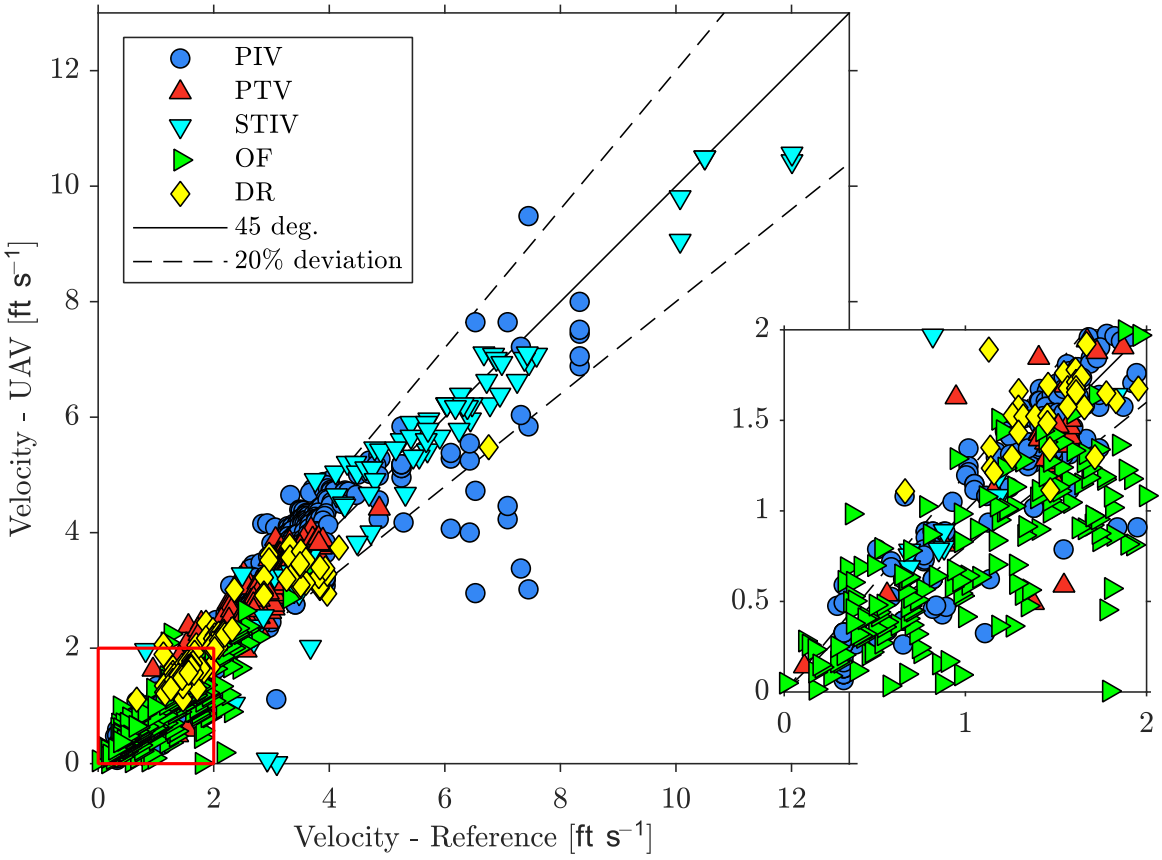

Figure 2.15 Comparison of UAV-derived and reference surface velocities from published datasets employing PIV, PTV, STIV, optical flow (OF), and Doppler radar (DR). The solid line denotes 1:1 agreement, and dashed lines indicate ±20% deviation. The inset shows a magnified view of the low-velocity region (0–2 ft s^{-1}).

Error statistics summarized in Table 2–4 indicate that PIV and PTV deliver high accuracy, with mean absolute percentage errors (MAPE) of 14.4% and 10.7%, respectively. These methods benefit from strong tracking capability when distinct surface features are present. STIV also shows high accuracy, with a MAPE of 12.3%, reflecting its reliance on consistent patterns along user-defined lines or broader image gradients. DR exhibits higher errors in this dataset, largely influenced by platform stability, beam geometry, and sensitivity to incidence angle. OF shows the largest error, mainly due to wind-induced surface disturbances, variable lighting, and surface reflections that degrade motion estimation accuracy.

Table 2-4 Error statistics for UAV-derived surface velocity estimates using PIV, PTV, STIV, OF, and DR.

	No. of data points	**Mean Absolute Percentage Error (MAPE) [%]**	**Mean Percentage Error (MPE) [%]**
PIV	508	14.4	+1.2
PTV	169	10.7	+4.0
STIV	86	12.3	-2.1
OF	183	37.7	-19.5
DR	74	13.4	+5.3
Total	1020	17.7	-2.0

Across all methods, the combined MAPE (17.7%) and near-zero average bias (MPE = -2.0%) demonstrate that UAV-based surface-velocity techniques provide reliable and unbiased measurements over a wide range of flow conditions. These findings confirm that UAV video-based velocimetry, when applied with appropriate method selection and quality control, can serve as an effective alternative to conventional field measurements.

2.5. Discharge

UAV-based discharge estimation integrates remotely sensed hydraulic parameters, such as channel geometry, water-surface elevation, depth, and surface velocity, to compute flow using standard hydrologic formulations. Current approaches fall broadly into three categories: geometric methods (GM), which rely on UAV-derived topography and hydraulic equations; surface-velocity methods (SV), which combine UAV-measured surface velocities with cross-sectional geometry; and hybrid GM–SV methods, which incorporate elements of both. Each approach offers different advantages depending on site conditions, available data, and the complexity of channel hydraulics. The following subsections summarize these methods and evaluate their applicability for UAV-based discharge estimation in natural streams.

2.5.1 Geometric Methods (GM)

River discharge can be estimated using UAV-derived topography combined with empirical hydraulic equations such as Manning's or Manning–Strickler's formulations for a given UAV measured WSE. In this approach, digital elevation models (DEM) and orthophotos obtained from UAV photogrammetry are used to extract channel cross sections, slopes, and roughness parameters. Compared to traditional point-based survey methods, UAV surveys provide spatially continuous channel geometry over extended reaches and can be conducted rapidly and safely, particularly in areas that are difficult to access.

Although geometric methods can provide reasonable discharge estimates under stable uniform flow conditions, they require additional field effort and may be constrained by safety, accessibility, and flow depth. Furthermore, these methods do not directly measure flow velocity and therefore may not capture spatial variations or complex flow structures that occur near bridge openings, abutments, or floodplains.

The empirical Manning's equation can be derived as (Equation 2.2):

$$Q = \frac{1}{n} A R^{\frac{2}{3}} S^{\frac{1}{2}}$$

where *n* is the Manning's roughness coefficient; *A* is the cross-sectional area; *R* is the hydraulic radius; and *S* is the channel slope.

Equation 2.2. Empirical Manning's equation

The Manning equation relates discharge to channel geometry, roughness, and slope, and is commonly used in hydraulic modeling for open-channel flow. The terms in this formulation are illustrated in Figure 2.16, which defines key hydraulic parameters including flow depth, wetted perimeter, top width, and hydraulic radius. The hydraulic radius represents the ratio of cross-sectional area to wetted perimeter and is used to describe the efficiency of flow conveyance within the channel.

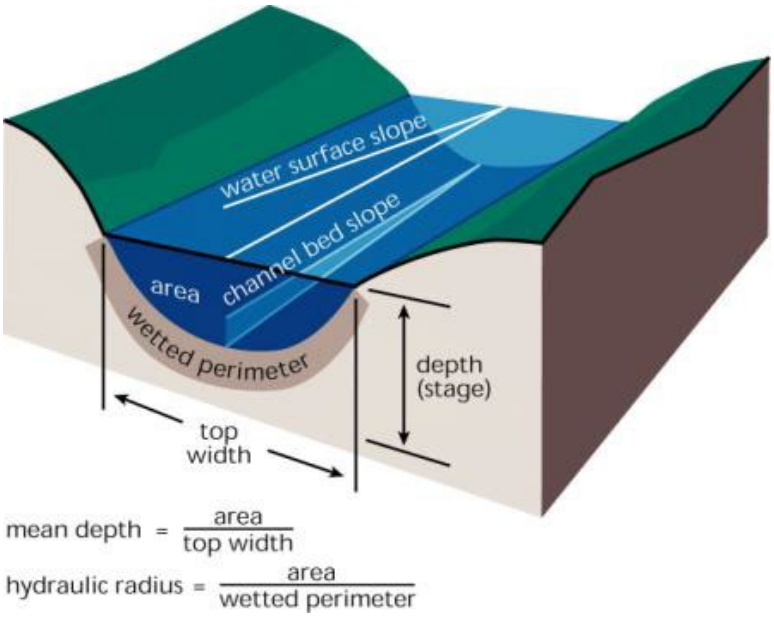

Figure 2.16 Definition of terms used in uniform flow equations (adapted from *Stream Corridor Restoration: Principles, Processes, and Practices,* Federal Interagency Stream Restoration Working Group, 1998).

Geometric methods offer a simple and tracer-independent approach to estimating discharge, using only UAV-derived channel geometry and slope, and they perform well under steady, uniform flow conditions. However, their accuracy depends on assumptions about roughness and hydraulic resistance, and they may not capture spatial velocity variations or complex flow structures, particularly near bridges, bends, or irregular channels. For practical application, locations with anticipated near uniform flow should be identified and targeted for UAV flow measurements when GM is to be used. In other words, GM measurements should be completed at a location near the proposed bridge that may be up or downstream as needed to find uniform flow, so long as the flow rate can be reasonably assumed to be the same as at the bridge location.

2.5.2 Surface Velocity Methods (SV)

Surface-velocity–based methods provide a non-contact alternative for characterizing streamflow using UAV-mounted imaging systems. Short video sequences of the water surface are captured from a hovering UAV, and optical velocimetry algorithms, such as Particle Image Velocimetry (PIV) and Particle Tracking Velocimetry (PTV), are applied to track the motion of natural or introduced surface tracers (e.g., biodegradable mulch) between successive frames. These techniques yield spatially distributed two-dimensional surface velocity fields that characterize the flow structure across the channel.

To compute discharge, the depth-averaged velocity can be defined as (Equation 2.3):

$$U = \alpha U_s$$

where the measured surface velocity U_s is converted to depth-averaged velocity U using a surface-to-depth velocity coefficient α, typically between 0.8 and 0.95 depending on flow roughness and turbulence.

Equation 2.3. Relationship between surface velocity and depth-averaged velocity

This depth-averaged velocity is multiplied by the cross-sectional area A to obtain total discharge ($Q = U \times A$). As illustrated in Figure 2.17, the velocity–area method divides the channel cross-section into multiple vertical subsections. Each subsection is defined by a local flow depth and corresponding mean velocity, and the total discharge is computed by summing the products of sub-sectional areas and their mean velocities.

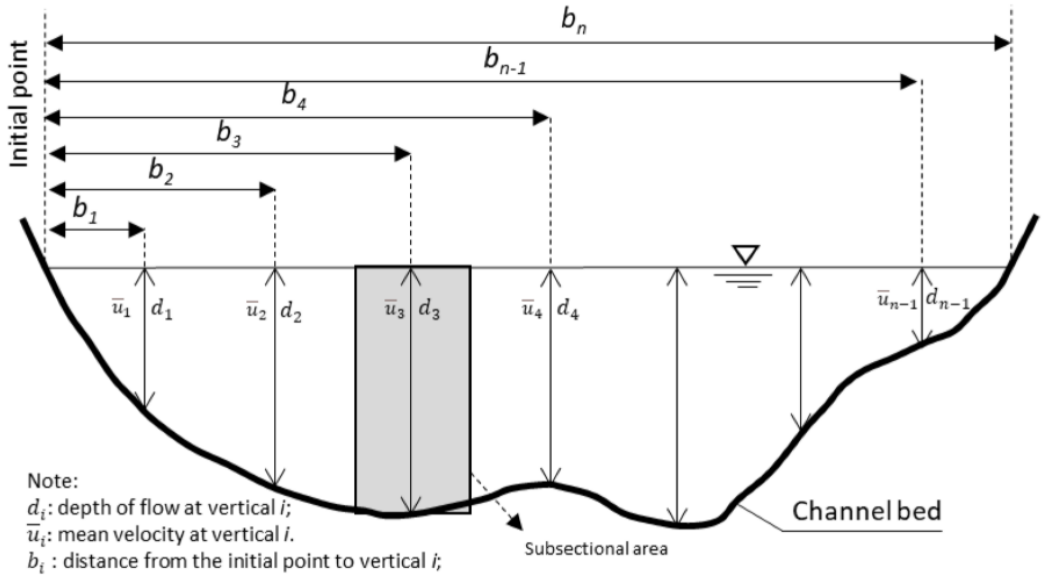

Figure 2.17 Schematic illustration of the velocity–area method (adapted from Chen et al., 2022, licensed under CC BY 4.0). The discharge is obtained by dividing the channel cross section into multiple verticals, each defined by flow depth ($d_1, d_2, \ldots, d_n$) and mean velocity ($\bar{u}_1, \bar{u}_2, \ldots, \bar{u}_n$). The total discharge is computed as the sum of sub-sectional areas multiplied by the corresponding mean velocities across the channel.

Surface velocity methods (SV) provide a fast, non-contact way to estimate discharge by extracting velocity fields from UAV video, improving safety and enabling measurements during high flows. They capture real spatial variability in surface velocity but rely on adequate surface texture or tracers, stable imagery, and suitable viewing geometry. Performance decreases in smooth or low-contrast flows, and additional uncertainty is introduced when converting surface velocity to depth-averaged velocity. Despite these limitations, surface velocity methods remain an effective option when surface features are sufficient for tracking.

2.5.3 Comparative Assessment

A comparative evaluation of the three discharge estimation approaches, geometric (GM), surface-velocity (SV), and the combined both methods (GM–SV), was conducted using the available data in 24 published studies (shown in Figure 2.1c). Figure 2.18 presents the comparison between UAV derived discharge and reference values, demonstrating consistent overall agreement across the full range of flows. All three methods follow the 1:1 trend line, with most estimates falling within ±20% deviation. The inset panel presents performance at low to moderate discharges, where factors such as image quality, flow turbulence, and tracer availability more strongly influence the accuracy of UAV-based estimates.

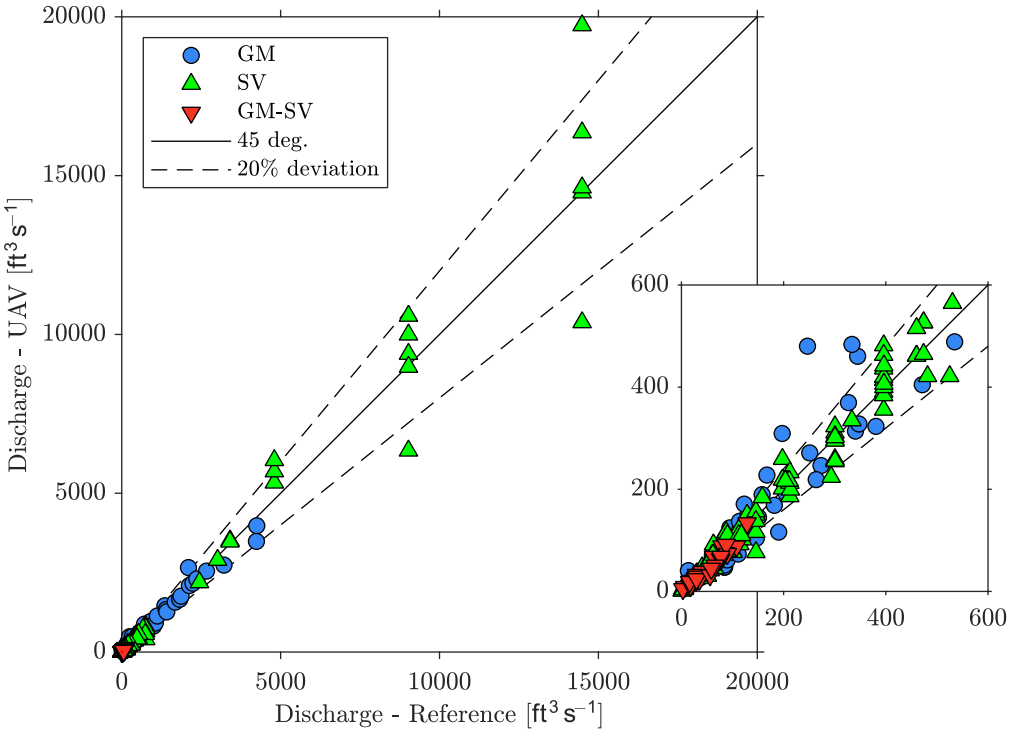

Figure 2.18 Comparison of UAV-derived discharge estimates with reference discharge values. Geometric method (GM), surface velocity method (SV), and combined (GM–SV) discharge estimates are plotted against reference values. The solid line represents the 1:1 agreement line, while dashed lines indicate ±20% deviation. The inset shows results for low to moderate flows.

Table 2-5 Error statistics for UAV-derived discharge estimates using geometric (GM), surface velocity (SV), and combined (GM–SV) methods.

	Mean Absolute Percentage Error (MAPE) [%]	**Mean Percentage Error (MPE) [%]**
Geometric method (GM)	17.9	-2.3
Surface velocity method (SV)	12.4	+1.4
Combined (GM-SV)	19.1	-6.6
Total	14.3	-1.0

Error statistics provided in Table 2-5 show that SV yields the lowest average error, with a MAPE of 12.4%. SV exhibits a slight positive bias (MPE = +1.4%), indicating minor overprediction on average. GM shows a higher MAPE of 17.9% and tends to slightly underpredict discharge (MPE = –2.3%), likely reflecting uncertainties in roughness selection and cross-section representation. The combined GM–SV method results in the highest MAPE (19.1%) and a more pronounced negative bias (MPE = –6.6%), suggesting that merging both methods without site-specific weighting may introduce additional uncertainty rather than improving accuracy.

Across all approaches, the total MAPE of 14.3% and near-zero MPE of –1.0% indicate that UAV-based discharge estimation provides reliable and nearly unbiased results, supporting its feasibility as a practical alternative for hydrologic monitoring, particularly where conventional measurements are difficult or unsafe.

3. Site Section

Selection of appropriate field sites is a critical step for evaluating UAV-based hydraulic measurement methods under a range of hydrologic and geomorphic conditions. The site-selection process for this project considered both hydraulic relevance and operational feasibility to ensure that UAVs could be safely deployed while capturing representative streamflow conditions in Missouri. The evaluation incorporated existing hydrologic information, UAV flight constraints, safety considerations, and logistical factors such as accessibility and travel efficiency. Stream gage availability was prioritized to enable comparison between UAV-derived measurements and reference discharge or stage data. Additional considerations included drainage area, expected lag time following rainfall, bridge conditions, and the presence of overhead utilities or dense tree cover that could limit UAV operation. This screening process allowed the project team to identify sites suitable for both method development and performance evaluation.

3.1 Initial UAV Test Site Selection

An initial pool of 21 candidate stream sites across central and eastern Missouri was evaluated based on key screening criteria. These sites were chosen to represent a diverse set of hydraulic conditions while ensuring practical accessibility for field operations. The primary screening factors included:

- stream gage availability, particularly USGS flow and stage data that support independent verification of UAV-derived measurements;
- UAV accessibility, including considerations of tree cover, bridge structure, and clear airspace for safe flight maneuvering;
- drainage area and hydrologic response characteristics, ensuring a range of flow regimes suitable for testing;
- safety factors, such as road access, presence of overhead utilities, and safe conditions for field personnel;
- proximity to Columbia, allowing efficient travel for repeated surveys and data-collection activities.

Figure 3.1 shows the geographic distribution of the evaluated sites across Missouri, illustrating their spatial spread and highlighting the diversity of watershed characteristics included in the selection process. The sites that best satisfied these criteria were advanced for subsequent UAV-based LiDAR, photogrammetry, and surface-velocity testing.

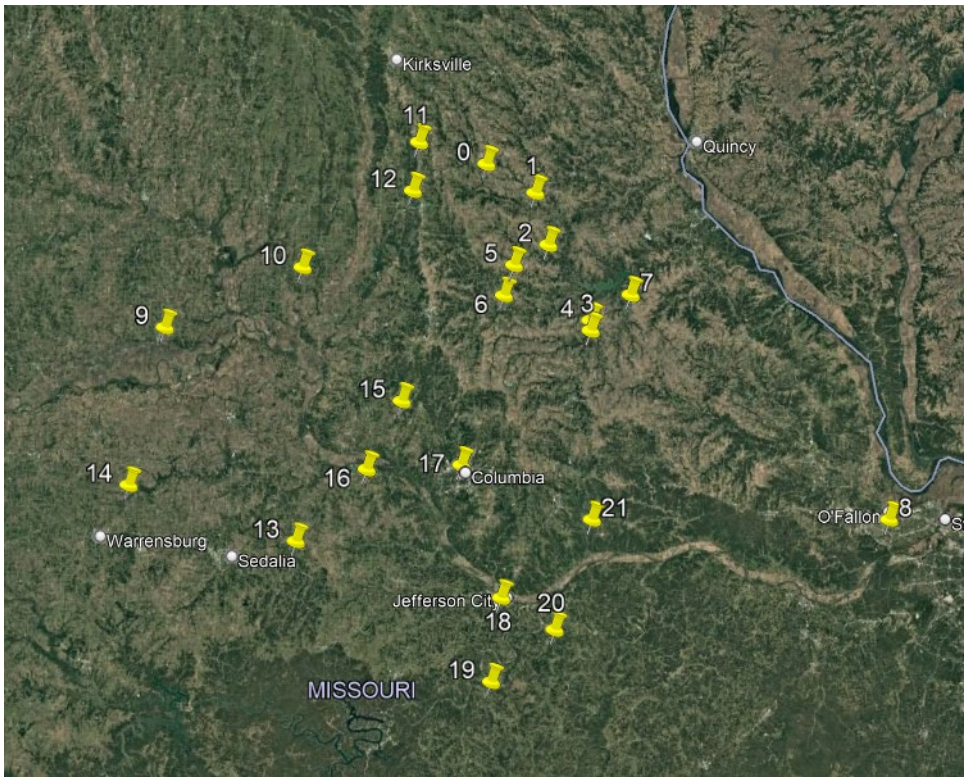

Figure 3.1 Comparison Initial UAV test site selection map. Geographic distribution of the 21 candidate stream sites evaluated during the initial screening process. Each pin represents a potential UAV test site reviewed based on stream gage availability, UAV accessibility, drainage characteristics, safety considerations, and proximity to Columbia, Missouri.

Figure 3.2 and Table 3.1 summarize the key characteristics of the Petite Saline Creek site selected for UAV testing. The satellite image highlights the bridge crossing, surrounding terrain, and overall visibility of the channel, while the inset map shows the site's regional location and proximity to the University of Missouri. The accompanying table outlines essential screening criteria, including drainage area, gage availability, accessibility, safety considerations, and travel time, which collectively support the suitability of this site for UAV-based hydraulic measurements.

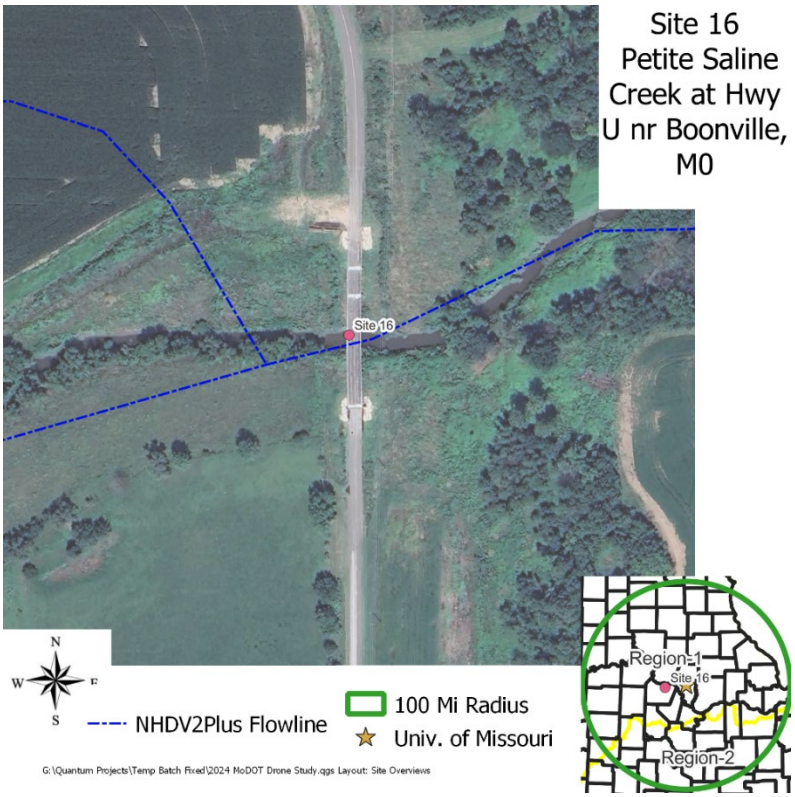

Figure 3.2 Petite Saline Creek at Hwy U near Boonville, Missouri. Satellite imagery of the selected UAV test site, showing the bridge crossing and surrounding terrain. The inset map indicates the site's regional location within Missouri and its proximity to the University of Missouri.

Table 3-1 Site screening summary for Petite Saline Creek at Hwy U near Boonville, Missouri.

Key site characteristics used for UAV test-site evaluation, including drainage area, accessibility constraints, safety considerations, and availability of stream gage data.

Field	Value
Site Name	Petite Saline Creek at Hwy U near Boonville, MO
Site # / Station ID	16 / US06909950
Lat / Lon	38.9172 / -92.7042
Drainage Area / Lag Time	136 mi^2 / 16.1 hr.
Gage Data Available?	Yes
Hydrologic Region	1
Tree Interference	No (clear, some trees west side of stream)
Utilities Nearby	Overhead power (downstream side)
Safety Notes	Pull-off area available, no shoulder on bridge
Travel Time from Columbia	32 min.
Use Priority	2 (medium)
Flood Stages (ft.)	Action: 11, Minor: 16, Mod: 19.5, Major: 26

A site-selection framework was developed to evaluate potential UAV test locations based on logistical, hydrological, and safety-related considerations. An initial screening spreadsheet was created to compile key site attributes, including location data, drainage characteristics, accessibility, and the presence of hydraulic monitoring infrastructure. This screening process ensured that selected sites were suitable for consistent UAV deployment while providing representative hydraulic conditions for method evaluation.

Key screening criteria included:

- Proximity to Columbia (travel time): to minimize travel burden for repeated surveys and allow timely mobilization during storm events.
- Availability of active USGS gages: enabling comparison of UAV-derived hydraulic parameters with independent stage and flow measurements.
- Tree interference and UAV visibility: assessing canopy density, bridge geometry, and obstacles that could limit flight safety or obstruct surface imaging.
- Drainage area and estimated lag time: to capture a range of hydrologic responses and to support scheduling of field deployments during rising or falling limbs of a hydrograph.
- Utility obstructions and roadside safety: including overhead power lines, narrow bridge shoulders, and constraints for safe takeoff and landing.
- Hydrologic region diversity: distributing sites across different physiographic and hydrologic regions within Missouri to evaluate method robustness under varying channel forms and flow characteristics.

The preliminary screening identified 21 candidate stream sites across central and eastern Missouri. These sites were then ranked based on UAV accessibility, safety considerations, and hydrologic relevance. A subset of representative locations was advanced for detailed UAV-based LiDAR, photogrammetry, and surface-velocity testing.

3.2 Field Experimental Location

Based on the initial screening of 21 candidate sites, a final set of six field locations was selected for UAV-based hydraulic data collection. These sites were chosen to represent a broad range of channel sizes, geomorphic settings, and hydrologic conditions while ensuring safe and consistent UAV operation. The final selection process emphasized feasibility and representativeness, prioritizing sites that provided clear UAV flight paths, reliable access points, adequate safety conditions, and the presence of nearby stream gages for comparison with UAV-derived measurements.

These locations span multiple hydrologic regions across central and eastern Missouri, offering diversity in watershed size, channel morphology, vegetation cover, and flow characteristics. Their distribution also allowed the project team to conduct repeated field surveys with manageable travel times from Columbia. Figure 3.3 shows the geographic arrangement of the selected sites within Missouri, and Table 3-2 provides a summary of site names, USGS station identifiers, coordinates, and county locations for each monitored stream reach.

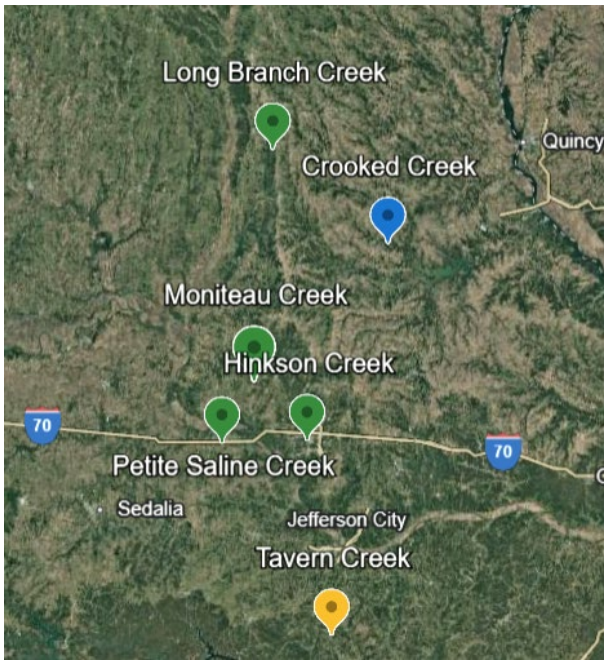

Figure 3.3 Locations of the experimental locations.

Table 3-2 Summary of field survey locations. This table lists the primary UAV survey sites, including site names, corresponding USGS station identifiers, geographic coordinates, and county locations for each monitored stream reach.

No.	Site Name	Station ID	Latitude	Longitude	County
1	Petite Saline Creek near Boonville, MO	US06909950	38.9172222	–92.7041667	Cooper
2	Hinkson Creek at Columbia, MO	US06910230	38.9277500	–92.3399444	Boone
3	Moniteau Creek near Fayette, MO	US06909500	39.1208333	–92.5672222	Howard
4	Long Branch Creek near Atlanta, MO	US06906150	39.8973056	–92.4932500	Macon
5	Tavern Creek below St. Elizabeth, MO	US06926290	38.2777778	–92.2333333	Miller

4. Data Processing & Results

This section presents the processing workflow and field results for each of the five monitored stream sites: Petite Saline Creek, Hinkson Creek, Moniteau Creek, Long Branch Creek, and Tavern Creek. For every site, UAV-derived datasets. including photogrammetry, LiDAR, surface-velocity measurements (PIV/PTV), and bathymetry measurements using boat or manual probing, were processed to extract hydraulic parameters such as water-surface elevation, channel geometry, surface velocity, and discharge. The subsections summarize the results of each dataset and describe the key findings relevant to flow characterization and comparison across sites.

4.1 Petite Saline Creek

4.1.1 Photogrammetry

An orthophoto of the Petite Saline Creek site was generated from imagery collected using the DJI M350 equipped with the P1 camera during a ~15-minute flight covering approximately 15.0 acres. As shown in Figure 4.1, the orthophoto captures the flooded area, bridge crossing, and overall channel alignment. Among the five surveyed sites, Petite Saline Creek showed the most extensive flooding during the survey, with overtopped banks and widespread overflowed area clearly visible in the imagery.

Figure 4.1 UAV-derived orthophoto of the Petite Saline Creek survey area. The orthophoto, generated from high-resolution imagery collected by the DJI M350–P1 system.

4.1.2 LiDAR

A UAV-based LiDAR survey was conducted at the Petite Saline Creek site using a DJI M350 equipped with the L2 LiDAR sensor. The flight covered approximately 14.8 acres with a total flight duration of roughly 12 minutes. The resulting point cloud was processed in DJI Terra to generate height and terrain models. As shown in Figure 4.2, the height data clearly differentiate vegetation, bridge structures, and surrounding floodplain features, while the classified terrain model isolates ground points to reveal the underlying channel geometry. Streamflow direction is visible in both results, and the high-density returns provide detailed elevation information suitable for cross-section extraction, slope estimation, and geometry-based hydraulic analysis.

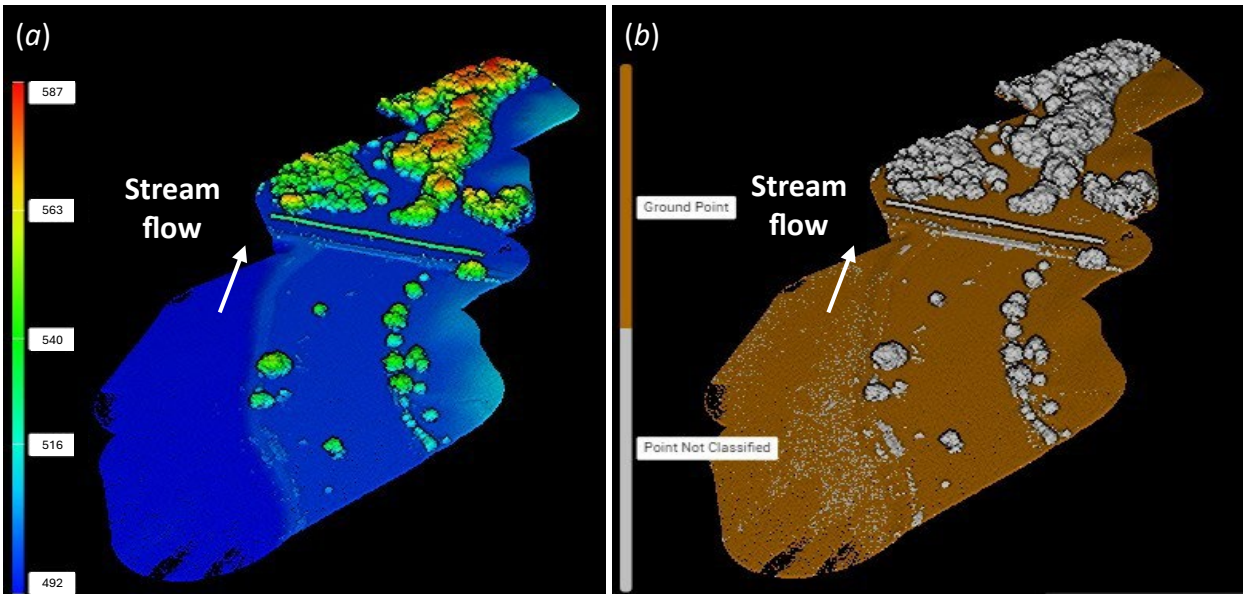

Figure 4.2 UAV LiDAR data for Petite Saline Creek. (*a*) Height map in ft and (*b*) classified terrain point-cloud representations derived from the UAV LiDAR survey.

Consequently, a Digital Elevation Model (DEM) was generated from the UAV LiDAR survey to evaluate longitudinal elevation changes along the Petite Saline Creek channel. The DEM (Figure 4.3a) provides a continuous surface representation from which the centerline of the stream was extracted. Elevation values sampled along this centerline were used to compute the local water-surface slope. A linear regression applied to the longitudinal profile shows a gradual decrease in elevation toward the downstream direction, consistent with the expected flow gradient (Figure 4.3b). The location of the nearby USGS streamgage is noted for reference and alignment. This slope information forms an important input for geometry-based discharge estimation and supports comparison between UAV-derived elevation data and independent gage measurements.

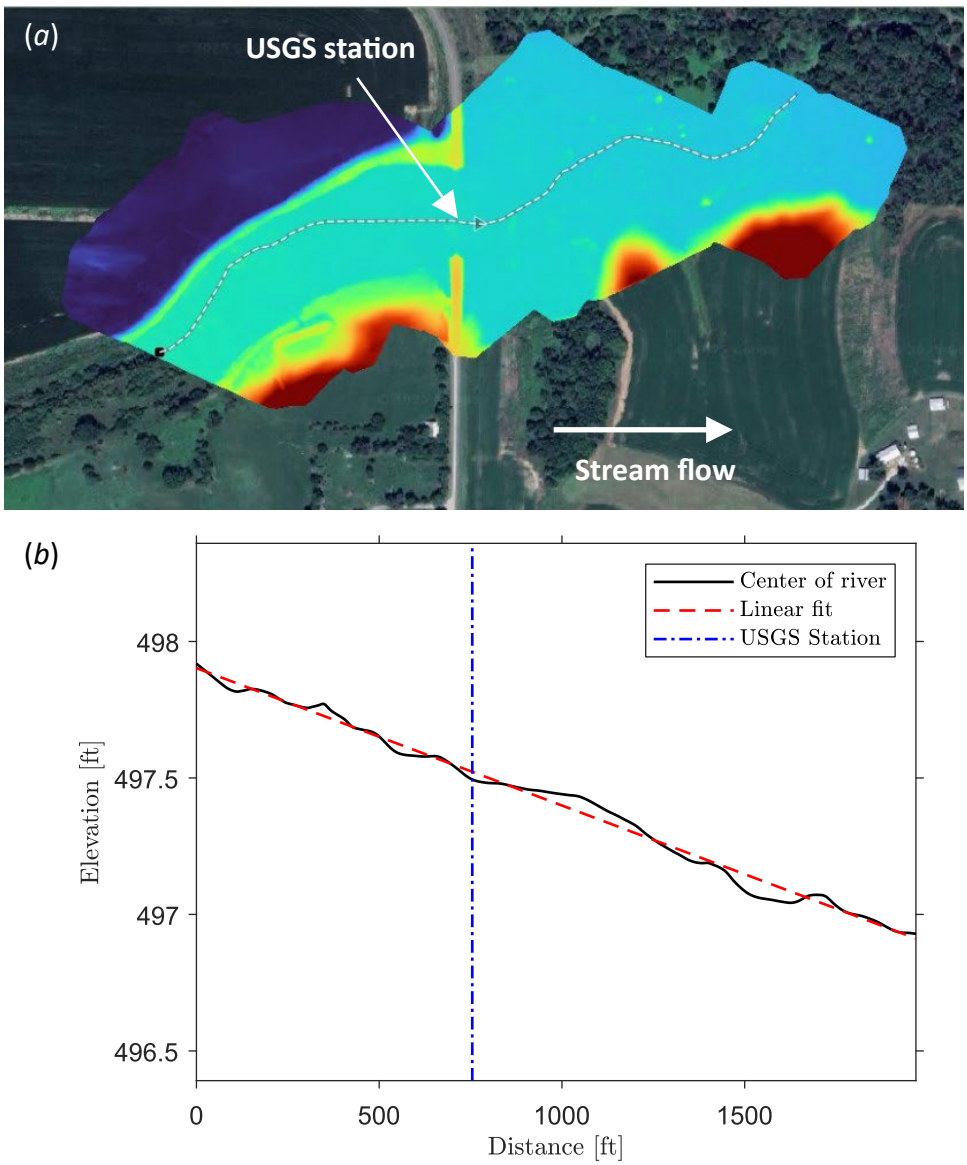

Figure 4.3 (a) Digital Elevation Model (DEM) from the UAV LiDAR survey overlaid on satellite imagery, showing streamflow direction and the location of the USGS station. (b) Longitudinal water surface elevation profile extracted along the channel centerline, with a linear-fit slope and the USGS station location indicated.

4.1.3 PIV

4.1.3.1 Upstream

The upstream computation window for PIV (Figure 4.4) was selected based on the presence of sufficient surface texture, such as foam patches, fine debris, and small brightness variations, that supports reliable cross-correlation in the PIV analysis. This region was also chosen to avoid interference from bridge shadows, vegetation, and bank-edge obstructions, ensuring consistent image quality throughout the video sequence. Within this window, stabilized UAV imagery enabled robust feature tracking and produced a spatially coherent velocity field.

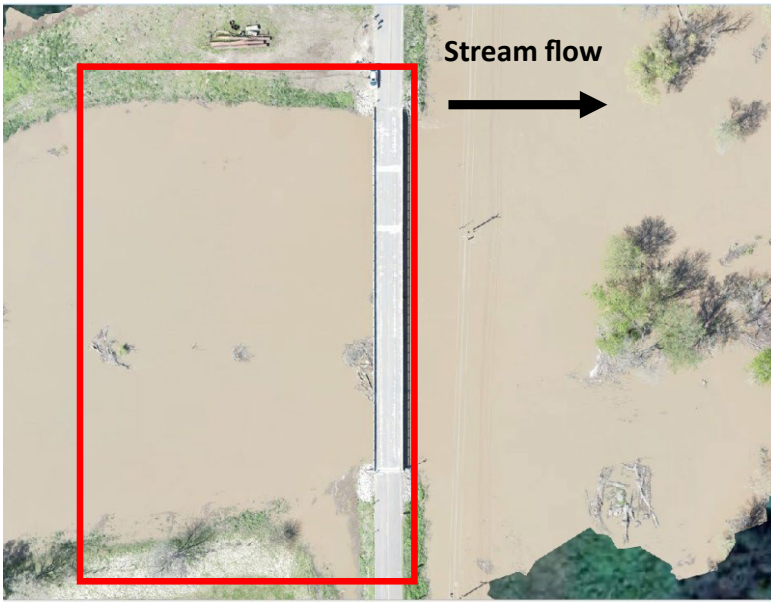

Figure 4.4 UAV orthoimage showing the selected analysis region for upstream surface velocity estimation. The red box indicates the area for PIV analysis, with flow direction shown by the white arrow.

Surface velocity measurements were obtained at both the upstream and downstream reaches of Petite Saline Creek using UAV-based Particle Image Velocimetry (PIV). A DJI M3E UAV was deployed, with each flight lasting approximately five minutes at an operating altitude of about 91 ft. Stabilized video imagery was collected to enable cross-correlation of surface patterns such as foam and floating debris within the designated analysis region.

The resulting upstream mean surface velocity map (Figure 4.5) illustrates the spatial distribution of flow across the channel, including locally accelerated zones near the center of the cross-section and reduced velocities toward the margins. These upstream velocity estimates provide essential input for discharge calculation when combined with channel bathymetry and slope information obtained from the UAV-LiDAR survey.

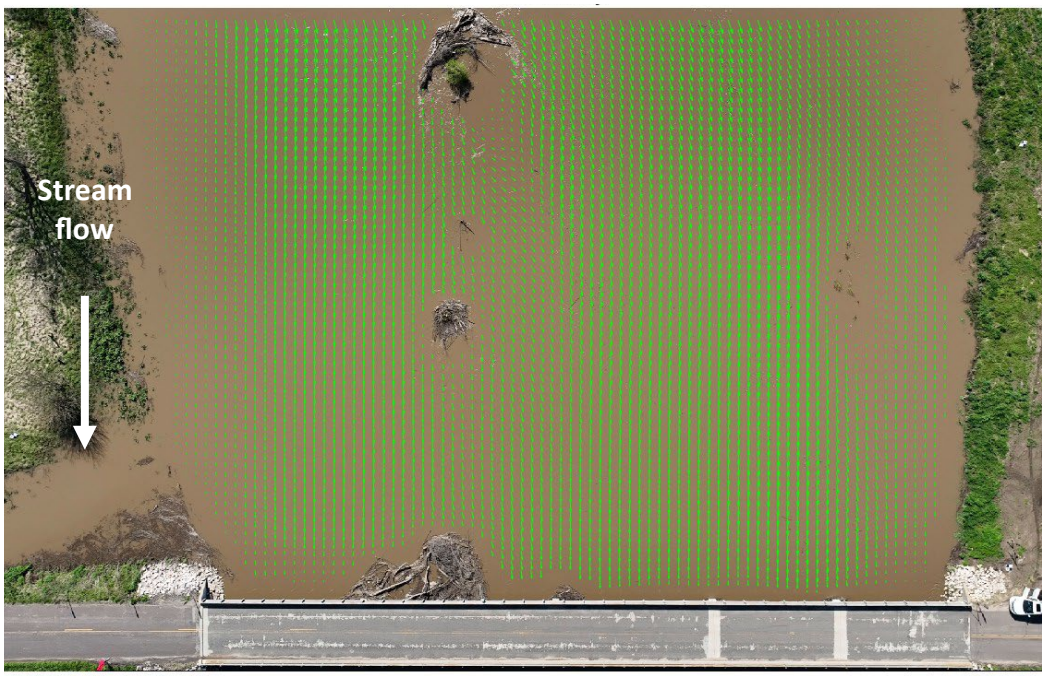

Figure 4.5 Upstream PIV mean velocity field for Petite Saline Creek overlaid over image from M3E.

4.1.3.2 Downstream

The downstream computation window for PIV (Figure 4.6) was selected along a stable portion of the channel where surface texture was sufficient for cross-correlation and interference from bridge shadows and bank vegetation was minimal. This region provided a clear field of view and consistent illumination, allowing the UAV-based PIV algorithm to track surface features effectively throughout the video sequence. The elongated rectangular window was oriented perpendicular to the bridge to capture the primary flow direction and to ensure uniform sampling across the width of the channel.

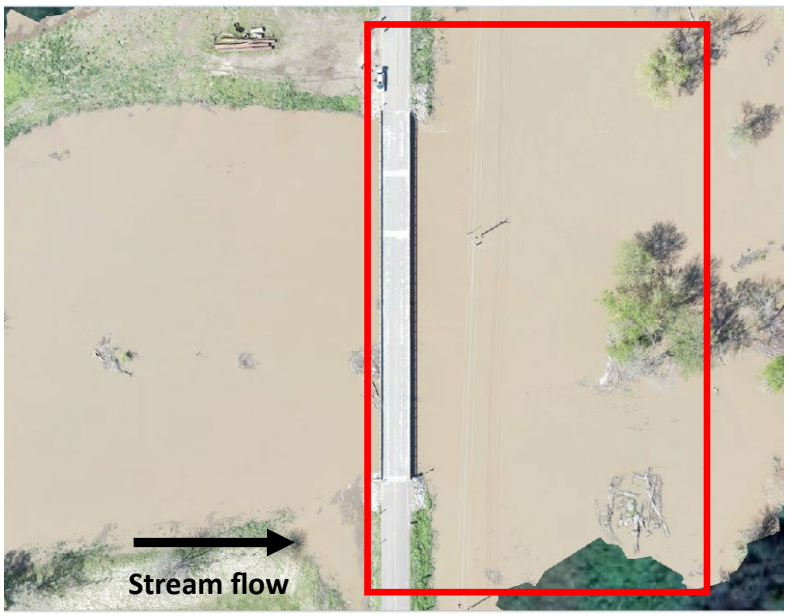

Figure 4.6 UAV orthoimage showing the selected analysis region for downstream surface velocity estimation. The red box indicates the area for PIV analysis.

The resulting downstream mean velocity field (Figure 4.7) shows a well-defined cross-channel velocity gradient, with higher velocities concentrated near the central portion of the flow and reduced velocities along the margins influenced by bridge piers, bank roughness, and localized vegetation. The corresponding downstream velocity profile (Figure 4.8) demonstrates a comparatively smoother distribution than the upstream section, indicating reduced variability and a more uniform flow structure. This difference reflects variations in channel geometry, bed configuration, and local hydraulic controls between the two reaches. The downstream velocity estimates, when combined with upstream measurements, provide an essential constraint for discharge calculations and support integration with LiDAR-derived channel geometry and water-surface slope.

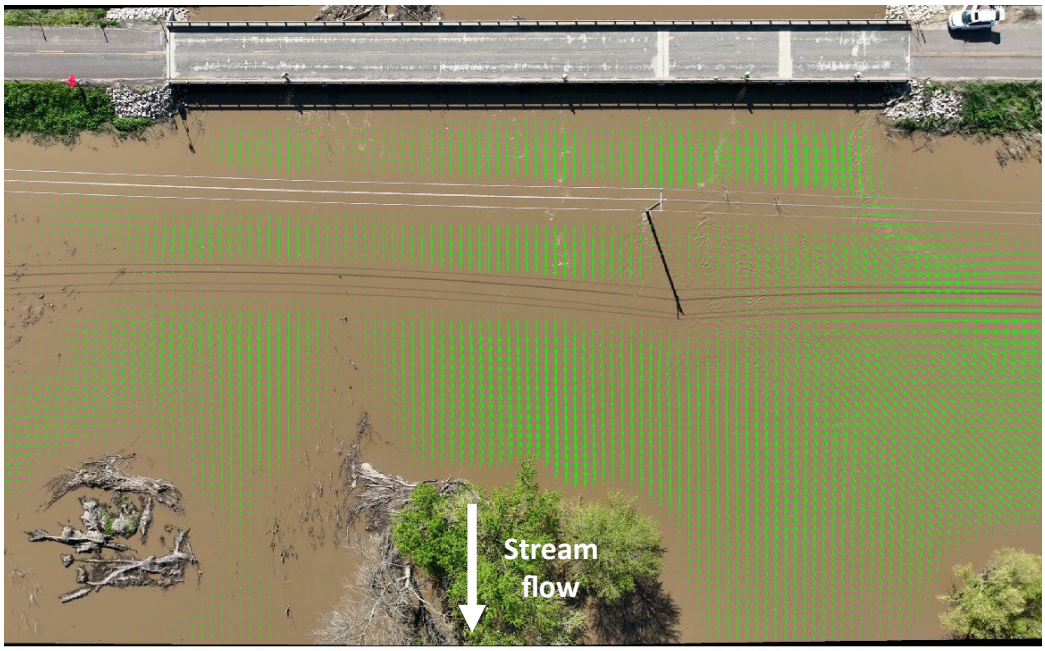

Figure 4.7 Downstream PIV mean velocity field for Petite Saline Creek overlaid over image from UAV. The red dashed box indicates the selected computation window used for velocity extraction.

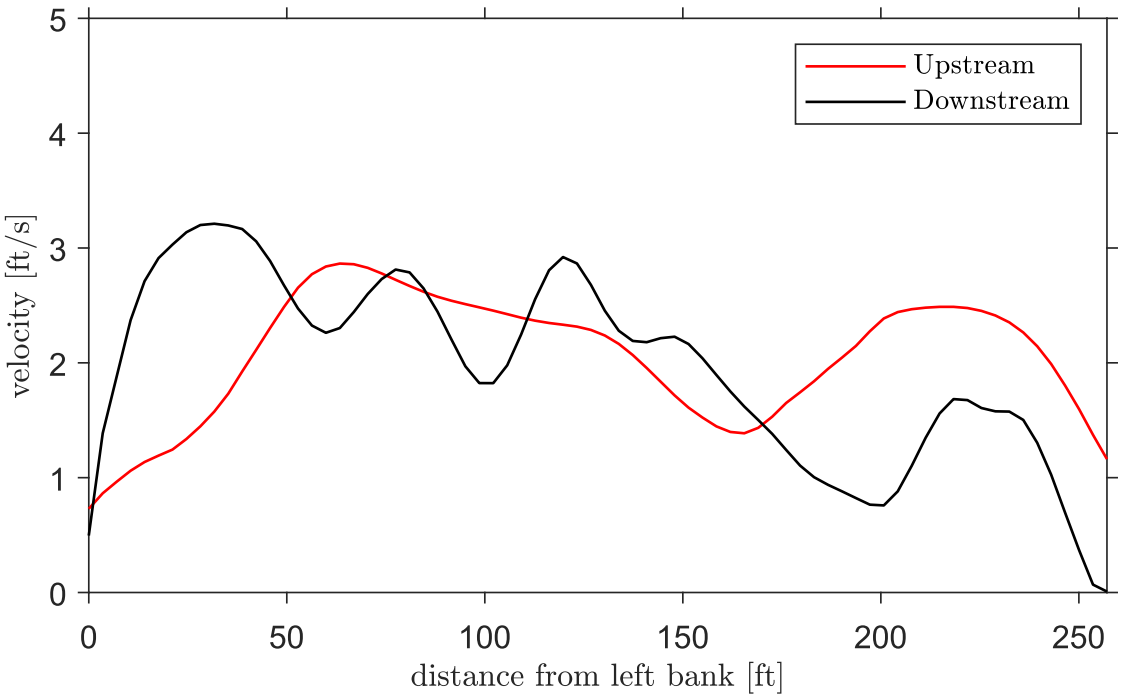

Figure 4.8 Cross-sectional surface velocity profiles derived from UAV-based image velocimetry. Velocity is plotted as a function of distance from the left bank along the flow direction.

4.1.4 Bathymetry

Bathymetry at Petite Saline Creek were evaluated using a combination of UAV-based LiDAR above the water surface and sonar measurements below the water surface using a remotely controlled boat mounted sonar detector. The depth map (Figure 4.9) illustrates spatial variations in sonar measured channel depth along the centerline transect, with warmer colors indicating deeper portions of the channel and cooler colors representing shallow regions. This mapping reveals a distinct deepened zone near the downstream bridge opening associated with constricted flow and structural influence.

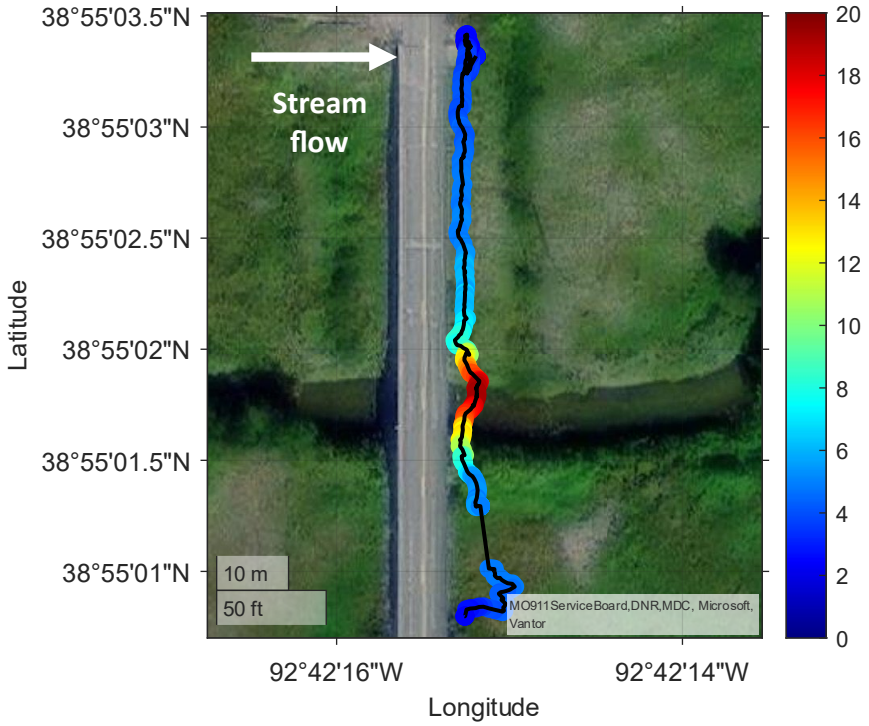

Figure 4.9 Bathymetry-derived channel depth from sonar sensor equipped boat overlaid on orthoimage of Petite Saline Creek. Depth measurements obtained from UAV-based bathymetric processing are shown along the centerline transect, with colors indicating local water depth in feet. Warmer colors represent deeper portions of the channel, while cooler colors correspond to shallow areas.

To further characterize the cross-sectional geometry, sonar-derived bed elevations were compared with LiDAR-derived water surface elevations (Figure 4.10). The sonar transect highlights a pronounced deep channel trough near mid-channel, while the LiDAR water-surface profile provides a fixed elevation reference for estimating absolute water depth. Together, these datasets provide a detailed representation of the channel geometry and depth variability, supporting subsequent discharge computations and hydraulic interpretation for the surveyed reach.

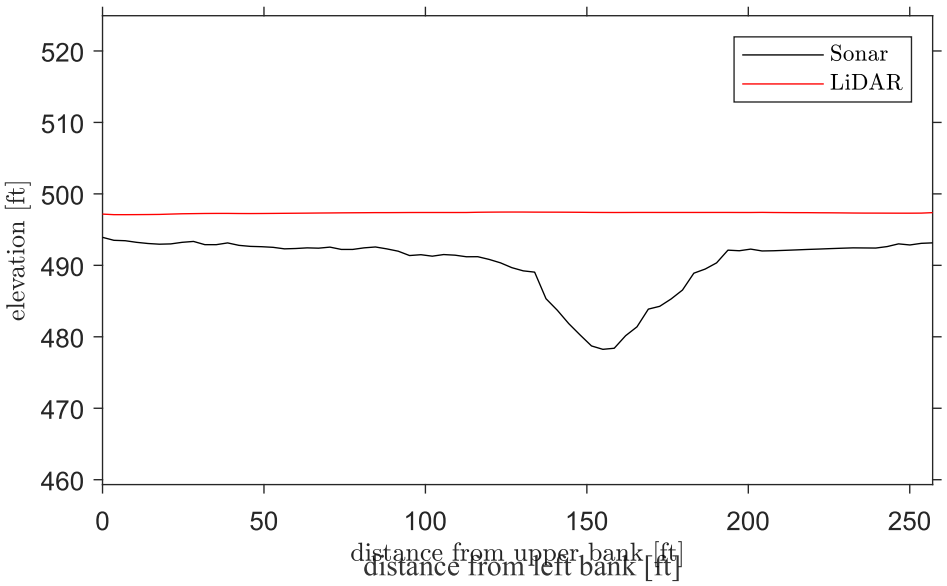

Figure 4.10 Elevation profile derived from LiDAR and sonar measurements. The black line represents the bed elevation measured from the sonar transect, while the red line indicates the corresponding LiDAR-derived water surface elevation as a function of distance from the left bank along the flow direction.

4.1.5 Discharge

Discharge at Petite Saline Creek was estimated using both geometry-based and UAV-derived surface-velocity methods. GM used Manning's equation with LiDAR geometry, estimated roughness, water-surface slope, and bathymetry to compute discharge. SV based discharge estimates were obtained from UAV-based PIV analysis at the upstream and downstream reaches, and converted to mean velocity using an appropriate velocity coefficient. These independent estimates were compared with the corresponding USGS gage discharge for the survey period, as summarized in Table 4-1.

Table 4-1 Comparison of discharge estimates at the upstream and downstream reaches for Petite Saline Creek. The table summarizes discharge derived from gauge measurements (Station), the geometric–method (GM) using Mannings' equation, and UAV-based surface velocity (SV). Percentage differences represent deviations from the station discharge for each method and location. Note that US and DS refer to upstream and downstream, respectively.

Discharge-Station (ft^3/s)	**Discharge-GM (ft^3/s)**	**Discharge-SV (ft^3/s)**	**Difference-GM (%)**	**Difference-SV (%)**
3650	4621	2973 (US) 2949 (DS)	26.6	18.5 (US) 19.2 (DS)

Across the two reaches, GM discharge values were generally higher than the gage measurement, reflecting the sensitivity of Manning's equation to assumed roughness and channel irregularity. A Manning's roughness coefficient of n = 0.035 was used for the GM calculations. SV-based discharge values showed closer agreement but tended to slightly underpredict discharge, consistent with expected limitations related to tracer availability, flow nonuniformity, and uncertainty in velocity-coefficient selection. When plotted on the USGS stage–discharge rating curve (Figure 4.11), the UAV-derived estimates align with the established trend, indicating that both methods capture the overall hydraulic response of the channel.

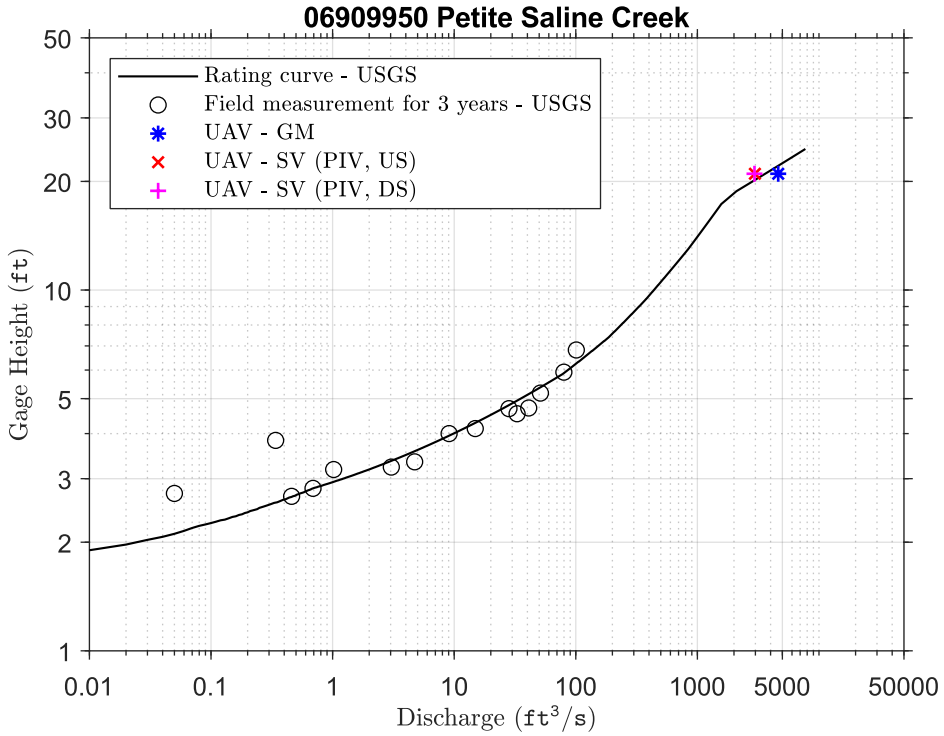

Figure 4.11 Comparison of UAV-derived discharge estimates with the USGS rating curve at gage 06909950 (Petite Saline Creek). The solid line represents the USGS rating curve, and open circles denote three years of historical field measurements.

Together, the GM and SV approaches provide complementary perspectives on discharge at Petite Saline Creek. The GM method leverages detailed channel geometry derived from UAV-LiDAR, while the SV method incorporates directly observed surface flow kinematics from UAV video analysis. Both approaches yielded discharge values within approximately 30% of the USGS station measurement, with SV-based estimates generally lower than those obtained from the GM method. The consistency between the two independent UAV-derived techniques strengthens confidence in the final discharge estimates and demonstrates the practicality and reliability of UAV-based hydraulic assessment for small and medium streams where conventional field measurements may be hazardous, impractical, or resource-intensive.

4.2 Hinkson Creek

4.2.1 Photogrammetry

For Hinkson Creek, using a DJI M350 equipped with the P1 camera, the survey covered 10.4-acre area, with a total flight duration of approximately 17 minutes. High-resolution images were processed to generate an orthophoto of the channel region (Figure 4.12), providing detailed information on channel region, bank conditions, vegetation distribution, and adjacent floodplain features. These photogrammetric products also support alignment of LiDAR data, establishment of ground control, and subsequent hydraulic interpretation throughout the Hinkson Creek analysis.

Figure 4.12 UAV-derived orthophoto of the Hinkson Creek survey area captured with the DJI P1 camera.

4.2.2 LiDAR

A UAV-based LiDAR survey was carried out at the Hinkson Creek site using a DJI M350 equipped with the L2 LiDAR sensor. The mission covered approximately 10.4 acres with a total flight duration of about 21 minutes. The resulting point cloud was processed in DJI Terra to produce both height and classified terrain models. As shown in Figure 4.13, the height map captures vegetation along the banks, overhead utility lines, and bridge structures. The tree canopy is denser in this area, and structures such as power lines and bridges are crowded. The high-density LiDAR returns provide sufficient spatial resolution for cross-section extraction, water-surface slope estimation, and geometry-based hydraulic analysis, forming a core dataset for discharge estimation and subsequent comparison with photogrammetric and surface-velocity measurements. After classification process the structures above ground can be filtered out for the digital elevation model (Figure 4.13b).

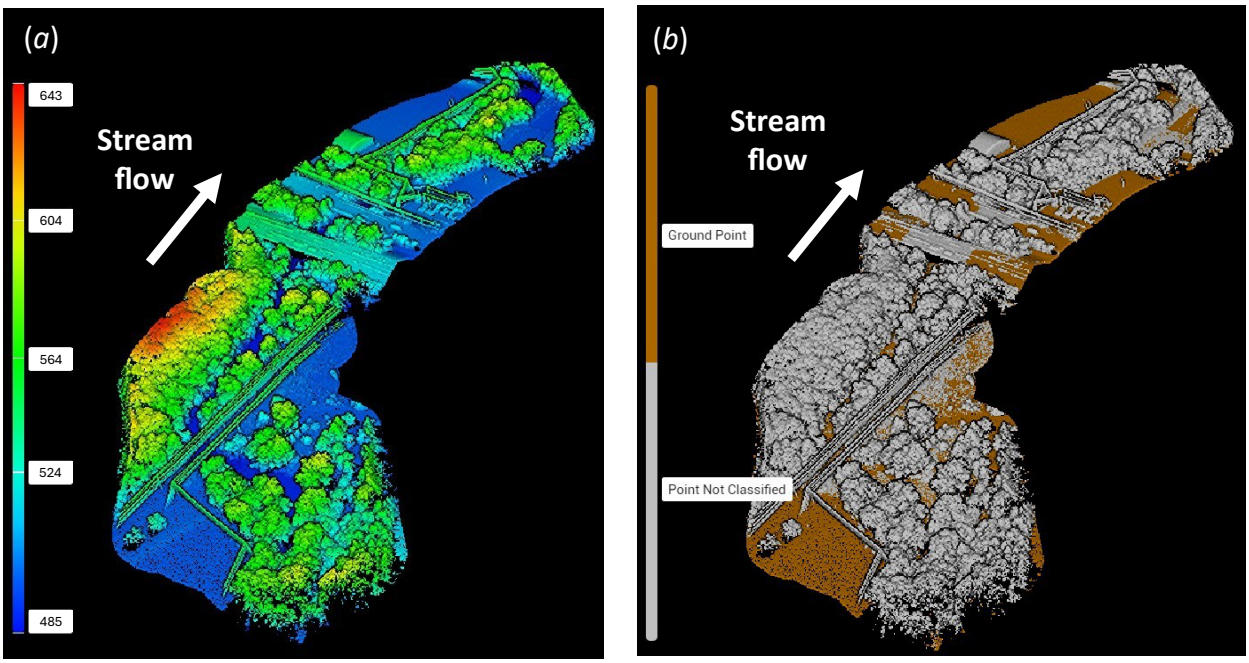

Figure 4.13 UAV LiDAR datasets (*a*) Height map in ft and (*b*) Classified terrain point cloud for the Hinkson Creek survey area.

For the Hinkson Creek channel, the generated DEM (Figure 4.14) provides a continuous surface representation from which the channel centerline was extracted. Elevation values sampled along this centerline were used to calculate the local bed and water-surface slope. A linear regression applied to the longitudinal profile indicates a gradual downstream decrease in elevation consistent with the expected hydraulic gradient. The location of the nearby USGS streamgage is shown for reference and alignment. This slope information serves as an essential input for geometry-based discharge estimation and enables comparison between UAV-derived elevation data and independent gage measurements.

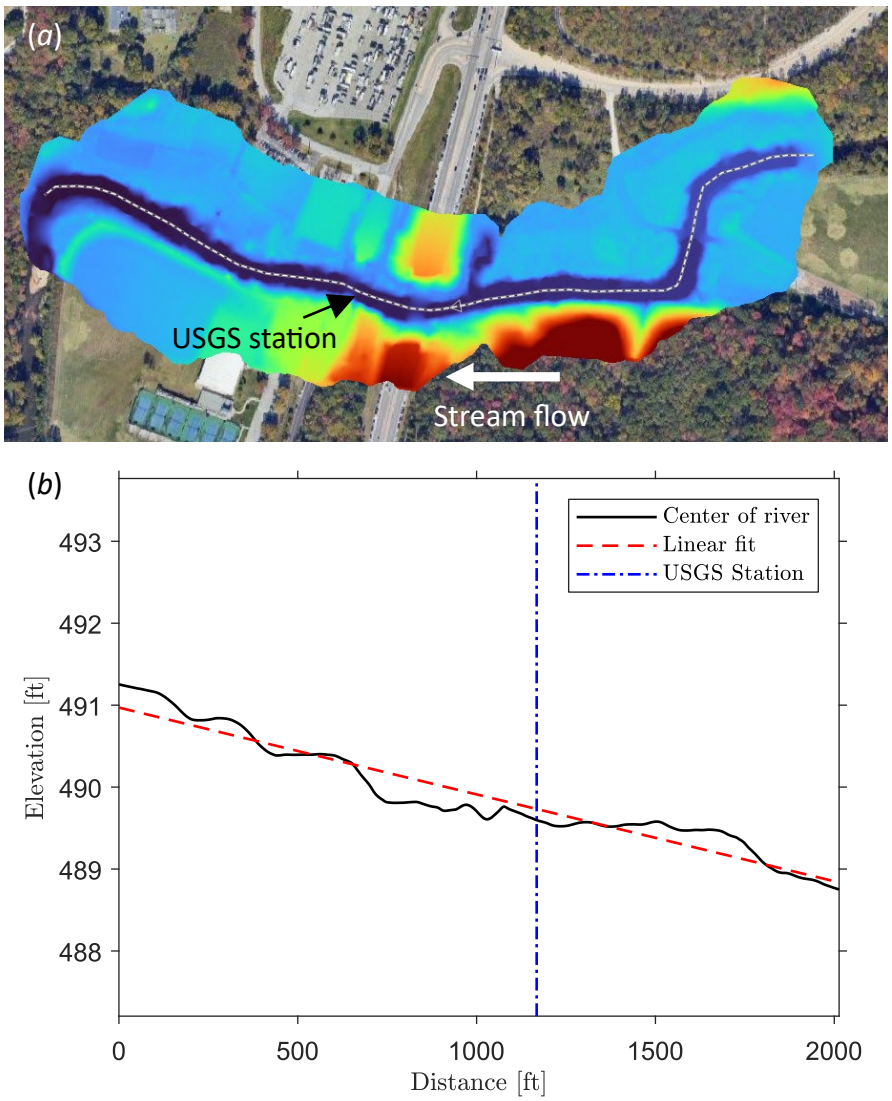

Figure 4.14 (a) Digital Elevation Model (DEM) from the UAV LiDAR survey overlaid on satellite imagery, showing streamflow direction and the location of the USGS station. (b) Longitudinal water surface elevation profile extracted along the channel centerline, with a linear-fit slope and the USGS station location indicated.

4.2.3 PIV

For the upstream reach, the computation window for PIV (Figure 4.15) was selected in an area with adequate surface texture and minimal interference from bridge shadows, overhanging vegetation, and bank obstructions. This placement ensured consistent image quality across the video sequence and allowed the PIV algorithm to track surface features reliably.

Figure 4.15 UAV orthoimage showing the selected analysis region for upstream surface velocity estimation. The red box indicates the area for PIV analysis, with flow direction shown by the white arrow.

Surface velocity measurements were acquired at Hinkson Creek using PIV. A DJI M3E UAV was used for PIV measurements, each lasting approximately five minutes at an operating altitude of about 195 ft. Stabilized video imagery was collected to enable cross-correlation of surface features, including foam patches, floating debris, and subtle brightness variations, that serve as tracers for PIV analysis.

The resulting mean velocity field (Figure 4.16) shows the spatial distribution of surface flow across the channel, with higher velocities concentrated near the central portion of the section and reduced velocities toward the banks and vegetated margins. The computation window ensures that PIV processing focuses on regions with consistent surface texture and minimal interference from shadows or overhanging vegetation. Shadowed areas were avoided because they can distort feature tracking and affect the resulting velocity distribution.

Figure 4.16 PIV mean velocity field for Hinkson Creek overlaid over image from UAV.

The cross-sectional velocity profile for Hinkson Creek (Figure 4.17) shows a relatively smooth distribution across the channel, with peak velocities located near the central portion of the section and gradual decreases toward both banks. The water surface was turbid, which allowed the PIV method to perform well. However, tree cover affected portions of the imagery, leading to near-zero velocity values along the right bank.

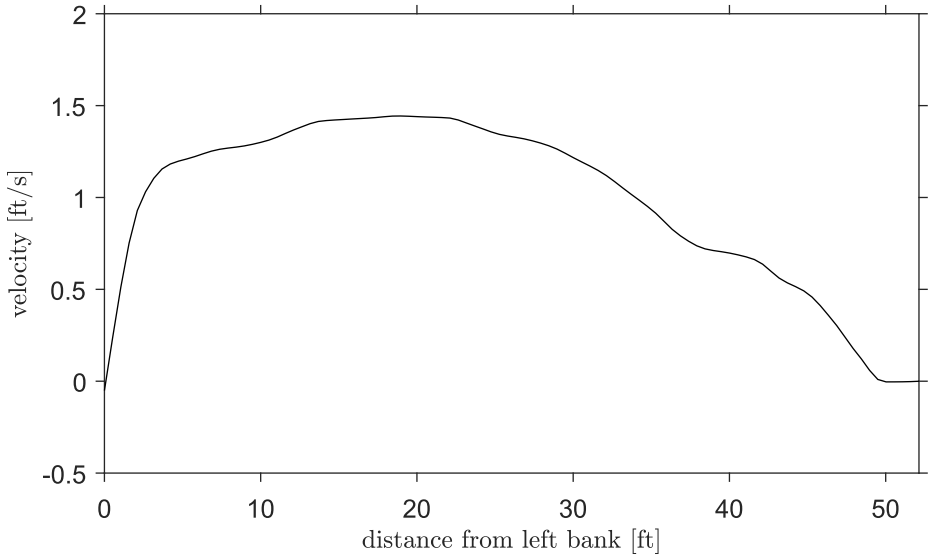

Figure 4.17 Cross-sectional surface velocity profiles derived from UAV-based image velocimetry as a function of distance from the left bank along the flow direction.

4.2.4 Bathymetry

Bathymetry at Hinkson Creek was evaluated using sonar measurements from a remote-controlled boat. The depth map (Figure 4.18) illustrates spatial variations in channel depth along the centerline transect, with warmer colors indicating deeper portions of the channel and cooler colors representing shallow regions.

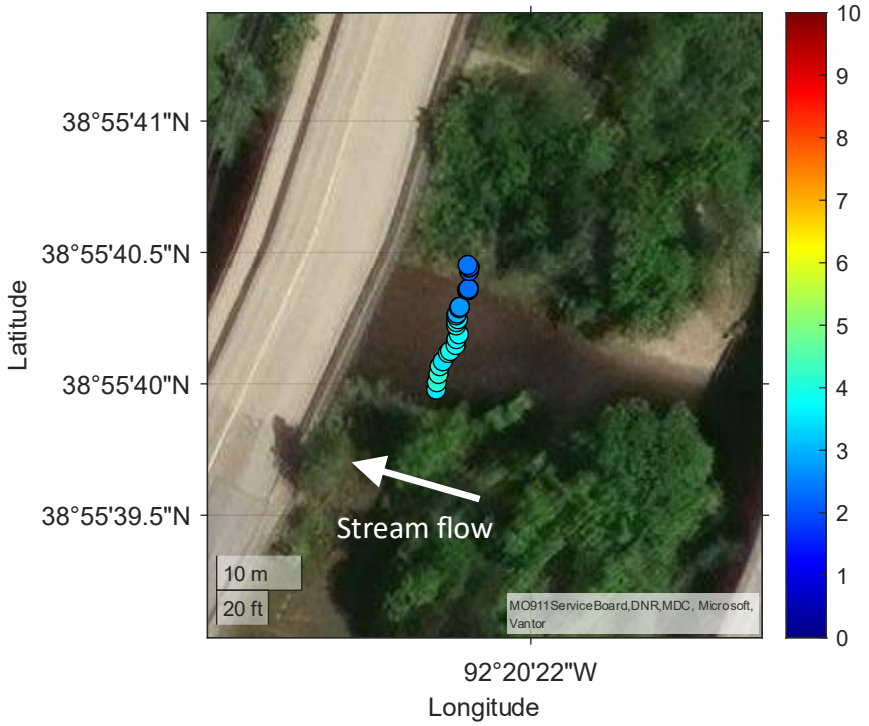

Figure 4.18 Bathymetry-derived channel depth from sonar sensor equipped boat overlaid on satellite image of Hinkson Creek. Depth measurements obtained from UAV-based bathymetric processing are shown along the centerline transect, with colors indicating local water depth in feet. Warmer colors represent deeper portions of the channel, while cooler colors correspond to shallow areas.

To further characterize the cross-sectional geometry, sonar-derived bathymetry was collected along a single transect across the channel (Figure 4.19). The bathymetric profile indicates a mid-channel deepening, with gradually shallower depths toward both banks but left bank was deeper. This distribution reflects the channel's asymmetric bed shape and supplies key geometric parameters for hydraulic analysis, including discharge estimation and integration with UAV-based surface-velocity observations.

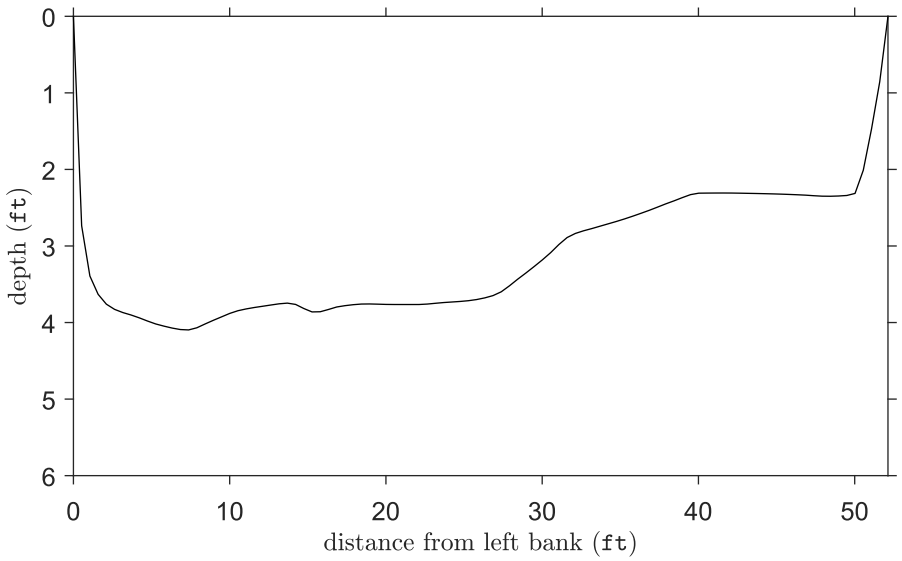

Figure 4.19 Bathymetry profile using sonar measurements. The black line represents the bed depth measured from the sonar transect as a function of distance from the left bank along the flow direction.

4.2.5 Discharge

Discharge at Hinkson Creek was estimated using both geometry-based and surface-velocity methods. Table 4-2 shows the comparison of discharge estimates using geometric and surface velocity methods. GM discharge values were consistently higher than the gage measurement, reflecting the sensitivity of Manning's equation to assumed roughness values and channel irregularities. A Manning's roughness coefficient of n = 0.035 was used for the GM calculations. In contrast, SV-based discharge estimates showed slightly closer agreement with the gage but tended to underpredict discharge.

Table 4-2 Comparison of discharge estimates at the upstream and downstream reaches for Hinkson Creek. The table summarizes discharge derived from gauge measurements (Station), the geometric–method (GM) using Mannings' equation, and UAV-based surface velocity (SV). Percentage differences represent deviations from the station discharge for each method and location.

Discharge-Station (ft^3/s)	**Discharge-GM (ft^3/s)**	**Discharge-SV (ft^3/s)**	**Difference-GM (%)**	**Difference-SV (%)**
226	318	152	40.7	32.7

When the UAV-derived estimates are plotted on the USGS stage–discharge rating curve (Figure 4.20), both GM and SV results fall along the established trend, indicating that each method successfully captures the overall hydraulic behavior of the channel.

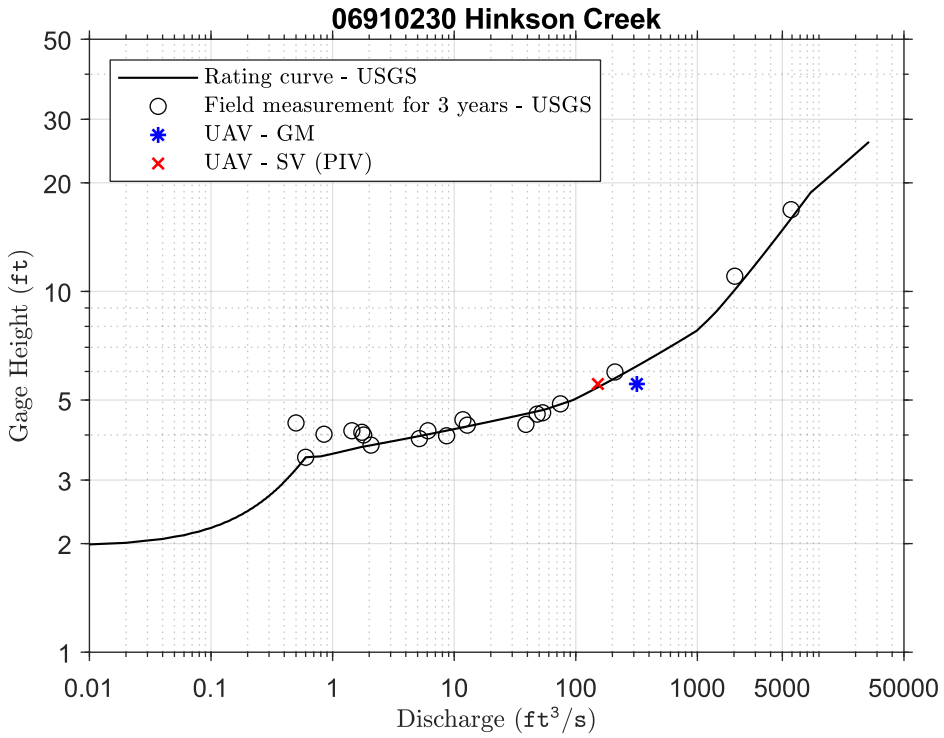

Figure 4.20 Comparison of UAV-derived discharge estimates with the USGS rating curve at gage 06910230 (Hinkson Creek). The solid line represents the USGS rating curve, and open circles denote three years of historical field measurements.

Together, the GM and SV approaches provide complementary perspectives on discharge at Hinkson Creek. The GM method, which uses channel geometry from UAV-LiDAR and Manning's equation, produced a discharge estimate of 318 ft³/s, approximately 40.7% higher than the USGS station value of 226 ft³/s. In contrast, the SV method, based on UAV-derived surface velocities, yielded a lower discharge estimate of 152 ft³/s, representing a 32.7% underestimation relative to the gage measurement.

4.3 Moniteau Creek

4.3.1 Photogrammetry

A UAV-based photogrammetric survey was conducted at the Moniteau Creek site using a DJI M350 equipped with the P1 camera. The mission covered approximately 24.7 acres with a total flight duration of about 16 minutes. High-resolution imagery was processed to generate an orthophoto of the channel corridor (Figure 4.21). The orthophoto shows the extent of tree coverage along the riverbank.

Figure 4.21 UAV-derived orthophoto of the Moniteau Creek survey area captured using the DJI P1 camera, overlaid on satellite imagery.

4.3.2 LiDAR

A UAV-based LiDAR survey was conducted at the Moniteau Creek site using a DJI M350 equipped with the L2 LiDAR sensor. The mission covered approximately the same area of Photogrammetry with a total flight duration of about 21 minutes. As shown in Figure 4.22, the height model clearly differentiates vegetation, while the classified terrain model isolates ground returns, revealing the underlying channel geometry and bank structure.

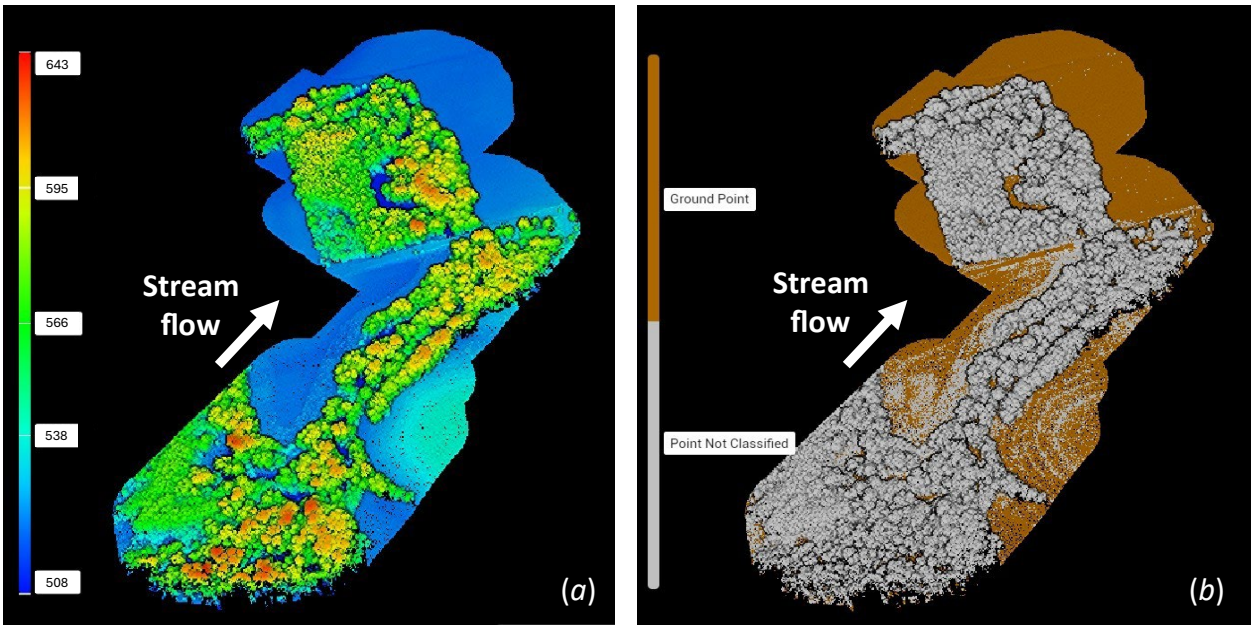

Figure 4.22 UAV LiDAR datasets for the Moniteau Creek survey area. (*a*) Height map in ft showing elevation variations, vegetation structure, roadway embankments, and floodplain topography.
(*b*) Classified terrain point cloud in which non-ground returns have been removed to reveal the underlying channel morphology. Streamflow direction is indicated for reference.

For Moniteau Creek, the DEM (Figure 4.23) provides a continuous elevation surface from which the channel centerline was extracted. Elevation samples extracted along this centerline were used to compute the water-surface slope. A linear regression applied to the longitudinal profile shows a gradual downstream decrease in elevation, consistent with the expected hydraulic gradient. The location of the nearby USGS streamgage is indicated for spatial reference and validation.

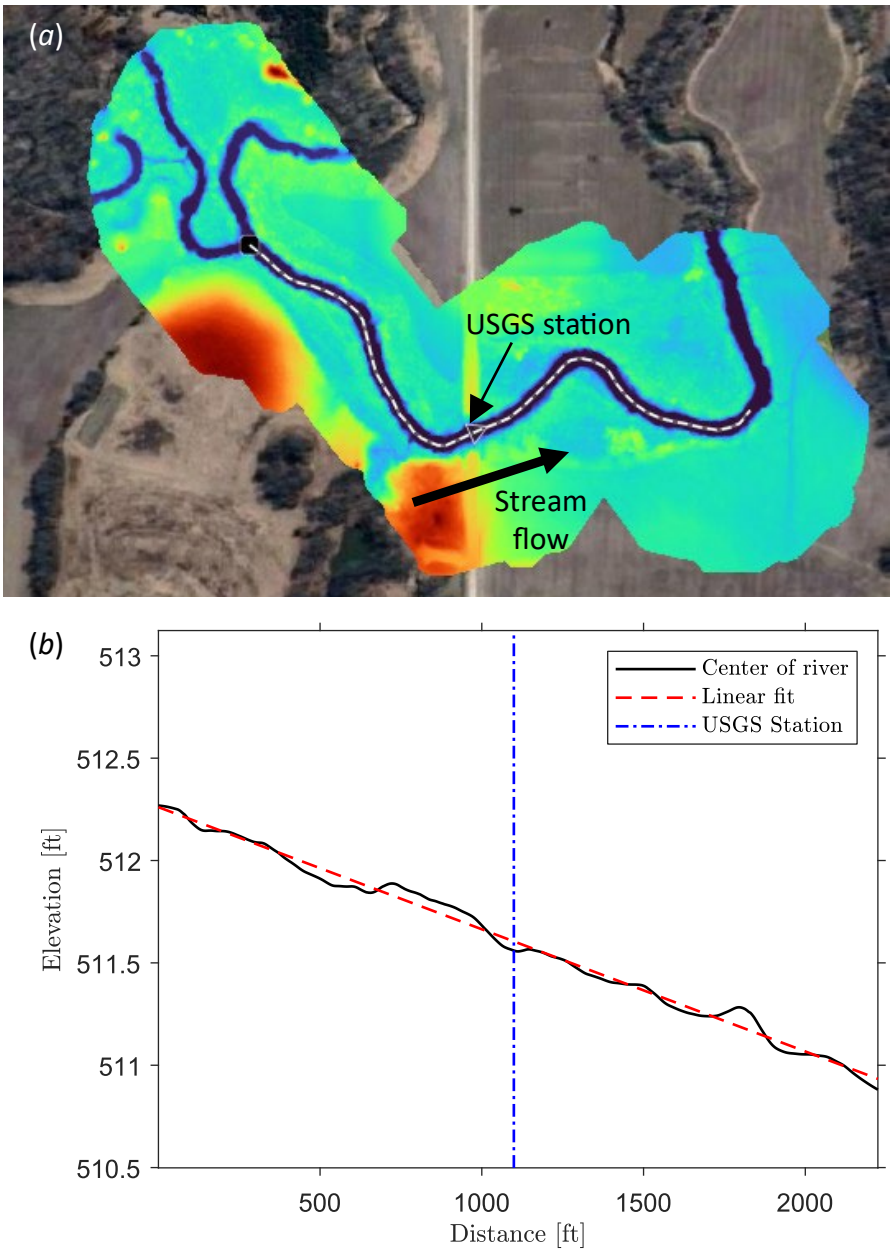

Figure 4.23 (*a*) Digital Elevation Model (DEM) derived from the UAV LiDAR survey overlaid on satellite imagery and the direction of streamflow. (*b*) Longitudinal elevation profile extracted along the channel centerline, with the linear-fit slope shown in red and the USGS station location marked for reference.

4.3.3 PIV

For the upstream reach, the computation window for PIV was selected (Figure 4.24). As shown in the figure, the tree coverage is dense, which limits the effectiveness of UAV-based surface velocity methods. This placement ensured consistent image quality across the video sequence and allowed the PIV algorithm to track surface features reliably. Within this selected window, the stabilized imagery produced a well-resolved and spatially coherent velocity field that characterizes the upstream flow structure.

Figure 4.24 UAV orthoimage showing the selected analysis region for upstream surface velocity estimation for Moniteau Creek. The red box indicates the area for PIV analysis, with flow direction shown by the white arrow.

The resulting mean velocity field (Figure 4.25a) illustrates the spatial distribution of surface flow across Moniteau Creek, with higher velocities concentrated near the central portion of the channel and reduced velocities toward the banks and vegetated margins. Power line motion introduced noise into the PIV measurements; therefore, the affected areas were masked out. The corresponding cross-sectional velocity profile (Figure 4.25b) shows a smooth distribution, with peak velocities occurring near the right bank and gradual decreases toward both channel banks, reflecting the influence of channel geometry and bank roughness on the flow structure.

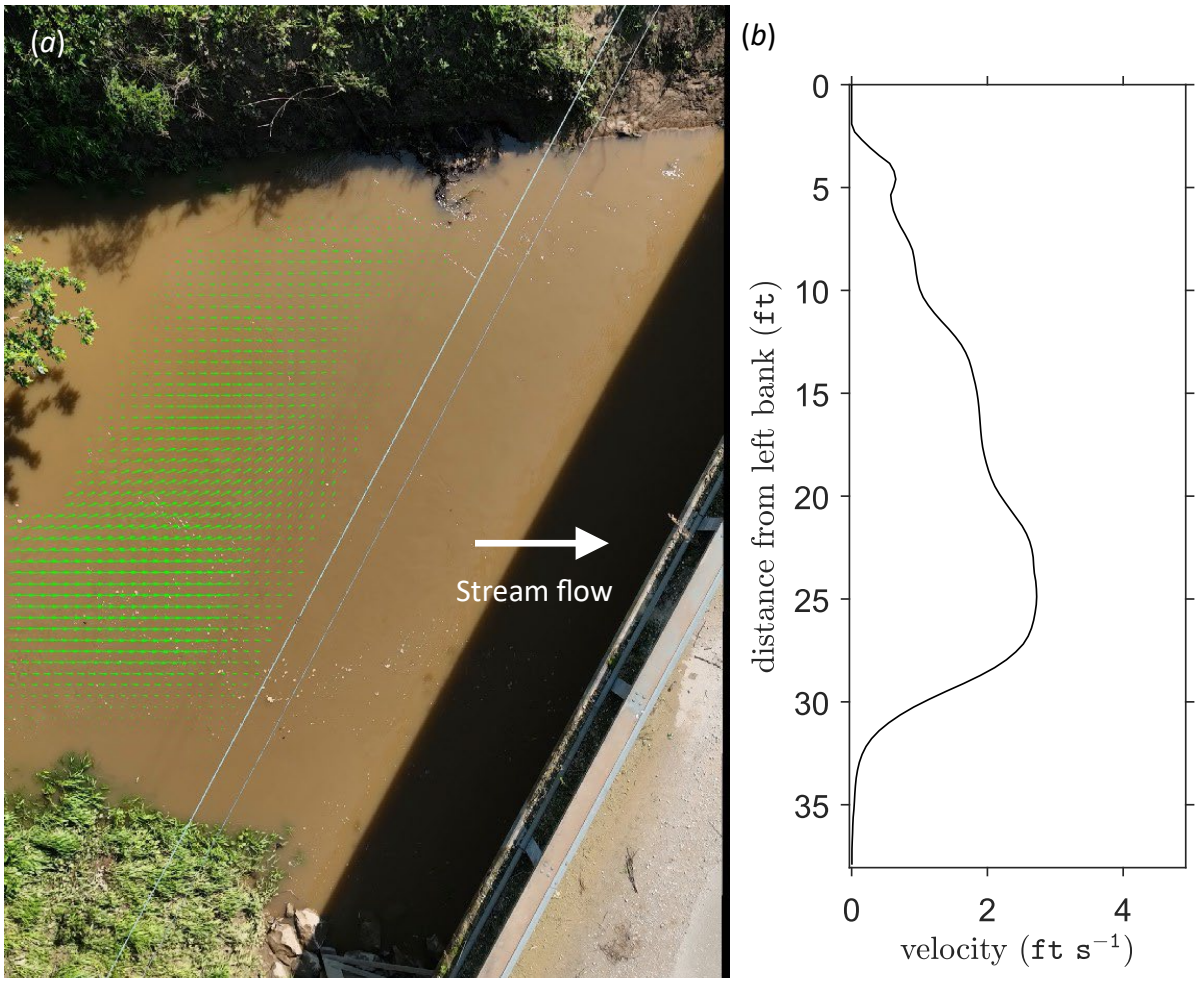

Figure 4.25 (*a*) Mean surface velocity field derived from UAV-based PIV analysis (*b*) Cross-sectional surface velocity profile extracted from the PIV results, plotted as a function of distance from the left bank along with the flow direction for Moniteau Creek.

4.3.4 Bathymetry

Bathymetric measurements obtained from UAV-based sonar mapping at Moniteau Creek. As shown in Figure 4.26, depth estimates vary across the surveyed section, with deeper zones highlighted by warmer colors and shallower areas by cooler colors. The corresponding cross-sectional profile further illustrates the asymmetric channel shape and supports integration of bathymetry with surface-velocity and LiDAR-derived slope information for discharge estimation.

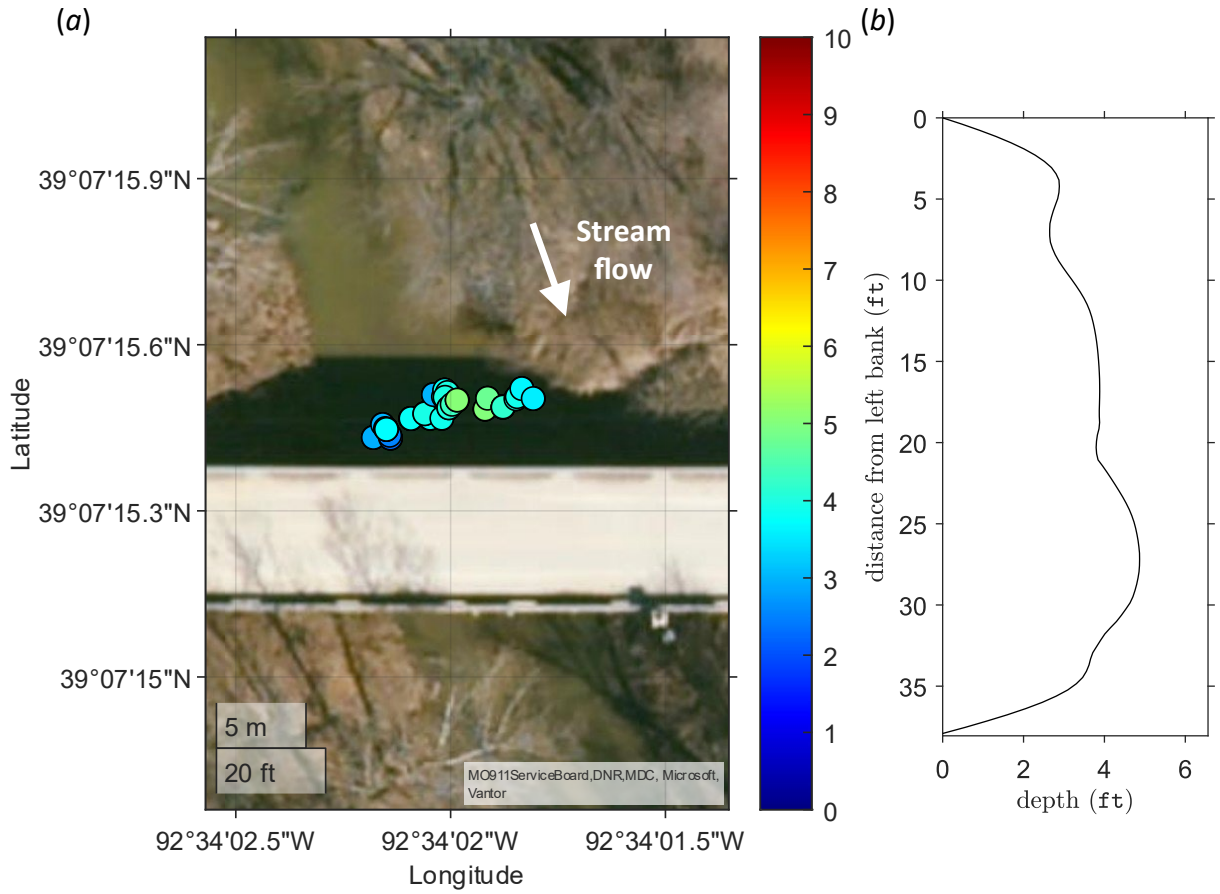

Figure 4.26 Bathymetry measurements from sonar sensor equipped boat for Moniteau Creek. (*a*) Depth scatter plot overlaid on satellite image, with color indicating measured water depth in feet. (*b*) Cross-sectional bathymetry profile extracted from the sonar transect, plotted as a function of distance from the left bank along with the flow direction.

4.3.5 Discharge

Discharge at Moniteau Creek was estimated using both geometry-based and UAV-derived surface-velocity approaches. The geometric–manometric (GM) method produced a discharge estimate of 302 ft^3/s, essentially matching the USGS gage value of 301 ft^3/s (Table 4-3). This corresponds to a difference of only 0.3%, indicating that the LiDAR-based geometric characterization and estimated roughness parameter were well aligned with actual hydraulic conditions at the site. A Manning's roughness coefficient of n = 0.035 was used for the GM calculations.

Table 4-3 Comparison of discharge estimates at the upstream and downstream reaches for Moniteau Creek. The table summarizes discharge derived from gauge measurements (Station), the geometric–method (GM) using Mannings' equation, and UAV-based surface velocity (SV). Percentage differences represent deviations from the station discharge for each method and location.

Discharge-Station (ft^3/s)	**Discharge-GM (ft^3/s)**	**Discharge-SV (ft^3/s)**	**Difference-GM (%)**	**Difference-SV (%)**
301	302	171	0.3	43.2

Surface-velocity (SV) estimates obtained from UAV-based PIV analysis yielded a discharge of 171 ft^3/s, which is approximately 43.2% lower than the gage measurement. This underestimation may be due to the limited area for observing from tree coverage and power lines.

When plotted on the USGS stage–discharge rating curve (Figure 4.27), the UAV-derived GM and SV estimates bracket the established curve, with the GM estimate aligning almost exactly and the SV estimate falling below the curve. This comparison highlights that:

- The GM method provides highly accurate discharge at this site due to well-defined channel geometry and reliable slope estimation.
- The SV method captures the correct hydraulic trend but underpredicts discharge, reflecting sensitivity to surface-texture quality during the UAV survey.

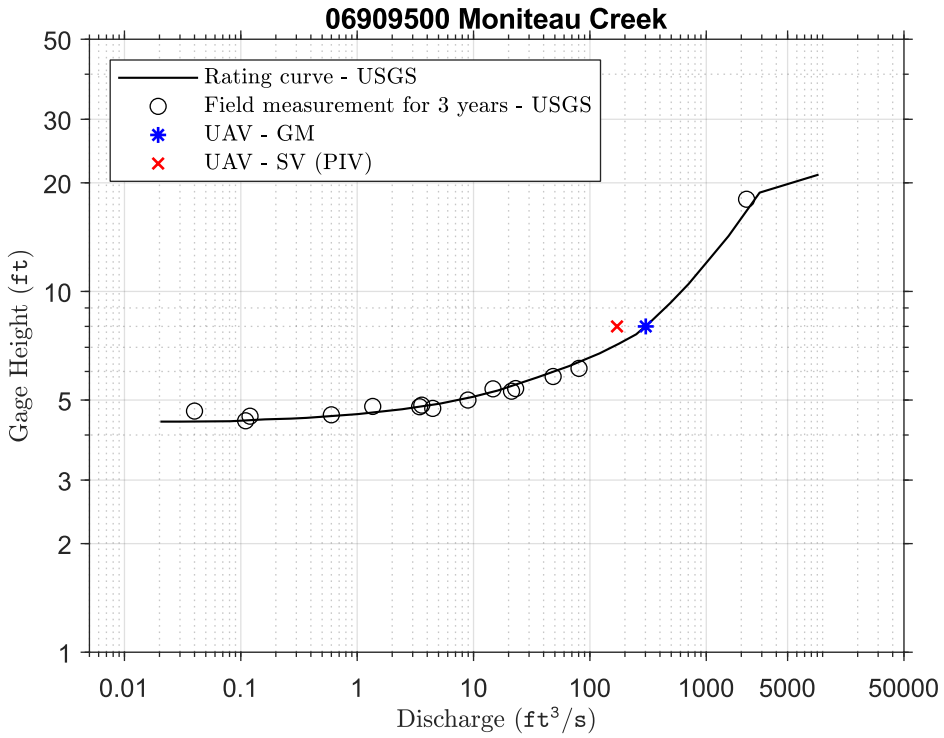

Figure 4.27 Comparison of UAV-derived discharge estimates with the USGS rating curve at gage 06909500 (Moniteau Creek). The solid line represents the USGS rating curve, and open circles denote three years of historical field measurements.

4.4 Long Branch Creek

4.4.1 Photogrammetry

For Long Branch Creek, using a DJI M350 equipped with the P1 camera, the mission covered approximately 11.8 acres with a total flight duration of about 10 minutes. High-resolution imagery was processed to generate an orthophoto of the channel corridor (Figure 4.28), capturing detailed information on channel planform, bank conditions, vegetation patterns, and surrounding floodplain features.

Figure 4.28 UAV-derived orthophoto of the Long Branch Creek survey area captured with the DJI P1 camera.

4.4.2 LiDAR

A UAV-based LiDAR survey was conducted at the Long Branch Creek site using a DJI M350 equipped with the L2 LiDAR sensor. The mission covered approximately 11.8 acres with a total flight duration of about 13 minutes. The acquired point cloud was processed in DJI Terra to generate both height and classified terrain models. Figure 4.29 shows the height model and the classified terrain model with streamflow direction. The generated DEM (Figure 4.30) provides a continuous elevation surface from which the channel centerline was delineated. A linear regression applied to the longitudinal profile shows a gradual downstream decrease in elevation, consistent with the expected hydraulic gradient.

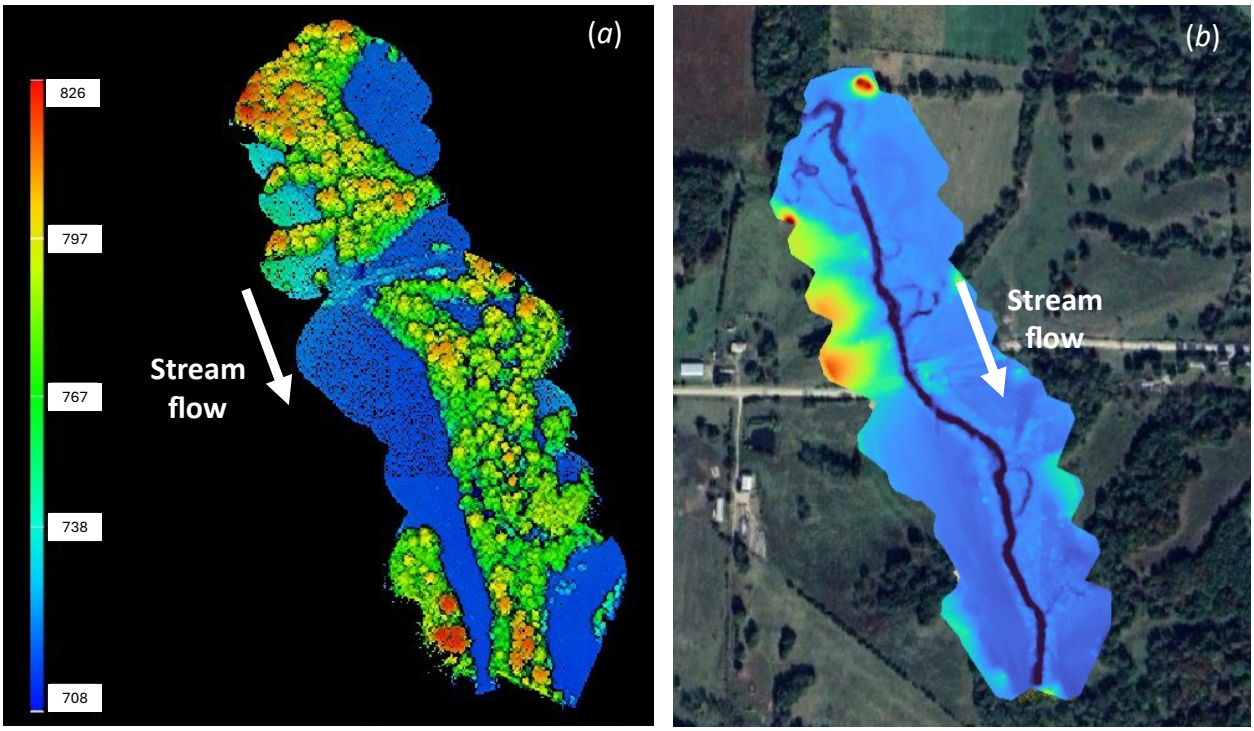

Figure 4.29 UAV LiDAR datasets (*a*) Height map in ft and (*b*) the generated digital elevation model for the Long Branch Creek survey area.

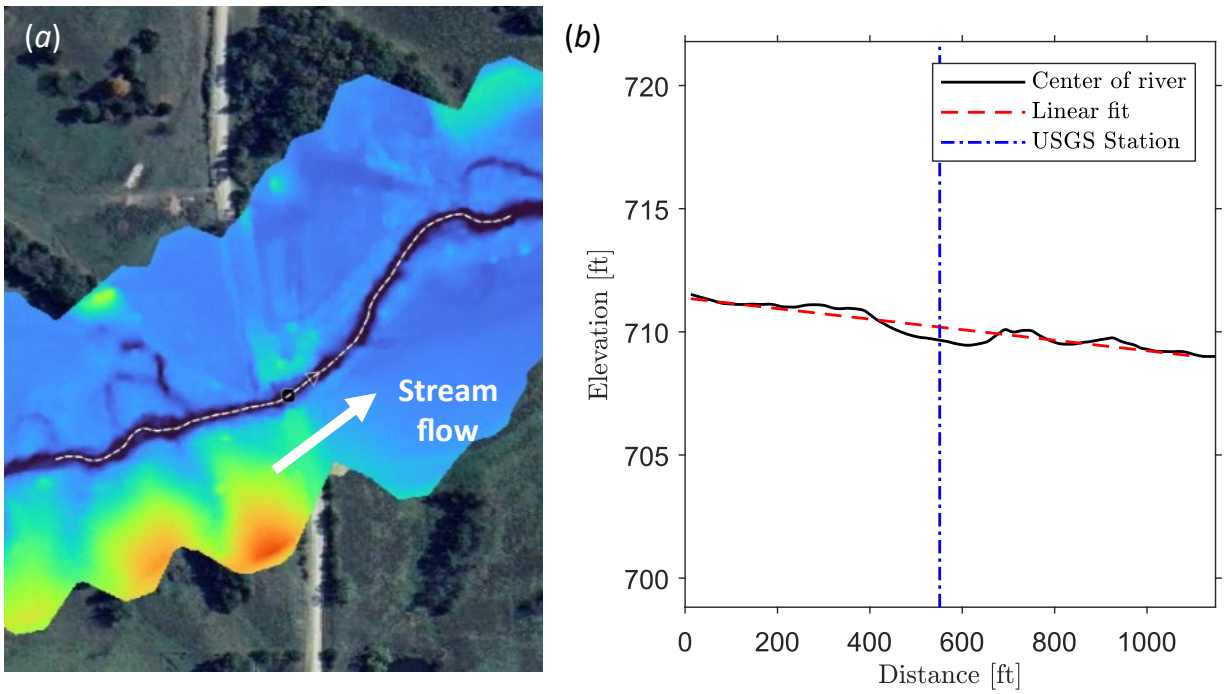

Figure 4.30 (*a*) Digital Elevation Model (DEM) of Long Branch Creek derived from the UAV LiDAR survey overlaid on satellite imagery, illustrating elevation gradients and the direction of streamflow. (*b*) Longitudinal elevation profile extracted along the channel centerline, with the linear-fit slope shown in red and the USGS station location marked for reference.

4.4.3 PIV

For the upstream reach, the computation window for PIV (Figure 4.31a) was selected in an unshadow area to ensure consistent surface texture for feature tracking. As shown in Figure 4.31b, dense tree coverage along the left bank likely influenced the velocity estimates, resulting in near-zero values in that region. This reduction reflects both shading effects and limited surface texture beneath the canopy, which can affect the reliability of PIV measurements.

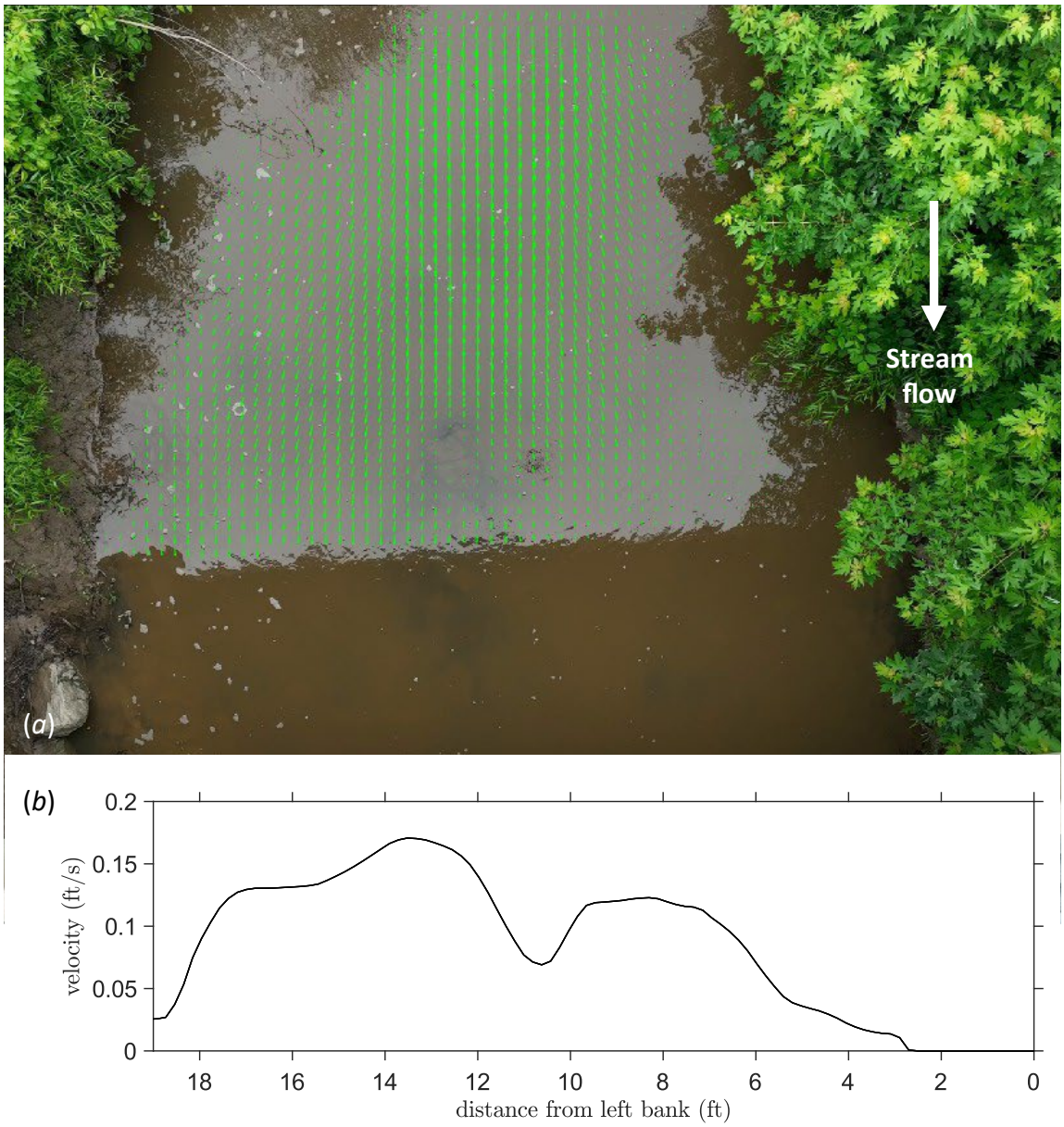

Figure 4.31 (*a*) Mean surface velocity field derived from UAV-based PIV analysis (*b*) Cross-sectional surface velocity profile extracted from the PIV results, plotted as a function of distance from the left bank along with the flow direction for Long Branch Creek.

4.4.4 Bathymetry

Bathymetric measurements at Long Branch Creek were obtained using a sonar sensor. Because the water was shallow, the sonar sensor was mounted on a rod and manually lowered from the bridge to capture depth measurements. As shown in Figure 4.32a, depth estimates vary across the surveyed section, with deeper zones highlighted by warmer colors and shallower areas by cooler colors.

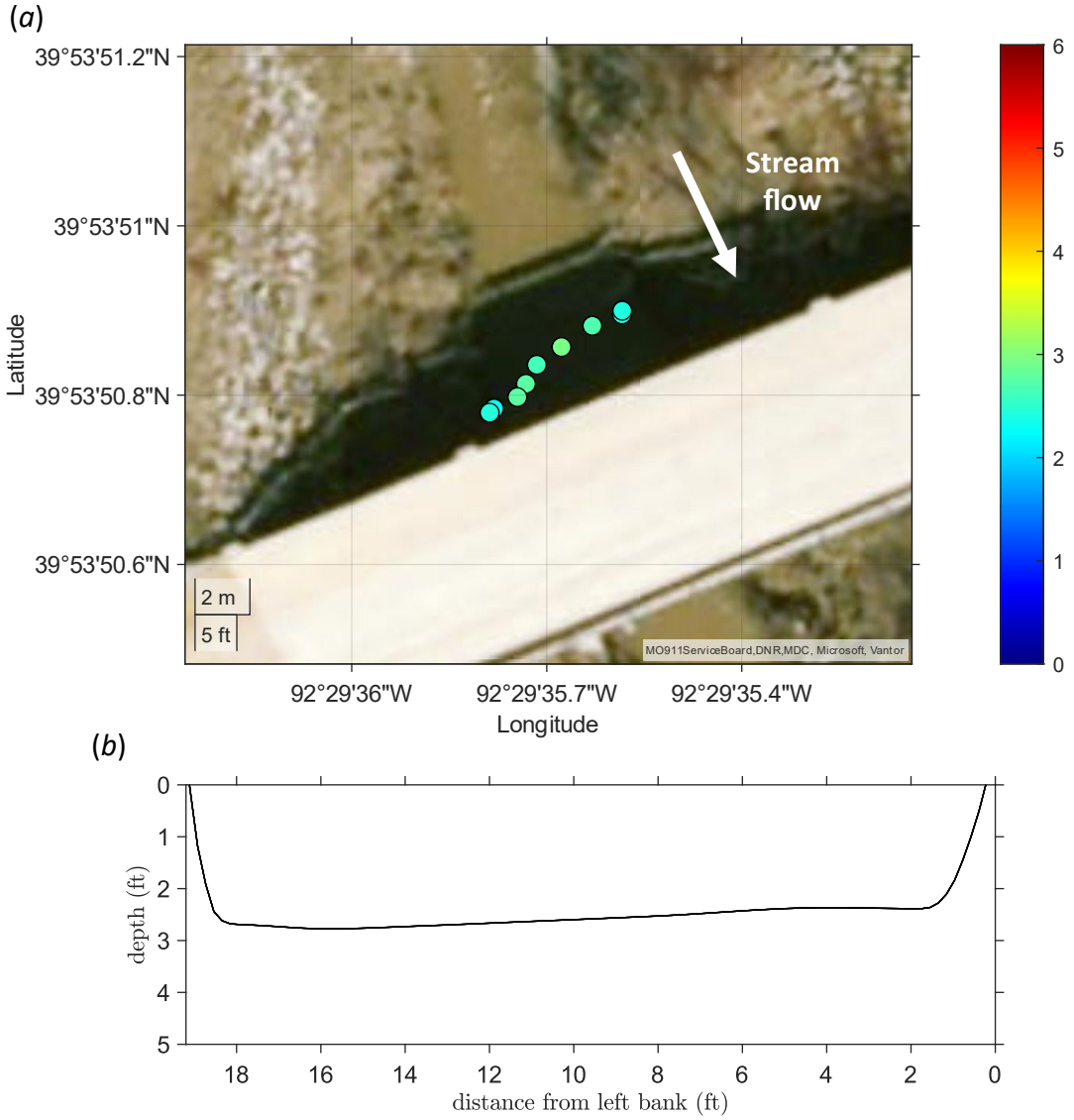

Figure 4.32 Bathymetry measurements from sonar sensor equipped boat for Long Branch Creek. (*a*) Depth scatter plot overlaid on satellite image, with color indicating measured water depth in feet. (*b*) Cross-sectional bathymetry profile extracted from the sonar transect, plotted as a function of distance from the left bank along with the flow direction.

The corresponding cross-sectional profile (Figure 4.32b) shows a relatively flat channel bed, with steeper gradients occurring near the banks. These bathymetric data will be integrated with surface-velocity measurements and LiDAR-derived slope information to support discharge estimation.

4.4.5 Discharge

Discharge at Long Branch Creek was estimated using both geometry-based and UAV-derived surface-velocity approaches (SV) as listed in Table 4-4. The geometric–manometric (GM) method produced a discharge estimate of 49.4 ft^3/s, compared with the USGS gage value of 5.5 ft^3/s. This corresponds to an error of approximately 798%, indicating that the LiDAR based geometric characterization and estimated roughness parameter did not accurately represent the hydraulic conditions at the site. A Manning's roughness coefficient of n = 0.035 was used for the GM calculations. In contrast, the SV produced an estimate of 4.0 ft^3/s, with a 27.3 % difference compared to station discharge value. This demonstrates that UAV-based surface-velocity methods provide a more reliable discharge estimate for this small, shallow stream where geometric assumptions are highly sensitive to roughness and channel form.

Table 4-4 Comparison of discharge estimates at the upstream and downstream reaches for Long Branch Creek. The table summarizes discharge derived from gauge measurements (Station), the geometric–method (GM) using Mannings' equation, and UAV-based surface velocity (SV). Percentage differences represent deviations from the station discharge for each method and location.

Discharge-Station (ft^3/s)	**Discharge-GM (ft^3/s)**	**Discharge-SV (ft^3/s)**	**Difference-GM (%)**	**Difference-SV (%)**
5.5	49.4	4.0	798	27.3

Figure 4.33 shows the comparison of the discharge estimates with the USGS rating curve. When plotted against the curve, the UAV-derived SV estimate falls on the discharge values in the curve, with deviations smaller than those observed in the field measurements. In contrast, the GM discharge estimate is noticeably offset, although it remains within the range of the highest field-measured deviation. This result suggests the GM method may be less accurate under low-flow conditions.

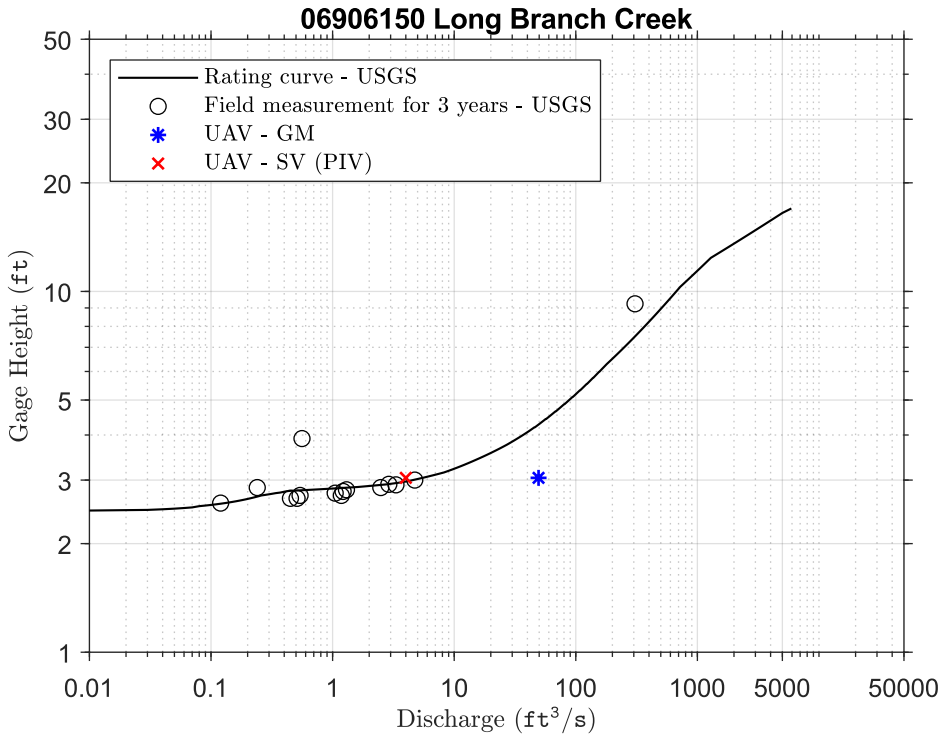

Figure 4.33 Comparison of UAV-derived discharge estimates with the USGS rating curve at gage 06906150 (Long Branch Creek). The solid line represents the USGS rating curve, and open circles denote three years of historical field measurements.

4.5 Tavern Creek

4.5.1 Photogrammetry

The photogrammetric survey at the Tavern Creek site covered approximately 24.6 acres with a total flight duration of about 12 minutes. High-resolution imagery was processed to generate an orthophoto of the channel corridor (Figure 4.34), showing a large open area with low tree density and noticeable changes in channel structure downstream of the bridge.

Figure 4.34 UAV-derived orthophoto of the Tavern Creek survey area captured with the DJI P1 camera.

4.5.2 LiDAR

At the Tavern Creek site, LiDAR survey covered approximately 39.5 acres with a total flight duration of about 12 minutes. Figure 4.35 shows the height model and the generated digital elevation model.

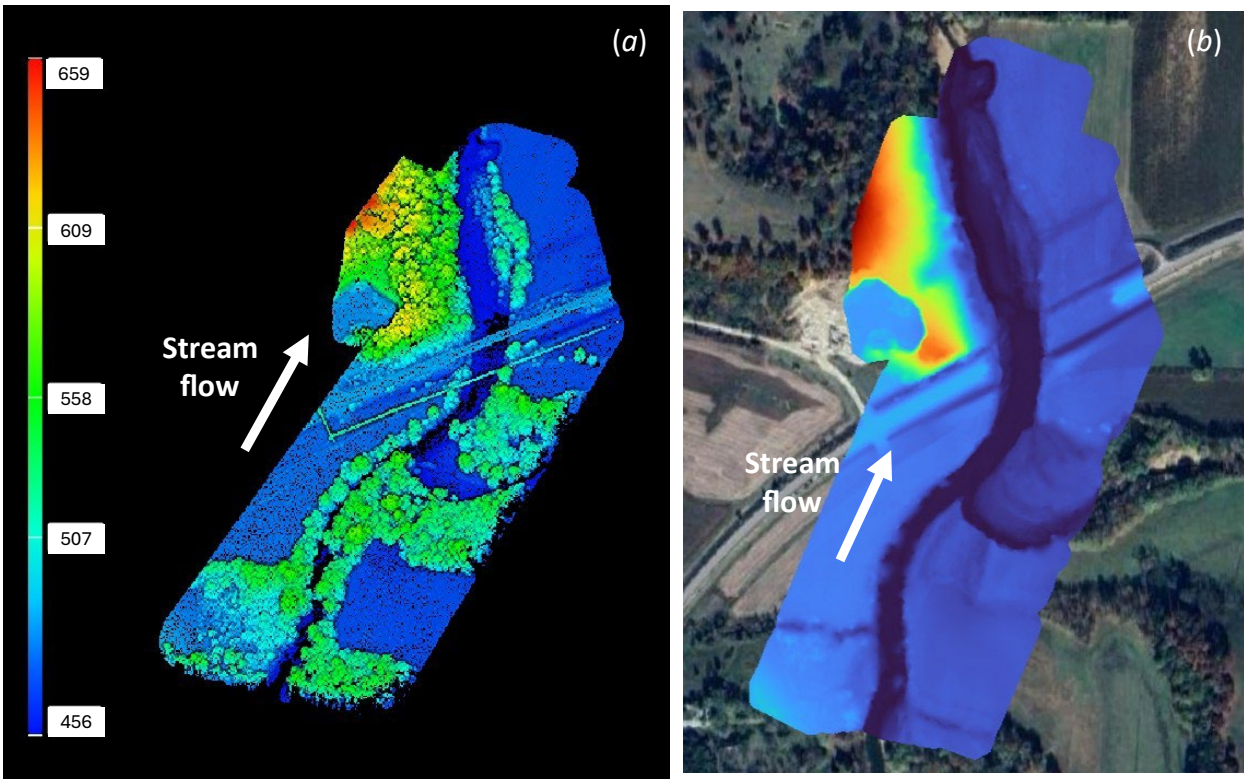

Figure 4.35 UAV LiDAR datasets for the Tavern Creek survey area. (*a*) Height map in ft and (*b*) the generated digital elevation model.

The slope calculation was performed downstream of the bridge because the flow beneath the bridge was too slow to provide reliable surface motion for analysis. Consequently, the evaluation section was shifted closer to the USGS gage location, where flow conditions were more suitable. This downstream area will also be used for PIV/PTV measurements to ensure consistency across all comparisons. As shown in Figure 4.36b, the selected slope-calculation region lies further downstream, where the channel geometry also changes rapidly within the measurement area.

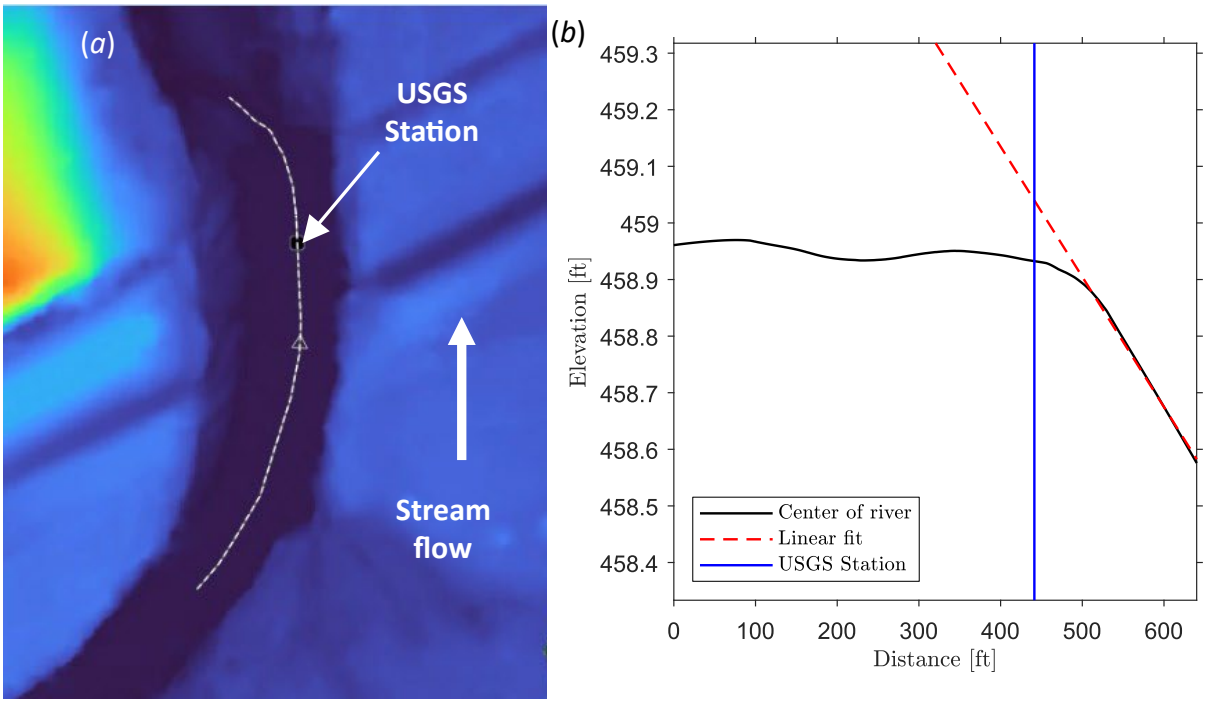

Figure 4.36 UAV LiDAR datasets for the Tavern Creek survey area. (*a*) Digital Elevation Model (DEM) with centerline (*b*) Longitudinal elevation profile extracted along the channel centerline, with the linear-fit slope shown in red and the USGS station location marked for reference.

4.5.3 PIV/PTV

PIV and PTV velocity measurements were conducted slightly downstream of the bridge. At the Tavern Creek site, biodegradable mulch was released upstream to provide adequate surface seeding. Figure 4.37 presents the resulting PIV and PTV velocity fields, along with their cross-sectional mean velocity profiles. The PIV results show limited coverage near the banks due to insufficient seeding density in those areas. In contrast, the PTV analysis captures more reliable velocity vectors near the banks, resulting in improved spatial coverage. Consequently, as shown in Figure 4.37c, the mean velocities from PTV are generally higher than those from PIV across most of the channel width.

In Tavern Creek, the water surface conditions differed notably from those at the other stream sites. Whereas the other locations showed developed flow or flooded conditions with naturally occurring surface tracers, Tavern Creek had moderate flow and clear water. Because the surface lacked sufficient natural texture for optical velocimetry, this was the only site where artificial seeding particles were required to enable PIV and PTV measurements.

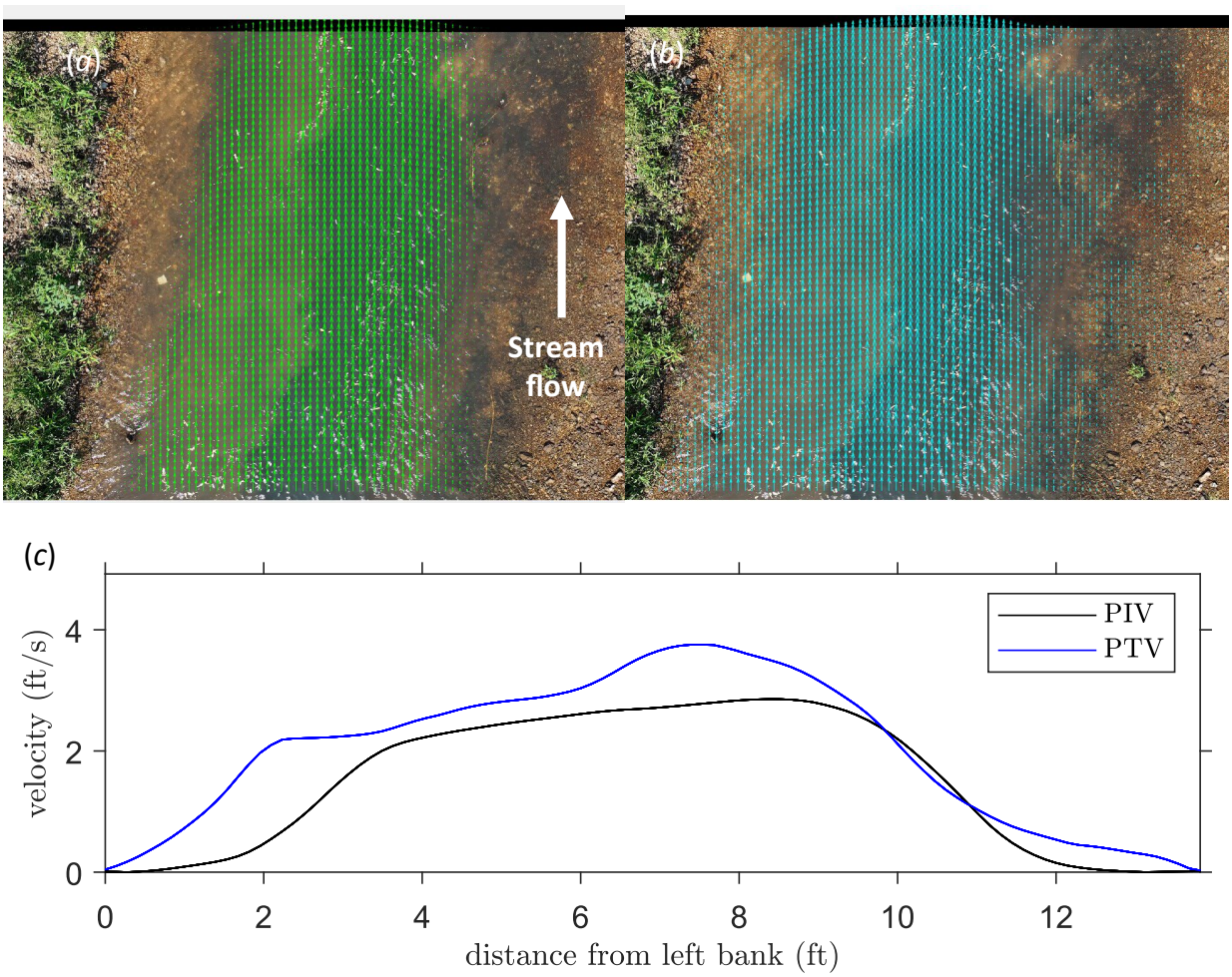

Figure 4.37 (*a*) Mean surface velocity field derived from UAV-based PIV analysis and (*b*) PTV analysis (*c*) Cross-sectional surface velocity profile extracted from the PIV results, plotted as a function of distance from the left bank for Tavern Creek.

4.5.4 Bathymetry

Because Tavern Creek was too shallow for boat-mounted sonar to operate effectively, bathymetric data were collected manually using field photographs and reference body measurements. Water depth at multiple points across the channel was estimated based on the photographs and references. This approach provided sufficient accuracy for shallow, wadable flows where acoustic methods could not be deployed. Figure 4.38 shows the resulting cross-sectional bathymetry profile, plotted as a function of distance from the left bank. The manually derived depths capture the shallow channel geometry at the site and were subsequently used in the velocity–area discharge calculations.

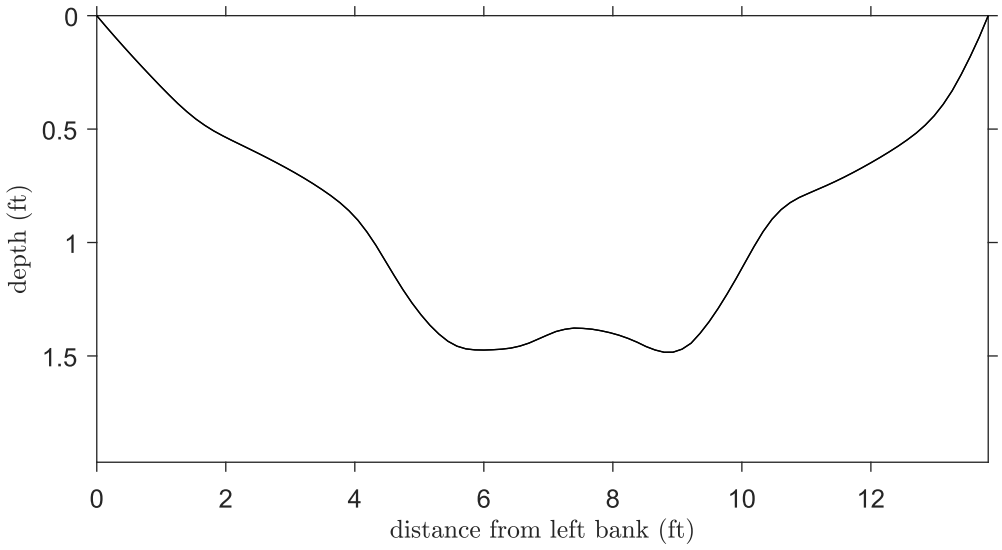

Figure 4.38 Cross-sectional bathymetry profile manually derived from field-based depth estimates, plotted as a function of distance from the left bank along with the flow direction.

4.5.5 Discharge

The calculated discharge information for Tavern Creek is summarized in Table 4-5. The geometric–manometric (GM) method produced a discharge estimate of 23.3 ft^3/s, compared with the USGS gage value of 29.5 ft^3/s, resulting in an error of approximately 21.1%. This suggests that the LiDAR-based geometric characterization and the selected roughness parameter were reasonably representative of the hydraulic conditions at the site. A Manning's roughness coefficient of n = 0.035 was used for the GM calculations. In contrast, the surface-velocity (SV) method produced estimates of 21.1 ft^3/s (PIV) and 25.3 ft^3/s (PTV), corresponding to errors of 28.4% and 14.2%, respectively.

Table 4-5 Comparison of discharge estimates at the upstream and downstream reaches for Tavern Creek. The table summarizes discharge derived from gauge measurements (Station), the geometric–method (GM) using Mannings' equation, and UAV-based surface velocity (SV). Percentage differences represent deviations from the station discharge for each method and location.

Discharge-Station (ft^3/s)	**Discharge-GM (ft^3/s)**	**Discharge-SV (ft^3/s)**	**Difference-GM (%)**	**Difference-SV (%)**
29.5	23.3	21.1 (PIV) 25.3 (PTV)	21.1	28.4 (PIV) 14.2

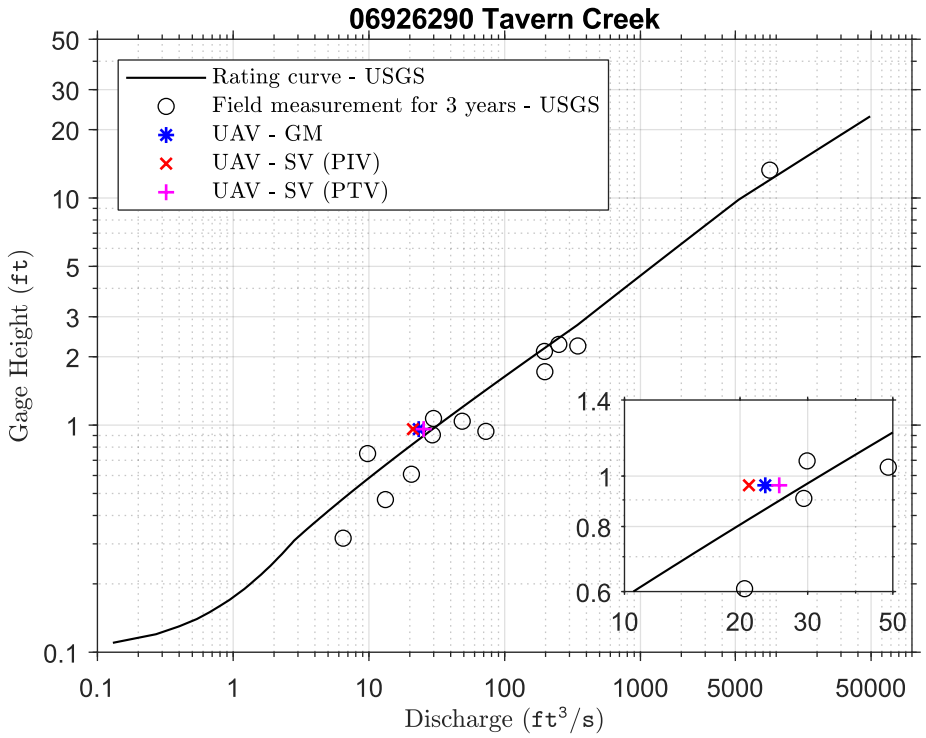

Figure 4.39 Comparison of UAV-derived discharge estimates with the USGS rating curve at gage 06926290 (Tavern Creek). The solid line represents the USGS rating curve, and open circles denote three years of historical field measurements. The inset highlights the low-discharge range (10–50 ft³/s) for improved visual comparison.

Figure 4.39 shows the comparison of the discharge estimates with the USGS rating curve. When plotted against the curve, the UAV-derived estimates fall close to the expected discharge values, with deviations smaller than those observed in the field measurements. Overall, the three methods yielded differences of 14–28% relative to the USGS discharge. Among them, the PTV-based SV estimate showed the lowest error. Under the clear-water conditions at Tavern Creek, the PTV method appears to provide the most reliable discharge estimate.

5. Summary and Recommendations

5.1 Summary

From the literature review, UAV-based water-surface elevation (WSE) measurement errors (ME) range from 0.16 to 0.61 ft, with radar-based WSE measurements showing the lowest error (ME = 0.16 ft). For bathymetry, measurement errors range from 0.3 to 1.0 ft, with hyperspectral/multispectral sensors (ME = 0.31 ft) and bathymetric LiDAR (ME = 0.30 ft) providing the highest accuracy among the reviewed methods. Surface-velocity measurements show mean absolute percentage errors (MAPE) ranging from 10.7% to 37.7%, with PTV yielding the lowest error (MAPE = 10.7%). For discharge estimation, MAPE ranges from 12.4% to 19.1%, with the surface velocity method (SV) providing the lowest error (MAPE = 12.4%). However, PTV and GM give mean percentage errors (MPE) of approximately +4.0% and –2.3%, respectively, which are larger in magnitude than the average MPE reported for surface-velocity measurements (-2.0%) and for overall discharge estimates (–1.0%). This indicates the presence of small systematic biases in both methods.

UAV-based discharge was estimated using two different approaches: the geometric method (GM) and the surface-velocity method (SV). Using the bathymetry data, LiDAR-derived hydraulic parameters, including hydraulic radius, flow area, and roughness coefficients, were used in the GM approach to compute discharge. For the SV method, PIV was applied at all sites except Tavern Creek, where clear-water conditions required the use of seeded tracers. Surface velocities obtained from PIV (or PTV at Tavern Creek) were then converted to discharge using the velocity–area method.

Table 5-1 provides a comparison of discharge estimates across all surveyed sites, illustrating the performance of both geometry-based and UAV-derived surface-velocity methods. The geometric–manometric method generally produced higher discharge estimates, especially in narrow or rough channels where Manning's *n* was difficult to constrain. In contrast, the SV-based methods, including PIV and PTV implementations, tended to underestimate discharge relative to the station values, reflecting the sensitivity of these techniques to tracer availability, camera angle, and velocity-coefficient selection. Across the sites, errors for SV-based estimates ranged from approximately 14% to 43%, while GM errors varied more widely, particularly at very small streams where uncertainties in wetted geometry dominate the calculation.

Table 5-1 Summary of discharge estimates across all surveyed sites. The table compares discharge derived from USGS station measurements, the geometric–manometric (GM) method, and UAV-based surface velocity (SV) methods. Percent differences indicate deviations from the station discharge for each technique. SV estimates include upstream (US), downstream (DS), or method-specific values (PIV, PTV), with applied velocity coefficients shown where relevant.

	Discharge			**Difference**	
Site Name	**Station (ft^3/s)**	**GM (ft^3/s)**	**SV (ft^3/s)**	**GM (%)**	**SV (%)**
Petite Saline Creek	3650	4621 (n1, n2, n3 = 0.1, 0.035, 0.1)	US: 2973 DS: 2949 (α1, α2, α3 = 0.8,0.9,0.8)	26.6	18.9 18.5(US) 19.2(DS)
Hinkson Creek	226	318 (n = 0.035)	US: 152 (α=0.9)	40.7	32.7
Moniteau Creek	301	302 (n = 0.035)	US: 171 (α=0.9)	0.3	43.2
Long Branch Creek	5.5	49.4 (n = 0.035)	US:4.0 (α=0.9)	798*	27.3
Tavern Creek	29.5	23.3 (n = 0.035)	PIV: 21.1 (α=0.9) PTV: 25.3 (α=0.9)	21.1	28.4 (PIV) 14.2 (PTV)
Total mean	842	1063	903	22.2 (*set as outlier)	25.3

Overall, UAV-based discharge estimation resulted in measurement errors of 22.2–25.3% compared with the USGS rating curve. Based on these results, GM is generally applicable except in very small streams. GM produced an average error of 22.2%, while SV method produced an average error of 25.3%. However, GM errors ranged widely from 0.3% to 798% (the extreme value was treated as an outlier when computing the mean), whereas SV errors were consistently within 14.2–43.2%. This indicates that SV provides more stable accuracy across different sites, while GM can exhibit large deviations when channel geometry or roughness estimates are uncertain. Therefore, when testing time is limited, SV may be the preferred approach; when sufficient time and site information are available, GM is recommended.

Across the field deployments, PTV provides more stable and accurate velocity estimates than PIV when seeding particles or natural tracers were present, in clear-water environments. PTV's ability to track discrete features improves robustness in low-texture scenes, which is a common condition in Missouri's small to medium drainage basins. PIV remained useful in highly textured or turbid flows but was more sensitive to stabilization errors and illumination variability. The findings establish a standardized workflow, integrating LiDAR, photogrammetry, bathymetry, and surface velocimetry, that supports reliable, repeatable UAV-based discharge estimation across a diverse range of hydraulic settings.

5.2 Recommendations

Based on field experience and data-processing outcomes, several recommendations are proposed to improve the reliability and efficiency of UAV-based hydraulic measurements:

- Adopt PTV with seeding particles for clear-water conditions. While PIV provides faster computation, PTV offers higher accuracy in resolving surface flow trajectories, especially when natural or artificial tracers are sparse. Despite its longer processing time, PTV is preferred for low-turbidity or smooth-surface flows where PIV correlation may be unreliable.
- Adopt PIV under flooded conditions. Although PTV yields better accuracy in clear water, it becomes less effective in flooded or highly reflective environments due to weak tracer contrast. PIV is recommended in such cases, as its correlation-based approach performs more robustly under variable lighting or surface disturbance.
- Establish standardized seeding protocols. Biodegradable tracers such as wood mulch improved surface texture and PTV detection. Seeding density and release location should be adjusted based on flow velocity and channel width to ensure uniform tracer distribution.
- Automate velocity extraction and discharge estimation. Developing semi-automated workflows in MATLAB or Python that integrate PIV/PTV outputs with DEM-based cross-sections can streamline data processing, reduce operator workload, and improve reproducibility.

These recommendations aim to improve both field efficiency and data fidelity, supporting the Missouri Department of Transportation (MoDOT) in developing a reliable, repeatable framework for UAV-based streamflow monitoring.

References

Bandini, F, L Kooij, BK Mortensen, et al. 2023. “Mapping Inland Water Bathymetry with Ground Penetrating Radar (GPR) on Board Unmanned Aerial Systems (UASs).” JOURNAL OF HYDROLOGY 616 (January). https://doi.org/10.1016/j.jhydrol.2022.128789.

Bandini, F, TP Sunding, J Linde, et al. 2020. “Unmanned Aerial System (UAS) Observations of Water Surface Elevation in a Small Stream: Comparison of Radar Altimetry, LIDAR and Photogrammetry Techniques.” REMOTE SENSING OF ENVIRONMENT 237 (February). https://doi.org/10.1016/j.rse.2019.111487.

Bandini, Filippo. 2017. “Hydraulics and Drones: Observations of Water Level, Bathymetry and Water Surface Velocity from Unmanned Aerial Vehicles.” https://api.semanticscholar.org/CorpusID:55025661.

Bernard Jerry M. and Tuttle Ronald W. 2012. “Stream Corridor Restoration: Principles, Processes, and Practices.” In Engineering Approaches to Ecosystem Restoration. Proceedings. https://doi.org/10.1061/40382(1998)55.

Chen, Yen-Chang, Yung-Chia Hsu, and Eben O. Zai. 2022. “Streamflow Measurement Using Mean Surface Velocity.” Water 14 (15). https://doi.org/10.3390/w14152370.

Dietrich, JT. 2017. “Bathymetric Structure-from-Motion: Extracting Shallow Stream Bathymetry from Multi-View Stereo Photogrammetry.” EARTH SURFACE PROCESSES AND LANDFORMS 42 (2): 355–64. https://doi.org/10.1002/esp.4060.

Emanuele, P, G Nives, C Andrea, C Carlo, D Paolo, and LA Maria. 2020. “Bathymetric Detection of Fluvial Environments through UASs and Machine Learning Systems.” REMOTE SENSING 12 (24). https://doi.org/10.3390/rs12244148.

Fujita, I, Y Notoya, and M Shimono. 2015. “DEVELOPMENT OF UAV-BASED RIVER SURFACE VELOCITY MEASUREMENT BY STIV BASED ON HIGH-ACCURATE IMAGE STABILIZATION TECHNIQUES.” Edited by A Mynett.

Godfroy, J, J Lejot, L Demarchi, S Bizzi, and H Piégay. 2024. “Assessing the Feasibility of Mapping Channel Bathymetry of Long River Corridors from Hyperspectral Data across a Range of Flow Conditions.” INTERNATIONAL JOURNAL OF REMOTE SENSING 45 (22): 8123–56. https://doi.org/10.1080/01431161.2024.2398817.

Patalano, Antoine, Carlos Marcelo García, and Andrés Rodríguez. 2017. “Rectification of Image Velocity Results (RIVeR): A Simple and User-Friendly Toolbox for Large Scale Water Surface Particle Image Velocimetry (PIV) and Particle Tracking Velocimetry (PTV).” Computers & Geosciences 109 (December): 323–30. https://doi.org/10.1016/j.cageo.2017.07.009.

Perks, MT. 2020. “KLT-IV v1.0: Image Velocimetry Software for Use with Fixed and Mobile Platforms.” GEOSCIENTIFIC MODEL DEVELOPMENT 13 (12): 6111–30. https://doi.org/10.5194/gmd-13-6111-2020.

Zhou, Z, L Riis-Klinkvort, EA Jorgensen, et al. 2024. “Measuring River Surface Velocity Using UAS-Borne Doppler Radar.” WATER RESOURCES RESEARCH 60 (11). https://doi.org/10.1029/2024WR037375.